Shocks and Instabilities in Traffic

Thesis by
Rachel Shinn-Mendoza

In Partial Fullfillment of the Requirement
for the Degree of
Doctor of Philosophy

California Institute of Technology
Pasadena, California

1990
(submitted Nov. 28, 1989)

In this thesis, we study several models for traffic flow. Our interest is in finding periodic solutions and to study the effect of including a time lag on the propagation of shocks through a line of cars. The periodic solution was stimulated by a problem from water waves in which a periodic solution is created in the unstable region of the parameters by connecting segments of the growing solution with shocks. This results in a finite amplitude solution in the region of instability. The analysis of this is presented and then applied to a continuum model for traffic flow. We look for a smooth version of this periodic shock solution by considering a car following model for traffic. Car following models define the n^{th} car's velocity in a line of cars as a function of the distance between the n^{th} and $n-1^{st}$ cars and are thus a system of differential-difference equations which define the motion of the cars.

The model we study is attributed to G.F. Newell who found a transformation which makes the nonlinear equation linear. We discuss this exact solution and in particular, look at the shock solutions. These solutions, however, do not include the effect of a time lag. When this is included, we have the possibility of instabilities. We look at the shock solutions with the time lag included numerically and find that after some critical value, the smooth shock profile breaks up into oscillations about the final velocity state. We modify the equation by modeling the time lag continuously and look at these same shock solutions. We then find periodic solutions to this in the form of steady profile waves and compare the results with a continuum theory which also has smooth periodic solutions.

Contents

List of Figures

List of Tables

Introduction

Roll waves are a type of water flow in open inclined channels in which the flow becomes turbulent. These roll waves depend on the resistance provided by the roughness of the channel surface. If the resistance is absent, roll waves will not form. Roll waves are considered any steady wave form, which is periodic in distance, that results from turbulent flow down an inclined channel. What distinguishes these roll waves from bores is their fundamental dependence on the friction resulting from the roughness of the channel surfaces. In 1949, R.F. Dressler proposed a solution to the equations associated with roll waves. He found that roll waves arise from instabilities in the flow due to the steepness and roughness of the channel. Small disturbances on the surface of the water will grow into finite amplitude waves which propagate down the channel. The analytical solution to this problem is found by looking for a traveling wave solution to the shallow water equations augmented by the Chezy formula. The Chezy formula is an empirical term which expresses the turbulent frictional force. The solution is obtained by connecting segments of the growing solution with shocks to obtain a periodic solution. The analysis presented by Dressler is repeated in Chapter 1. Since the continuous traffic flow equations also exhibit instabilities and are similar to these shallow

water equations, we apply the ideas of the roll wave solution to the problem of traffic flow. The instability in traffic is based on a relationship between the mean velocity and the time lag. The presence of the time lag is required for instabilities to occur.

In channel flow, roll waves do occur and experiments have been done that illustrate this. Roll waves in traffic are the stop and go waves that everyone who drives on freeways is familiar with. These stop and go waves are a series of waves which travel down a line of cars. That this is caused by an instability may be a reasonable conjecture for the following reason. When there is a car stopped on the shoulder of the freeway, in heavy traffic, there is usually a traffic jam before the stopped car and much less so after the stopped car. When a car is stopped on the side of the road, people turn and look as they pass, causing them to slow down just slightly. The theory would suggest that this small change in speed, due to one car, causes the following cars to slow down even more until further down the line there is a traffic jam. Thus, it seems plausible that the phenomenon of 'roll waves', or periodic waves, in traffic exists.

There are two basic ways to deterministically model traffic flow. One way is with a continuum theory. This theory determines the density and flow of the traffic as continuous quantities in terms of location and time. The density and flow can be thought of as averaged quantities which give overall characteristics of the flow as opposed to precise motions of individual cars. The second way to model traffic is with car following models. These models assume that the velocity or acceleration of each individual car is determined

from some function of the headway — distance between consecutive cars — and/or the velocity difference between consecutive cars at a time T seconds earlier. T is then the time lag, or time that it takes for the driver to respond to some change in front of him. The function of the headway or velocity difference is usually based on some empirical data defining steady state values for the velocity and headway.

In Chapter 1, we consider a continuum model for traffic. Since the ideas we will pursue are based on the problem mentioned above from water waves, we review the roll waves solution and then apply these ideas to a continuum model of traffic flow. We then look at ways of smoothing out these discontinuities both in water and in traffic.

In the second chapter, we study a particular car following model. This model was presented by G.F. Newell in 1960 and is particularly interesting because it is a nonlinear model for which there is a transformation which makes the equation linear and thus has exact solutions. This transformation is possible when the time lag is zero. We study shock solutions of this model and find that there is a striking comparison to Burgers equation. When the effect of a time lag is introduced, exact solutions cannot be obtained and the new feature of instabilities arises. We examine these instabilities and then see how they affect the shocks that we studied when the time lag was zero.

In Chapter 3, we revise the model from Chapter 2 slightly by modeling the time lag differently. We have instabilities, as in Chapter 2, and we see how this instability affects shocks in this case and compare the results with those of Chapter 2. We then look for a periodic solution in the form of traveling

waves. This changes the equation from a differential-difference equation to a differential-delay equation. We linearize about a uniform state and find the conditions under which periodic solutions are possible. One of these conditions is that we are in the unstable region. We use this linear solution as a starting point for a perturbation expansion and find the circumstances under which we may expect periodic solutions. The analysis follows closely the ideas for limit cycle solutions to differential equations without a delay. We proceed to look at these limit cycles numerically and see how the character of the solution changes as we vary the two important parameters in the problem, the wave speed and the time lag.

In Chapter 4, we look again at the car following model of Chapter 2 and apply the perturbation analysis of Chapter 3 to this equation. The perturbation suggests that there are periodic solutions but perhaps only for a certain value of the wave speed (as opposed to a range of values).

In Chapter 5, we consider another continuum model for traffic flow which has smooth periodic solutions in the form of traveling waves. We apply the perturbation analysis of Chapter 3 to this model and then look at the periodic solution numerically. We find that this continuum model provides a bridge between the car following model and the continuum model with discontinuous shocks of Chapter 1.

We conclude by tying together the approaches to periodic solutions of Chapters 1, 3 and 5 and making a hueristic comparison with one piece of actual data.

Chapter 1

Review of Continuum Theories in Traffic and Water Waves

In this chapter, we introduce a continuum model for traffic flow and discuss its stability. We then review the roll waves solution to the problem of turbulent flow down an inclined channel which was solved by Dressler in 1949. The periodic solutions which are found model, qualitatively, the effect of a series of hydraulic jumps propagating down stream. Physically, the more common phenomenon is a series of these hydraulic jumps which are not periodic and not steady, they move at different speeds and hence, merge to form waves with different amplitudes. The periodic solution is a simplification and generalization of this. We study the periodic solution in particular because of its simplicity in comparison to the non-uniform case. In this thesis, we are primarily interested in the problem of traffic flow. We present the channel flow problem because it is the motivation for the approach we take to study traffic flow.

After we look at the water waves problem, we return to the equations

for traffic flow and apply the ideas from the roll waves problem to obtain a discontinuous periodic shock solution for traffic flow. We then discuss ways to alter the equations of shallow water and traffic to obtain smooth periodic solutions.

1.1 The Simplest Continuum Model for Traffic

The simplest continuum model for traffic flow is the conservation equation:

$$\rho_t + q_x = 0,$$

where $\rho(x,t)$ is the density of cars per unit area, and $q(x,t)$ is the flow of cars passing a position, x, per unit time. For this simple model, we assume that the flow is a function of the density alone,

$$q = Q(\rho).$$

The waves travel with speed $c(\rho) = Q'(\rho)$ and this equation can lead to shocks as discontinuities which travel with a velocity

$$U = \frac{Q(\rho_2) - Q(\rho_1)}{\rho_2 - \rho_1}.$$

The subscripts 1 and 2 denote the state ahead and behind the shock respectively. A simple jump between two uniform states is illustrated in figure (1.1). This corresponds to driving in light traffic and suddenly, at the position, x^*, slowing down and driving through heavier traffic. Additional terms added to this equation smooth out these shocks. We introduce a model which includes

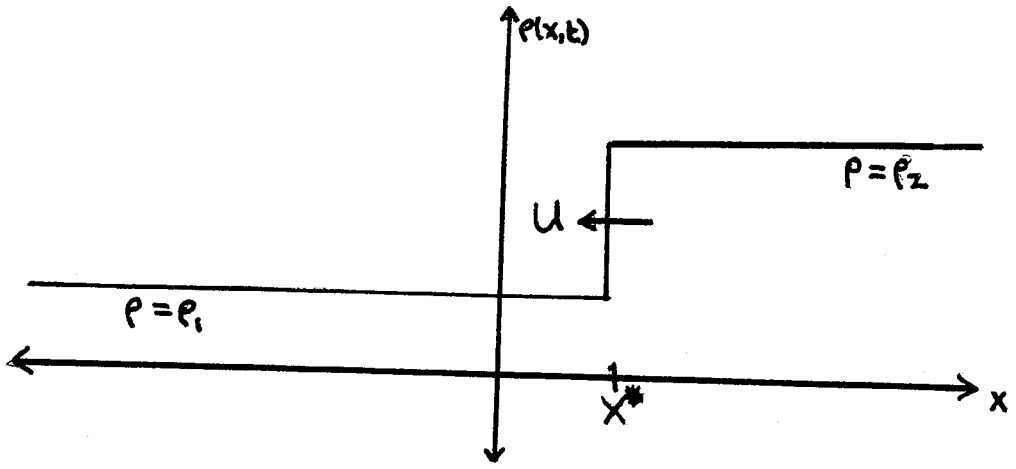

Figure 1.1: A simple jump discontinuity.

higher order effects. The first effect we include is the dependence on changes in the density, i.e., q depends on ρ_x as well as ρ: $q = Q(\rho) - \nu\rho_x$. The other effect we include is that of a time lag. The equations are:

$$\begin{aligned} &\rho_t + (\rho v)_x = 0 \\ &v_t + vv_x = -\tfrac{1}{\tau}(v - V(\rho) + \tfrac{\nu}{\rho}\rho_x). \end{aligned} \tag{1.1}$$

The first equation is the conservation equation where $v(x,t)$ is the velocity and hence, ρv is the flow, q. The second equation is the acceleration, where the quantity $V(\rho) - \frac{\nu}{\rho}\rho_x$ is the velocity the driver accelerates towards and τ is a measure of the drivers reaction time. We write the second equation in conservation form to illustrate the shock conditions:

$$(\rho v)_t + (\frac{\rho v^2}{2} + \frac{\nu}{\tau}\rho)_x = -\frac{1}{\tau}(\rho v - Q(\rho)),$$

where we have used the relation that $Q(\rho) = \rho V(\rho)$. This set of equations, however, also includes a different family of shocks with speed U defined by:

$$v_1 - U = \sqrt{\frac{\nu}{\tau}\frac{\rho_2}{\rho_1}}$$
$$v_2 - U = \sqrt{\frac{\nu}{\tau}\frac{\rho_1}{\rho_2}}.$$

Notice that here, the shock speed, U, is always less than the velocity.

An interesting phenomenon in these equations is the appearance of linear instabilities. To analyze the instabilities, we linearize about a uniform state v_0 and ρ_0 by setting $v = v_0 + w$, and $\rho = \rho_0 + r$, $(v_0 = V(\rho_0))$. Thus the linear equations are:

$$(w_t + v_0 w_x) = -\frac{1}{\tau}(w - V'(\rho_0)r + \frac{\nu}{\rho_0}r_x)$$
$$r_t + v_0 r_x + \rho_0 w_x = 0.$$

Eliminating w, we have:

$$r_t + (v_0 + \rho_0 V'(\rho_0))r_x = \nu r_{xx} - \tau(\frac{\partial}{\partial t} + v_0\frac{\partial}{\partial x})^2 r. \qquad (1.2)$$

Recognizing the first order wave speed on the left hand side of equation (1.2), we let $c_0 = v_0 + \rho_0 V'(\rho_0)$. To look for instabilities, it is sufficient to make the approximation $\frac{\partial}{\partial t} \simeq -c_0\frac{\partial}{\partial x}$ on the right hand side of equation (1.2) to obtain the equation:

$$r_t + c_0 r_x = (\nu - \tau(c_0 - v_0)^2)r_{xx}.$$

We know that $\nu - \tau(c_0 - v_0)^2 > 0$ corresponds to stable diffusion and that $\nu - \tau(c_0 - v_0)^2 < 0$ corresponds to instability. Therefore, we get instability if $\sqrt{\frac{\nu}{\tau}} < (c_0 - v_0)$. With the use of the shock conditions given above, we can

show that these instabilities develop into finite amplitude waves, analogous to the problem in water waves with similar equations.

1.2 Discontinuous Roll Waves in Shallow Water

We look now at the problem from water waves and review the roll wave solution. Figure (1.2) is a sketch of these waves. In water waves, the problem of

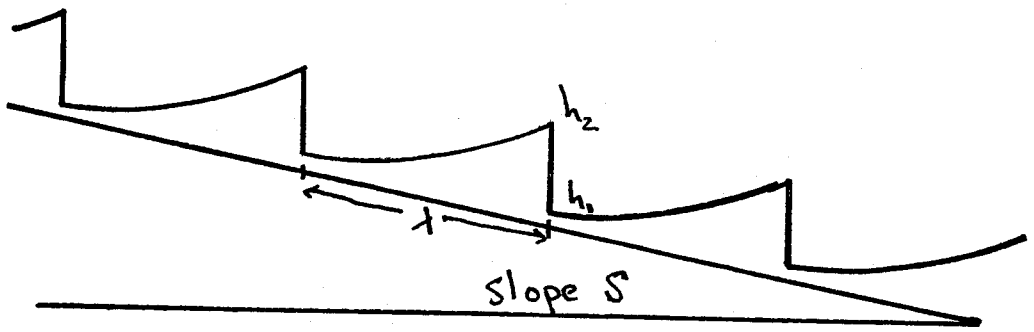

Figure 1.2: Roll waves down an inclined channel.

turbulent flow down an inclined channel leads to the shallow water equations augmented with the Chezy formula:

$$h_t + vh_x + hv_x = 0 \tag{1.3}$$

$$v_t + vv_x + gh_x = gS - C_f\frac{v^2}{h}. \tag{1.4}$$

Here, h is the height of the water and v is the velocity in the horizontal direction. S is the slope of the channel, C_f is the friction coefficient and g is gravity. The shock conditions are:

$$-U[h]_1^2 + [vh]_1^2 = 0 \tag{1.5}$$

$$-U[hv]_1^2 + [v^2h + \frac{1}{2}gh]_1^2 = 0, \tag{1.6}$$

where $[f]_1^2$ means the jump in f across the shock — the value of f behind the shock minus the value of f in front of the shock — and U is the shock velocity. The shock conditions are equivalent to:

$$U = v_1 + (\frac{gh_2(h_1+h_2)}{2h_1})^{1/2} \tag{1.7}$$

$$v_2 = v_1 + \frac{h_2 - h_1}{h_2}(\frac{gh_2(h_1+h_2)}{2h_1})^{1/2}. \tag{1.8}$$

We look for steady profile waves by setting $X = x - Ut$. Using this in equations (1.3) and (1.4) and integrating equation (1.3), the equations can be written as:

$$v = U - \frac{B}{h} \tag{1.9}$$

$$\frac{dh}{dX} = \frac{gSh^3 - C_f(B - Uh)^2}{gh^3 - B^2}, \tag{1.10}$$

where B is the constant of integration. Solving (1.9) for B, the denominator of (1.10) can be written as:

$$gh^3 - B^2 = -h^2(U - (v - \sqrt{gh}))(U - v - \sqrt{gh}).$$

Since $U > v$, U is always greater than $v - \sqrt{gh}$. Thus, the sign of the denominator depends on the sign of $U - v - \sqrt{gh}$. Using the shock conditions,

we find that at the lower end of the shock, we have

$$U - v_1 = \sqrt{\frac{gh_2(h_1 + h_2)}{2h_1}} > \sqrt{gh_1},$$

and hence $U - v_1 - \sqrt{gh_1}$ is positive. At the other end of the shock, we have

$$U - v_2 = \sqrt{\frac{gh_1(h_1 + h_2)}{2h_2}} < \sqrt{gh_2}$$

and thus, $U - v_2 - \sqrt{gh_2} < 0$. Therefore, $gh^3 - B^2$ changes sign for h between h_1 and h_2 and the denominator of (1.10) vanishes for $h = (\frac{B^2}{g})^{1/3} = h_c$ inside the interval $[h_1, h_2]$. Thus, the shock conditions require $h_2 > h_c > h_1$. Since we don't allow waves with infinite slope, we require that the numerator of (1.10) also vanish at $h = h_c$. This restricts either U or B.

The numerator of (1.10) is

$$gSh^3 - C_f U^2 h^2 + 2C_f UBh - C_f B^2. \tag{1.11}$$

For h_c to be a zero of this, we divide expression (1.11) by $h - h_c$ and require that the remainder be zero. This requirement gives the restriction on U:

$$U = \frac{B}{h_c} \pm \sqrt{\frac{gS}{C_f}} h_c.$$

We take the plus sign since $U = v + \frac{B}{h}$ and hence, $U > \frac{B}{h_c}$. The numerator, (1.11), can then be written as

$$gS(h - h_c)\{h^2 + (h_c - \frac{C_f}{gS}U^2)h + \frac{C_f}{S}h_c^3\}.$$

The roots of the quadradic, h_a and h_b, are then

$$h_{a,b} = \frac{1}{2}\{\frac{C_f}{gS}U^2 - h_c \pm \sqrt{(\frac{C_f}{gS}U^2 - h_c)^2 - 4\frac{C_f}{S}h_c^2}\}.$$

Substituting the value for U, we find h_a and h_b in terms of h_c, C_f and S:

$$h_{a,b} = h_c(\frac{1}{2}\frac{C_f}{S} + \sqrt{\frac{C_f}{S}} \pm \sqrt{(\frac{C_f}{2S})^2 + (\frac{C_f}{S})^{3/2}}). \tag{1.12}$$

The shock conditions become:

$$\frac{B}{h_1} = (\frac{gh_2(h_1+h_2)}{2h_1})^{1/2}. \tag{1.13}$$

Using (1.9), evaluated at state 1 and state 2, we have:

$$v_1 = U - \frac{B}{h_1}$$
$$v_2 = U - \frac{B}{h_2}$$

So far, h_1 is determined in terms of h_2, and the rest of the parameters: v_1, v_2, U, h_a, h_b and h_c can be expressed in terms of B. Equation (1.10) becomes:

$$h_X = \frac{S(h-h_a)(h-h_b)}{h^2 + hh_c + h_c^2}. \tag{1.14}$$

We see from equation (1.14) that if $h = h_a$ or h_b, X must be equal to $\pm\infty$. Thus, the solutions are of the form illustrated in figure (1.3). If we are in the unstable region, it can be shown that $S > 4C_f$ and hence, $\sqrt{\frac{C_f}{S}} < \frac{1}{2}$. From this and equation (1.12), we see that h_a, the largest of h_a and h_b, is less than h_c. Thus, we piece together sections of the upper curve in figure (1.3), with $\frac{dh}{dX}$ always positive, to form a periodic solution. It can be shown (refer to Dressler's paper) that a periodic solution to this equation is not possible any other way. This equation can be integrated to get $X(h)$. Given this, we find the wavelength $\lambda = X(h_2) - X(h_1)$ which, in integral form is:

$$\int_{X(h_1)}^{X(h_2)} dX = \int_{h_1}^{h_2} \frac{h^2 + hh_c + h_c^2}{S(h-h_a)(h-h_b)} dh.$$

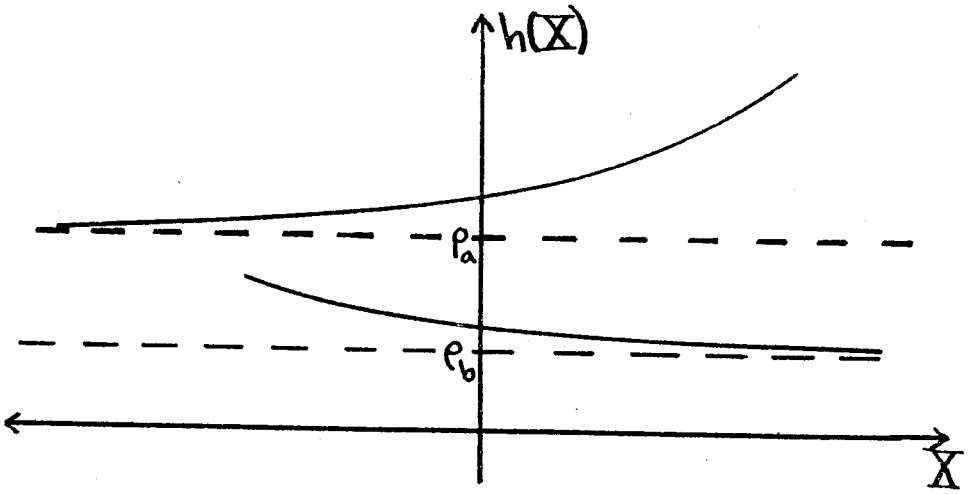

Figure 1.3: Possible solution types for $h(X)$.

Thus, the periodic roll wave solution is constructed with 2 free parameters, h_c and ρ_1, say, although this is not the only choice. We see that for $\frac{dh}{dX}|_{h_c} > 0$, we must have $4C_f < S$ which is the instability condition and the relationship between the friction and the slope that is required to produce roll waves, i.e., too much friction or too little slope will result in no roll waves.

1.3 Discontinuous 'Roll Waves' in Traffic

Since the traffic flow equations, equations (1.1), are similar to the shallow water equations studied in the previous section, we look for discontinuous periodic solutions for this problem. The first equation of (1.1) is already in conservation form. The second equation of (1.1) can be written in conserva-

form as:

$$(\rho v)_t + (\rho v^2 + \frac{\nu}{\tau}\rho)_x = -\frac{1}{\tau}(\rho v - Q(\rho)).$$

From the conservation form of the equations, the shock conditions are:

$$-U[\rho]_1^2 + [\rho v]_1^2 = 0$$
$$-U[\rho v]_1^2 + [\rho v^2 + \frac{\nu}{\tau}\rho]_1^2 = 0.$$

These can be rewritten as:

$$v_1 - U = \sqrt{\frac{\nu}{\tau}\frac{\rho_2}{\rho_1}}$$
$$v_2 - U = \sqrt{\frac{\nu}{\tau}\frac{\rho_1}{\rho_2}}.$$

As in section 1.2, we look for steady profile waves by setting $X = x - Ut$, where U is the shock velocity. Consequently, equations (1.1) become

$$\rho(v - U) = A = const \tag{1.15}$$
$$\frac{\nu}{\tau}\rho_X + \rho(v - U)v_X = \frac{1}{\tau}(Q(\rho) - \rho v) \tag{1.16}$$

Recall from the shock conditions that $v > U$ so that $A > 0$. Solving for v in (1.15) and substituting this into (1.16), we have:

$$\frac{d\rho}{dX} = \frac{\rho^2}{\tau}\frac{Q(\rho) - \rho U - A}{\frac{\nu}{\tau}\rho^2 - A^2}. \tag{1.17}$$

Using (1.15), the shock conditions can be written as:

$$\begin{aligned} v_1 &= U + \tfrac{A}{\rho_1} \\ v_2 &= U + \tfrac{A}{\rho_2} \end{aligned} \tag{1.18}$$

$$\frac{\nu}{\tau}\rho_1\rho_2 = A^2. \tag{1.19}$$

Note that the denominator of (1.17) vanishes at $\rho = \rho_a = \sqrt{\frac{\tau}{\nu}}A$. We see that ρ_a is between ρ_1 and ρ_2, and thus in the region of interest, since $A^2 = \frac{\nu}{\tau}\rho_1\rho_2$ and thus, $\rho_a^2 = \rho_1\rho_2$. We require finite slopes in the profile of ρ, so the numerator must also vanish at ρ_a. As a particular model, we take the case $Q(\rho) = \alpha\rho(\beta - \rho)$. This is the quadratic profile with $\beta = \rho_j$, the jam density. ρ_m is equal to the value of ρ where Q is a maximum, $\rho_m = \frac{1}{2}\beta$, with $Q(\rho_m) = \frac{1}{4}\alpha\beta^2 = q_m$. Using this form for Q in equation (1.17), we obtain:

$$\frac{d\rho}{dX} = -\frac{\rho^2}{\tau}\frac{\alpha\rho^2 + (U - \alpha\beta)\rho + A}{\frac{\nu}{\tau}\rho^2 - A^2} \tag{1.20}$$

which can be written as:

$$\frac{d\rho}{dX} = -\frac{\rho^2}{\tau}\frac{\alpha(\rho - \rho_a)(\rho - \rho_b)}{\frac{\nu}{\tau}(\rho - \rho_a)(\rho + \rho_a)}, \tag{1.21}$$

where $\rho_a = \sqrt{\frac{\tau}{\nu}}A$. Equating the numerators of equations (1.20) and (1.21), we have:

$$U = \alpha\beta - \alpha(\rho_a + \frac{1}{\alpha}\sqrt{\frac{\nu}{\tau}})$$
$$\rho_b = \sqrt{\frac{\nu}{\tau}}\frac{1}{\alpha}.$$

So far there is one free parameter — ρ_a or A. In terms of ρ_a equation (1.17) can be written as:

$$\frac{d\rho}{dX} = -\frac{\rho^2\alpha}{\nu}\frac{\rho - \frac{1}{\alpha}\sqrt{\frac{\nu}{\tau}}}{\rho + \rho_a}.$$

Expressing A in terms of ρ_a and ρ_b, equation(1.19) and the shock velocity can be written as:

$$\frac{\nu}{\tau}\rho_1\rho_2 = \alpha^2\rho_a^2\rho_b^2$$
$$U = -\alpha(\rho_a + \rho_b - \rho_j).$$

The shock conditions, equations (1.18), give v_1 and v_2 in terms of ρ_1 and ρ_2. The last relationship that we have is obtained from the requirement that the solution be periodic. This implies that the wavelength, λ, is related to the other parameters by:

$$\lambda = \int_{X(\rho_1)}^{X(\rho_2)} dX = -\frac{\alpha}{\nu}\int_{\rho_1}^{\rho_2} \frac{\rho+\rho_a}{\rho^2(\rho-\rho_b)}d\rho.$$

For roll waves in traffic, $\frac{d\rho}{dX}$ should be negative since we expect the shocks to jump from a low density to a higher one. This requires that $\rho > \rho_b$. Recall that the instability condition derived in section (1.1) was $(c_0 - v_0) > \sqrt{\frac{\nu}{\tau}}$. We relate the parameters in section (1.1) to those of this section by noting that $c_0 - v_0 = \rho_0 V'(\rho_0)$. Using the relation $\rho V(\rho) = Q(\rho)$ and the quadradic form for Q, we have $V(\rho) = \alpha(\beta - \rho)$ and $V'(\rho_0) = -\alpha$. Substituting the value of $\rho_0 V'(\rho_0)$ into the instability condition, we have $\alpha\rho_0 > \sqrt{\frac{\nu}{\tau}}$ or $\rho_0 > \frac{1}{\alpha}\sqrt{\frac{\nu}{\tau}} = \rho_b$. So the instability condition is required for roll waves to occur.

The equation for X is

$$X = -\frac{\alpha}{\nu}\int \frac{\rho+\rho_a}{\rho^2(\rho-\rho_b)}d\rho,$$

which integrates to

$$X = -\frac{\alpha}{\nu\rho_b^2}[(\rho_a+\rho_b)\ln(\frac{\rho-\rho_b}{\rho}) + \frac{\rho_a\rho_b}{\rho}] + C.$$

C is unimportant since it just fixes the origin on the X axis. The solution is thus determined in terms of two free parameters. If we took the two free parameters to be ρ_1 and ρ_a, both U and ρ_2 are determined in terms of these. Given particular values for ρ_1 and ρ_a, $\rho(X)$ could be plotted as a function of X as in figure (1.4).

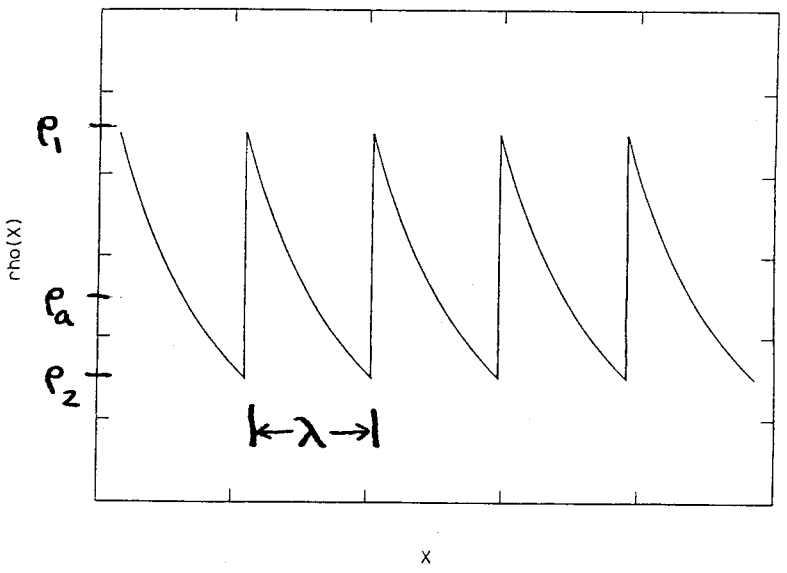

Figure 1.4: Plot of $\rho(X)$

1.4 Smooth Roll Wave Solutions in Water

In water, something like discontinuous hydraulic jumps is observed. However, it is possible to smooth out these discontinuities to obtain a continuous solution. This solution is a smoothed out version of figure (1.2). A continuous version of these shocks can be obtained in two ways. Dressler looked at the full two-dimensional water waves problem and took a perturbation approach to get a continuous periodic solution. Needham and Merkin added an eddy viscosity term to the shallow water equations that were presented

in section (1.2). Dressler takes the full equations for water waves:

$$\begin{aligned} u_x + v_y &= 0 \\ u_t + uu_x + vu_y &= -\frac{1}{\rho}p_x \\ v_t + uv_y + vv_x &= -\frac{1}{\rho}p_y \\ v_x &= u_y \end{aligned}$$

with boundary conditions

$$\eta_t + u\eta_x = v \qquad at \quad y = \eta$$

$$p = 0 \qquad at \quad y = \eta$$

$$ud_x - v = 0 \qquad at \quad y = d(x),$$

where $u(x,t)$ is the velocity in the horizontal direction, x, v is the velocity in the vertical direction, y, p is the pressure and ρ is the density. In the boundary conditions, we have that η is the surface displacement and $d(x)$ defines the bed of the channel. Dressler contends that it is possible to augment these equations in such a way that if a perturbation expansion for shallow water is done on the augmented equations, with the vertical height of the water equal to

$$Y^0 + \epsilon Y^1 + \cdots$$

and the horizontal velocity:

$$u = U^0 + \epsilon U^1 + \cdots,$$

the 0^{th} and 1^{st} order equations alone will give exactly the equations that Dressler used to construct the periodic shock solution. That is, the friction term, $C_f\frac{v^2}{h}$, will only come into the 0^{th} and 1^{st} order equations of the perturbation problem and the higher order equations will not include any friction terms except as part of the 0^{th} order solution. So, the higher order equations will be the same, formally, as those of the expanded, unaugmented hydrodynamic equations. Thus, to 0^{th} order we have the steady solution for the horizontal velocity that was obtained in section 1.2, and the vertical height, Y^0 is constant. We find from the 1^{st} order approximation (which can only be found after looking at the equations of 2^{nd} and 3^{rd} order) that Y^1 is linearly related to U^1 and that Y^1 can be expressed in terms of the *cn* function. Thus, a continuous periodic solution is found.

In their alternative view, Needham and Merkin add on an eddy viscosity term to the shallow water equations from section (1.2). They looked at the equations:

$$h_t + (hv)_x = 0$$
$$v_t + vv_x + gh_x = gS - C_f\frac{v^2}{h} + \nu_0 v_{xx}$$

and showed that a periodic solution could be obtained.

1.5 Equations for Smooth Roll Wave Solutions in Traffic

In traffic, higher derivitives correspond to Needham and Merkins approach. Discrete equations in the form of car following models have often been used.

A general car following equation is given by

$$v_n(t+T) = G(h_n)$$

where $v_n(t)$ is the velocity of the n^{th} car, $h_n(t) = s_{n-1}(t) - s_n(t)$ is the spacing between two consecutive cars with s_n equal to the position of the n^{th} car and G is a function of the spacing. These equations can be approximated

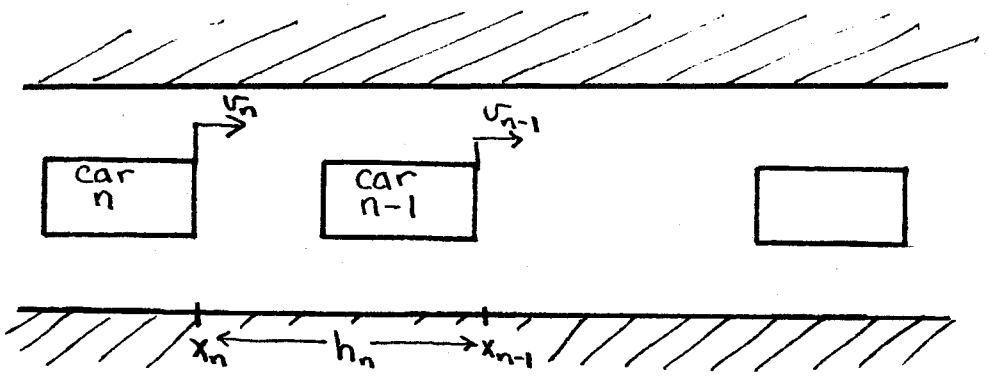

Figure 1.5: Diagram of car following.

by continuous differential equations by an expansion of the spacing between consecutive cars that appears in the discrete equations. If this expansion is cut off appropriately, we have an equation similar to Needham and Merkin's. We write the velocity and position as continuous variables:

$$v_n(t) = v(\xi_n, t)$$

$$s_n(t) = s(\xi_n, t)$$

where ξ_n is a label and equals the position of the n^{th} car at $t = 0$. The discrete equations become:

$$v(\xi_n, t+T) = G(s(\xi_{n-1}, t) - s(\xi_n, t))$$
$$\frac{ds}{dt}(\xi_n, t) = v(\xi_n, t).$$

If the cars are in a uniform state to begin with, then $\xi_n = -n\Delta\xi$ where $\Delta\xi = h_n(0)$ is the same for all n. In particular, $\Delta\xi = G^{-1}(v_0)$, where v_0 is the uniform flow. In general, ξ_n is just s_n at $t = 0$. However, we are interested in small perturbations from a uniform state, so we let $\xi_n = -n\Delta\xi$ with $\Delta\xi$ constant. This substitution yields

$$\begin{array}{c} v(-n\Delta\xi, t+T) = G\{s(-(n-1)\Delta\xi, t) - s(-n\Delta\xi, t)\} \\ \frac{ds}{dt}(-n\Delta\xi, t) = v(-n\Delta\xi, t) \end{array} \tag{1.22}$$

We now expand $s(-n\Delta\xi + \Delta\xi, t)$ about $-n\Delta\xi$:

$$s(-n\Delta\xi + \Delta\xi, t) = s(-n\Delta\xi, t) + \Delta\xi s_\xi(-n\Delta\xi, t) +$$
$$\frac{1}{2}(\Delta\xi)^2 s_{\xi\xi}(-n\Delta\xi, t) + \cdots.$$

Therefore, the difference $s(-(n-1)\Delta\xi, t) - s(-n\Delta\xi, t)$ becomes

$$(\Delta\xi)s_\xi(-n\Delta\xi, t) + \frac{1}{2}(\Delta\xi)^2 s_{\xi\xi} + \cdots.$$

If ρ, defined as $\frac{1}{h}$, is the density of cars, then in a Lagrangian description, we have that for a fixed time, t_0, $\rho\,\delta\xi|_{t=t_0} = \rho\,\delta s|_{t=t}$ which can be written as $\frac{\rho_0}{\rho} = \frac{\delta s}{\delta\xi} = s_\xi$. We choose $\rho_0 = \frac{1}{\Delta\xi}$ and let $\xi = -n\Delta\xi$. We expand $v(\xi, t+T)$ for T small in some sense and use this together with the expansion for $s(\xi + \Delta\xi, t) - s(\xi, t)$ in equation (1.22) to obtain:

$$v(\xi, t) + Tv_t(\xi, t) + \frac{1}{2}v_{tt}(\xi, t) + \cdots =$$

$$G(\frac{1}{\rho} + \frac{1}{2}\Delta\xi\frac{d}{d\xi}(\frac{1}{\rho}) + \cdots)$$

$$\frac{ds}{dt}(\xi, t) = v(\xi, t).$$

we now expand $G(u)$ for u near $\frac{1}{\rho}$:

$$G(u) = G(\frac{1}{\rho}) + [\frac{1}{2}\Delta\xi\frac{d}{d\xi}(\frac{1}{\rho}) + \cdots]G'(\frac{1}{\rho}) + \frac{1}{2}[\frac{1}{4}(\Delta\xi)^2(\frac{d}{d\xi}(\frac{1}{\rho}))^2 + \cdots]G''(\frac{1}{\rho}) + \cdots,$$

and write this as:

$$G(\frac{1}{\rho}) + \frac{1}{2}\Delta\xi\frac{d}{d\xi}(\frac{1}{\rho})G'(\frac{1}{\rho}) + (\Delta\xi)^2[\frac{1}{8}G''(\frac{1}{\rho})(\frac{d}{d\xi}(\frac{1}{\rho}))^2 + \frac{1}{6}\frac{d^2}{d\xi^2}(\frac{1}{\rho})G'(\frac{1}{\rho})] + \cdots.$$

If we keep terms up to and including order $(\Delta\xi)^2$ on the right, then we have an equation with the desired higher derivatives. If we choose some large number of cars, N, then we are assuming that $\Delta\xi$ is small in comparison to the total distance over which N cars are stretched. That is $\frac{\Delta\xi}{N\Delta\xi} \ll 1$, so that the approximation is good for a large number of cars. We are also assuming that T is small compared to some typical time scale.

In view of this expansion, we see that the equation $v_n(t+T) = G(h_n)$ can be viewed as an equation with an infinite number of derivatives. We expect these higher derivatives to smooth out the discontinuities in the first order continuous equation. Thus, in Chapter 3, we look for continuous roll wave type solutions from this type of equation.

Chapter 2

A Discrete Model

As noted earlier, one general form for car following models is:

$$v_n(t+T) = G(h_n(t)) \tag{2.1}$$

where various choices for G have been studied. In general, car following models give the velocity (or acceleration) of a car at time t as some function of the headway (distance between front bumpers of consecutive cars) evaluated at a time T seconds earlier. Acceleration models also include dependence on the velocity difference between consecutive cars. The simplest forms of these dependencies were studied initially. Small deviations from a uniform state were studied by R.E. Chandler, R. Herman, and E.W. Montroll in 1958 by considering the acceleration as a linear function of the velocity difference and headway. However, their experiments showed that the acceleration was more sensitive to the velocity difference than to the headway, so the headway dependence can be dropped. This leaves a perfectly integrable equation in the linear case and leads us back to considering equations of the form (2.1). Linear models have been studied in some detail but not much has been done

on nonlinear models. Nonlinear models in general illustrate more interesting phenomena and have the potential of illustrating effects that linear models do not contain at all.

The nonlinear model proposed by G.F. Newell that was alluded to earlier has the great advantage that it has exact solutions. Aside from that it has the properties that the shape is approximately correct for the steady state data, it gives what is expected at zero velocity and at infinite headway, and it is a fairly simple model. The equation is:

$$v_n(t+T) = v_f(n)(1 - e^{\frac{-\lambda(n)}{v_f(n)}[h_n(t)-d_n]}),$$

where $v_f(n)$ represents the n^{th} car's free speed, d_n, the n^{th} car's spacing when all the cars are at rest, and $\lambda(n)$, the slope of $V(h)$ at zero velocity. For simplicity, we study the case where λ and v_f are constant; independent of n. d_n can be eliminated from the equations by setting

$$y_n(t) = x_n(t) - \sum_{k=1}^{n} d_k.$$

Notice that letting d_n be a function of n allows for different size cars. Since it can be eliminated from the equation, there is no loss in taking it to be a constant, L. This is accepted in the following.

2.1 Case $T = 0$

Solution for $T = 0$ were obtained by Newell. The key step is that the transformation

$$z_n(t) = e^{-\frac{\lambda}{v_f} y_n(t)}$$

linearizes the equation exactly. For v_n, we have

$$v_n(t) = \frac{dy_n}{dt} = -\frac{v_f}{\lambda}\frac{\frac{dz_n}{dt}}{z_n}.$$

This transformation gives a linear equation in z_n:

$$\frac{1}{\lambda}\frac{dz_n}{dt} + z_n = z_{n-1}.$$

We can non-dimensionalize t by letting $\tau = \lambda t$ and the equation becomes

$$\frac{dz_n}{d\tau} + z_n = z_{n-1}.$$

Notice that a simple solution to the above equation is

$$z_n(\tau) = e^{-p\tau+qn},$$

where

$$q = q(p) = \log(\frac{1}{1-p}).$$

This solution is just the uniform flow:

$$v_n(t) = pv_f$$
$$h_n(t) = x_{n-1}(t) - x_n(t) = q\frac{v_f}{\lambda} - L.$$

In Newell's notation, $p = 1 - \alpha$.

If λ and v_f are left as functions of n, the transformation still yields a linear equation, but the simplicity of the solution is lost.

2.1.1 Shock Solution

Since the z_n equation is a linear equation, any superposition of these is also a solution. If we put two of these together, we get a shock profile for the solution $v_n(t)$. We add two and have:

$$z_n = e^{-p_1\tau+q_1 n} + e^{-p_2\tau+q_2 n}.$$

Therefore, the velocity, v_n, is:

$$v_n(\tau) = \frac{p_1 e^{-p_1\tau+q_1 n} + p_2 e^{-p_2\tau+q_2 n}}{e^{-p_1\tau+q_1 n} + e^{-p_2\tau+q_2 n}}$$

which, by rearranging the exponentials appropriately can be written as:

$$v_n(t) = \frac{v_f}{\lambda}\{\frac{1}{2}(p_1+p_2) - \frac{1}{2}(p_2-p_1)\tanh(\frac{1}{2}(p_2-p_1)X)\}. \qquad (2.2)$$

Here,

$$X = \lambda t - An$$

and

$$A = \frac{q_2-q_1}{p_2-p_1} = \frac{\log(\frac{1-p_1}{1-p_2})}{p_2-p_1}.$$

The corresponding y_n is then

$$y_n(t) = \frac{v_f}{\lambda}(\frac{1}{2}(p_1+p_2)t - \ln\{\cosh[\frac{1}{2}(p_2-p_1)X]\}).$$

The state ahead is $\frac{v_f}{\lambda}p_1$, and the state behind is $\frac{v_f}{\lambda}p_2$. In Newell's notation, $p_1 = 1-\alpha$ and $p_2 = 1-\beta$. See figure (2.1).

Newell also solved the equation by generating functions, where the general solution is given in terms of the displacement of the lead car and the initial displacement of all the cars. He then looked at the special case where the lead car decelerates instantaneously from a velocity v_1, to a new velocity v_2 and until $t = 0$, all the cars are traveling at speed v_1. The solution to this can be written in terms of Gamma functions. Newell does asymptotics on this for large n and shows that the velocity profiles of the cars tend to the same solution, (2.2). Notice that v_n is a function of $\tau - nA$ alone and otherwise independent of τ and n. The n^{th} car has the same velocity profile

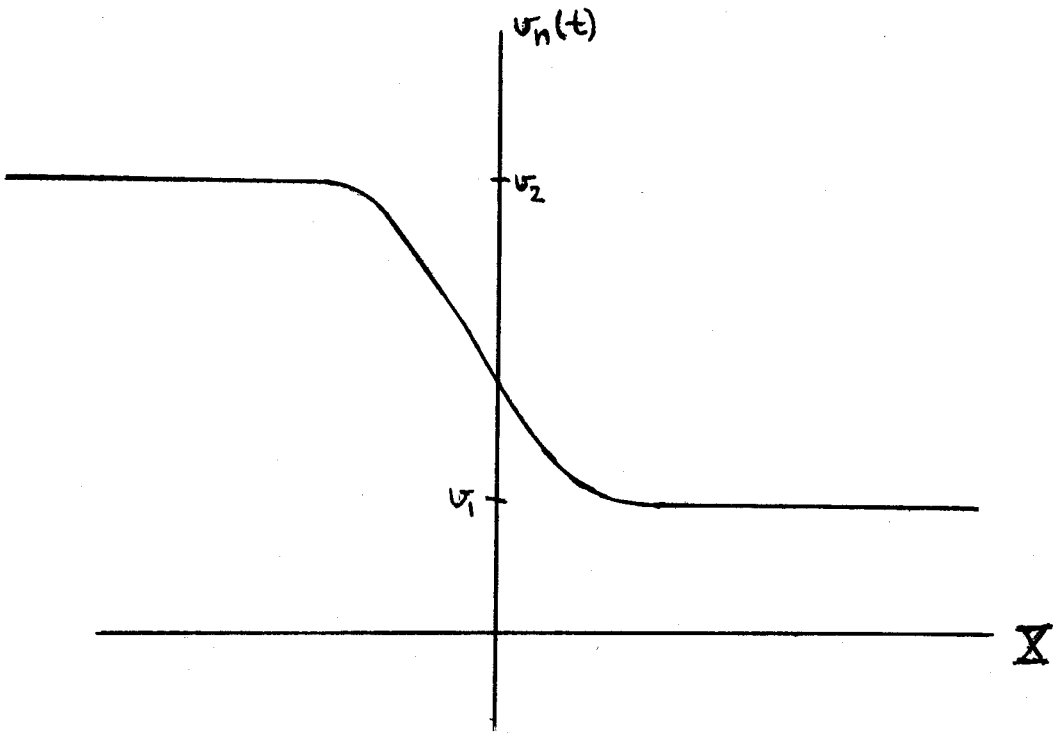

Figure 2.1: 1-shock solution for $T = 0$.

as the $(n-1)^{st}$ car at a time $\frac{A}{\lambda}$ later. Whereas in the simplest continuum theory discussed in the first chapter, the shock is discontinuous, the discrete equations give a smooth shock and give the details of the motion through it.

2.1.2 Expansion Wave

Newell also did the case where the lead car accelerates from a velocity v_1 up to a velocity v_2 which we would think of as an expansion wave. He does asymptotics for large n and obtains the velocity

$$v_n \sim \begin{cases} v_f(1-\alpha) & \text{if } \tau < \frac{n-1}{\alpha} \\ v_f(1-\frac{n-1}{\tau}) & \text{if } \frac{n-1}{\alpha} < \tau < \frac{n-1}{\beta} \\ v_f(1-\beta) & \text{if } \tau > \frac{n-1}{\beta} \end{cases} .$$

Notice here that each individual section is a solution to the equation. The two constant states are just the simple solutions shown earlier, and the middle case can be substituted into the equation for v_n and seen to satisfy the equation with

$$x_n(\tau) = x_1 + \frac{v_f}{\lambda} \ln(\frac{(n-1)!}{\tau^{n-1}}).$$

The corresponding z_n for this is

$$z_n(\tau) \sim \begin{cases} e^{-(1-\alpha)\tau - \ln(\alpha)} & \text{if } \tau < \frac{n-1}{\alpha} \\ (\frac{(n-1)!}{\tau^{n-1}})^{\frac{\lambda}{v_f}} & \text{if } \frac{n-1}{\alpha} < \tau < \frac{n-1}{\beta} \\ e^{-(1-\beta)\tau - \ln(\beta)} & \text{if } \tau > \frac{n-1}{\beta}. \end{cases} .$$

Notice that just as in Burgers equation,

$$c_t + cc_x = \nu c_{xx},$$

where the transformation

$$c = -2\nu(\log \phi)_x$$

transforms the equation into a linear one, here also, a logrithmic transformation yields a linear equation. Similar to $c = -2\nu\frac{\phi_x}{\phi}$, we have for Newell's equation that $v_n = -\frac{v_f}{\lambda}\frac{(z_n)_t}{z_n}$. The solution also looks similar to that of Burgers equation. We saw earlier that the sum of two simple solutions gave the shock profile. If we add three of these solutions together, we get interacting shocks just as in Burgers equation.

2.1.3 Multishocks

For three of these simple solutions, we have that

$$v_n(\tau) = \frac{v_f}{\lambda}\{\frac{p_1 e^{-p_1\tau+q_1 n} + p_2 e^{-p_2\tau+q_2 n} + p_3 e^{-p_3\tau+q_3 n}}{e^{-p_1\tau+q_1 n} + e^{-p_2\tau+q_2 n} + e^{-p_3\tau+q_3 n}}\}.$$

We want to see in what regions of (τ, n) space each exponential dominates. Lets call $f_i = e^{-p_i\tau+q_i n}$. First we look for where f_1 dominates. We rewrite v_n as :

$$v_n(\tau) = \frac{v_f}{\lambda}\{\frac{p_1 + p_2\frac{f_2}{f_1} + p_3\frac{f_3}{f_1}}{1 + \frac{f_2}{f_1} + \frac{f_3}{f_1}}\}.$$

Each $\frac{f_i}{f_j}$ can be written as $e^{-(p_i-p_j)(\tau-A_{ij}n)}$ where $A_{ij} = \frac{q_i-q_j}{p_i-p_j}$ which is $\frac{\log(\frac{1-p_j}{1-p_i})}{p_i-p_j}$. Notice that $A_{ij} = A_{ji}$ and also that $A_{ij} > 0$ since for $p_i > p_j$, $\frac{1-p_j}{1-p_i} > 1$. Thus, the numerator is positive and, by assumption, the denominator, $p_i - p_j$ is positive also. For f_1 to be domimant, we require the other exponentials to decay. This means that $\tau > A_{31}n$ and $\tau > A_{21}n$. Looking at

$$A_i(p) = \frac{\log(\frac{1-p_i}{1-p})}{p - p_i},$$

we can see that this is an increasing function of p, so that for $p_3 > p_2$, we have that $A_{31} > A_{21}$. Hence, $v_f \sim \frac{v_f}{\lambda}p_1$ for $\tau > A_{31}n$.

Next, we find where f_2 dominates. We write v_n as

$$v_n(\tau) = \frac{v_f}{\lambda}\{\frac{p_1\frac{f_1}{f_2} + p_2 + p_3\frac{f_3}{f_2}}{\frac{f_1}{f_2} + 1 + \frac{f_3}{f_2}}\}.$$

Again, for f_2 to dominate, the other exponentials must decay. This is true for $\tau < A_{12}n$ and $\tau > A_{32}n$. Since $A_i(p)$ is an increasing function of p, we have that $A_{32} > A_{12}$, so the only way for τ to be between $A_{32}n$ and $A_{21}n$ is for n and hence τ, to be negative. Thus, for $A_{32}n < \tau < A_{12}n$, we have $v_n(\tau) \sim \frac{v_f}{\lambda}p_2$.

Following the same reasoning for f_3, we find that for $\tau < A_{31}n$ and $\tau < A_{32}n$, we have:

$$v_n(\tau) \sim \frac{v_f}{\lambda}p_3 \quad \text{for} \quad \begin{cases} \tau < A_{31}n & , n > 0 \\ \tau < A_{32}n & , n < 0 \end{cases}.$$

Graphically, we draw the $\tau - n$ plane in figure (2.2) showing the regions of different velocities. Since we have a smooth solution, these lines in the $\tau - n$ plane do not represent discontinuous shocks, rather there is some transition region around these lines where the solution is changing. This same type of solution is seen in Burgers equation. This merging of two shocks into one can also be seen if you directly compute the car following equation with the lead car's velocity set to the sum of two hyperbolic tangent curves which represent the three velocity states:

$$v_0(t) = \frac{v_1 + v_3}{2} - \frac{v_1 - v_2}{2}\tanh(C(t - D)) - \frac{v_2 - v_3}{2}\tanh(C(t - E))$$

and initially have all the cars moving at the speed v_1. A sequence of cars following the lead car is shown in figure (2.3). We see that the two shocks, from v_1 to v_2, and v_2 to v_3, merge into one shock, from v_1 to v_3.

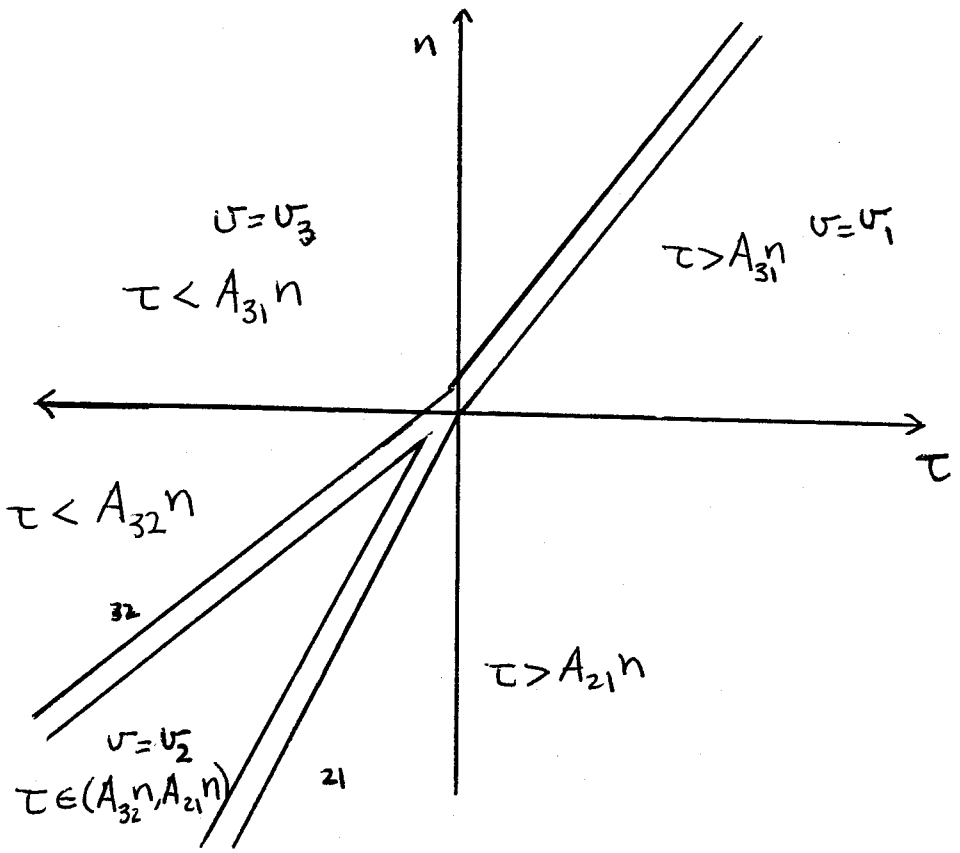

Figure 2.2: τ - n plane.

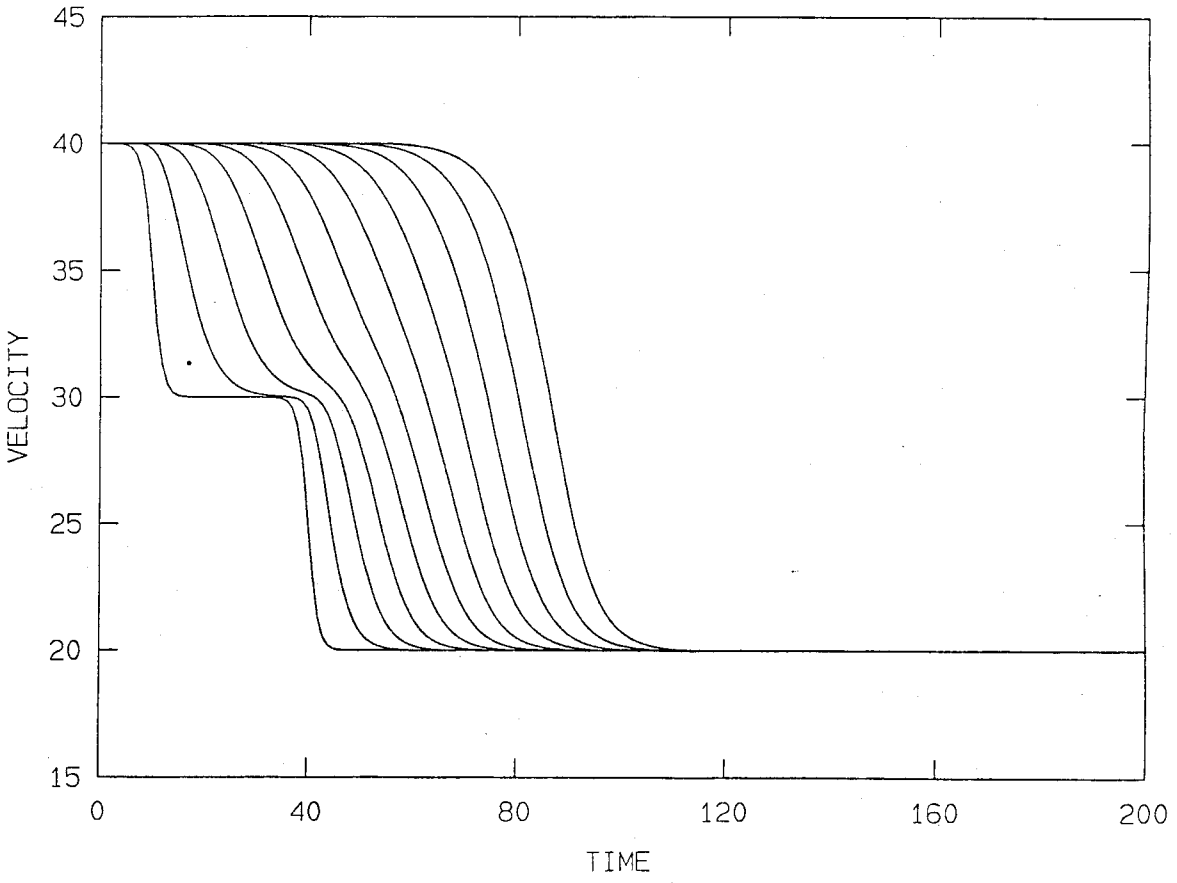

Figure 2.3: The merging of two shocks into one.

A superposition of k of these simple solutions:

$$z_n = \sum_{i=1}^{k} e^{-p_i\tau+q_in},$$

would then give for v_n,

$$v_n(\tau) = \frac{v_f}{\lambda}\{\frac{p_1e^{-p_1\tau+q_1n} + \cdots + p_ke^{-p_k\tau+q_kn}}{e^{-p_1\tau+q_1n} + \cdots + e^{-p_k\tau+q_kn}}\},$$

where $p_1 < p_2 < \cdots < p_k$. This solution has exactly the same structure as the solution to Burgers equation with x replaced by τ and t replaced by n.

2.2 Case $T \neq 0$

So far, we have only looked at the case where $T = 0$. When $T \neq 0$, we are not so fortunate as to have a transformation that makes the equation linear. In this case, the transformation that made the equation with $T = 0$ linear, yields the equation:

$$\frac{1}{\lambda}\frac{\dot{z}_n(t+T)}{z_n(t+T)} = \frac{z_{n-1}(t)}{z_n(t)} - 1$$

which is not linear. As Newell pointed out, the solution could be constructed by integrating the equations consecutively but this alone sheds little light on the characteristics of the solution. Asymptotics for small T can be used and some particular cases have been done by Newell. However, since computers are easily accessible, once we have some interesting cases to study, the solution can be obtained numerically. The important new feature with $T \neq 0$ is the possibility of instabilities which are not possible if $T = 0$.

2.2.1 Instabilities

Instabilities do arise for $T \neq 0$. To analyze them, we look at the linearized equation. We start with a car following equation of the form (2.1). There are two types of stability to look at. One is stability with respect to time, that is, whether two cars collide as $t \rightarrow \infty$. This analysis was done in a paper by Herman, Montroll, Potts, and Rothery in 1958, and is done by taking the Laplace transform of the linearized equation and analyzing the properties of the solution from the singularities of the transformed solution. To linearize the car following equation stated above about a uniform state, $v = v_0$, $h = G^{-1}(v_0) = h_0$, we set $x_n = v_0 t + y_n + x_n(0)$. Substituting this into the car following equation, expanding G about h_0 and linearizing, we have the equation:

$$\dot{y}_n(t+T) = \alpha[y_{n-1}(t) - y_n(t)],$$

where $\alpha = G'(h_0)$. Herman et al. determine that the acceleration, velocity and headway of the n^{th} car will have the following properties based on the single parameter αT.

1.) For $\alpha T > \frac{1}{2}\pi$, the motion is oscillatory with increasing amplitude.

2.) For $\alpha T = \frac{1}{2}\pi$, the motion is purely oscillatory.

3.) For $\frac{1}{e} < \alpha T < \frac{1}{2}\pi$, the motion is damped and oscillatory.

4.) For $\alpha T < \frac{1}{e}$, the motion is damped and non-oscillatory.

The second type of instability has to do with the character of the acceleration, velocity and headway as a disturbance propagates down the line of cars, i.e., if a small disturbance is created near the front of the line, we want

to know if it grows, decays or stays the same as it propagates down the line of cars. We are looking for linear instabilities now, so the possibility of finding stabilized growth (limit cycles) is ruled out at this point. To find this out, we again go to the linearized equation. We set $y_n(t) = f^n e^{i\omega t}$ and the linear equation becomes

$$e^{i\omega T} i\omega = \alpha(\frac{1}{f} - 1).$$

Solving for f, we have:

$$f = \frac{\alpha}{\alpha + i\omega e^{i\omega T}}.$$

For stability, we require that $|f| < 1$. The modulus is then:

$$|f|^2 = \frac{\alpha^2}{\alpha^2 - 2\omega\alpha \sin\omega T + \omega^2}$$

and the requirment that this to be less than 1 leads to the condition

$$2\alpha \sin\omega T < \omega.$$

If $\sin\omega T$ is negative, this is always true. If $\sin\omega T$ is positive, then we require $\alpha < \frac{\omega}{2\sin\omega T}$, the smallest value for which is $\frac{1}{2T}$. Therefore, we must have $\alpha T < \frac{1}{2}$ for stability. Notice that for αT in the range of $\frac{1}{2}$ to $\frac{1}{2}\pi$, we have a solution which is linearly stable in time but unstable in n. That is, the velocity of the n^{th} car will decay in time but the amplitude of the oscillations will grow from car to car. Also note that if $T = 0$ or is small enough, the solution will always be stable in time and in n. Since $\alpha = G'(h_0)$, it will be different for each steady state velocity v_0 and since in general, $G(h_0)$ is a decreasing function of h_0, it will be the smaller speeds which will be unstable for a fixed reaction time T.

2.2.2 Shock Velocity

We find the shock velocity independent of the model and the reaction time T. We do this here since the value is verified in the next section for the different cases studied. We assume a shock profile where to the left of the shock, all of the cars have velocity v_1 and headway h_1, and to the right, v_2 and h_2. We look at a piece of the shock profile in figure (2.4) and assume the shock moves with speed V to the left. We consider a car located a distance x_1 from the left boundary. In time δt the car moves a distance $v_1\delta t$ to the right, and the boundray, moving with the shock velocity, moves a distance $V\delta t$ to the left. For this car to enter the shaded region, we require

$$x_1 - V\delta t = v_1\delta t.$$

The number of cars in the distance x_1 is $\frac{x_1}{h_1}$, which in terms of V is $\frac{v_1+V}{h_1}\delta t$. This is the number of cars entering the shaded region. Similarly, we look at the cars in the distance x_2 and see that for them to pass out of the shaded region in time δt, we must have

$$x_2 - V\delta t = v_2\delta t$$

and the number of cars which pass out of the shaded region is $\frac{x_2}{h_2} = \frac{v_2+V}{h_2}\delta t$. The number of cars entering must equal the number of cars leaving and thus, we have the relation

$$V = \frac{v_1h_2 - v_2h_1}{h_1 - h_2}.$$

The velocity relative to the cars in state 1 is

$$v_1 + V = h_1\frac{v_1 - v_2}{h_1 - h_2}.$$

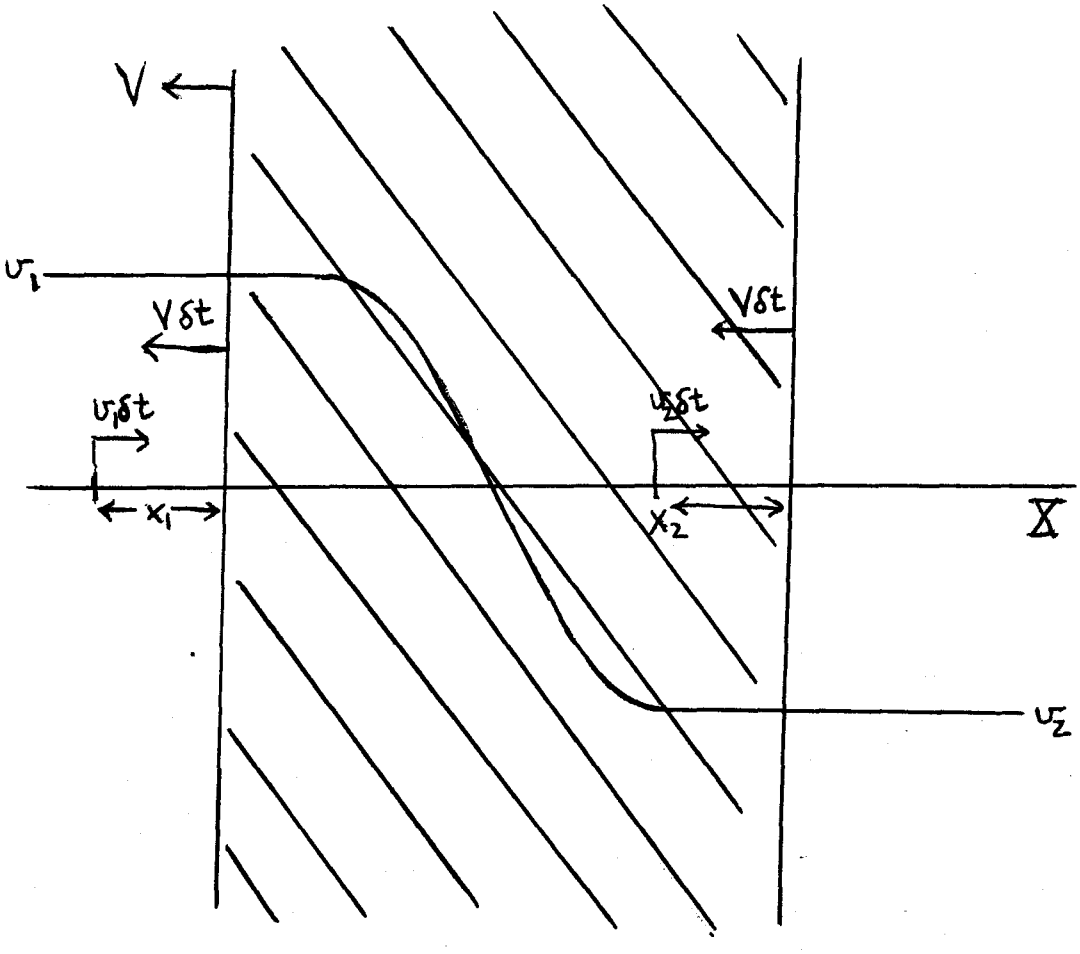

Figure 2.4: A piece of the shock profile.

This has velocity dimensions and we would like to have the shock speed in terms of number of cars per second. This is $\frac{v_1+V}{h_1} = U$ and we have

$$U = \frac{v_1 - v_2}{h_1 - h_2}. \tag{2.3}$$

This checks with the shock solution obtained in section 2.1.1. We also check this relation in the numerical calculations.

2.2.3 Numerical Studies

Because the introduction of non-zero T indicates that instabilities can occur, we investigate what happens to the solution with T now included. We carry out numerical studies for $T \neq 0$ for Newell's model:

$$v_n(t+T) = v_f(1 - e^{-\frac{\lambda}{v_f}(h_n - L)}).$$

Because of the time lag T, v_n must initially be given for a range of t: $t \in (-T, 0)$. We chose to let $v_n = v_0$ for $t \in (-T, 0)$ and then let the lead car produce some disturbance after $t = 0$ and watch how this disturbance propagates down the line of cars. Since x_{n-1} and x_n are known T seconds earlier, $v_n(t+T)$ can be computed immediately. We therefore march forward in time evaluating $v_n(t)$ at each step based on the values of x_{n-1} and x_n at time $t - T$. To make this easier, we choose Δt such that T is an integer multiple of it, $T = m\Delta t$. To obtain the values of x_n at t, we add to the previous value of x_n, Δt times the average of the current and previous velocities, i.e.,

$$x_n(t) = x_n(t - \Delta t) + \frac{\Delta t}{2}[v_n(t) + v_n(t - \Delta t)].$$

The disturbance that we study is that the lead car, initially at velocity v_1, slows down smoothly to a speed $v_2 < v_1$. We do this for various values of

$\alpha_2 T$ by keeping α_2 fixed, which corresponds to v_2 fixed, and varying T. α_2 is the value of α evaluated at $v_0 = v_2$. We also keep α_1 fixed with $\alpha_1 < \alpha_2$ and our choice of T keeps $\alpha_1 T < 1/2$.

We first see what happens when T is zero. The solution we obtain should mimic the asymptotic result obtained by Newell. Since we know the solution for T equal to zero, this case provides a check on the numerical procedure as well. Giving the lead car the actual shock solution profile gave each car down the line that same profile. This is expected since it is an exact solution. We give the lead car a velocity profile in the form of a hyperbolic tangent with the width and center adjustable. When the velocity profile of the lead car is very steep, we see that the successive velocity profiles spread out down the line of cars (the velocity profile of the 50^{th} car was steeper than that of the 100^{th}). The velocity profile of car number 100 was almost identical to the asymptotic shock solution but was slightly steeper.

We then increase T from 0, using the shock solution for $T = 0$ as the lead car's velocity. As $\alpha_2 T$ increases, the velocity profile steepens and the shock width narrows. The solution appears to be steady — car numbers 50 and 100 have almost the same profile. Figure (2.5) shows car numbers 50 and 100 for $\alpha_2 T$ equal to .1, .2, .3 and .4.

When $\alpha_2 T$ reaches 1/2, we see oscillations about the final velocity which die out in time (see figures (2.6) and (2.7)). We continue to increase $\alpha_2 T$ slowly. Figures (2.6) and (2.7) show that although the amplitude of the oscillation grows initially, the solution stabilizes and in fact looks to be a steady profile solution. Each car down the line repeats the same velocity

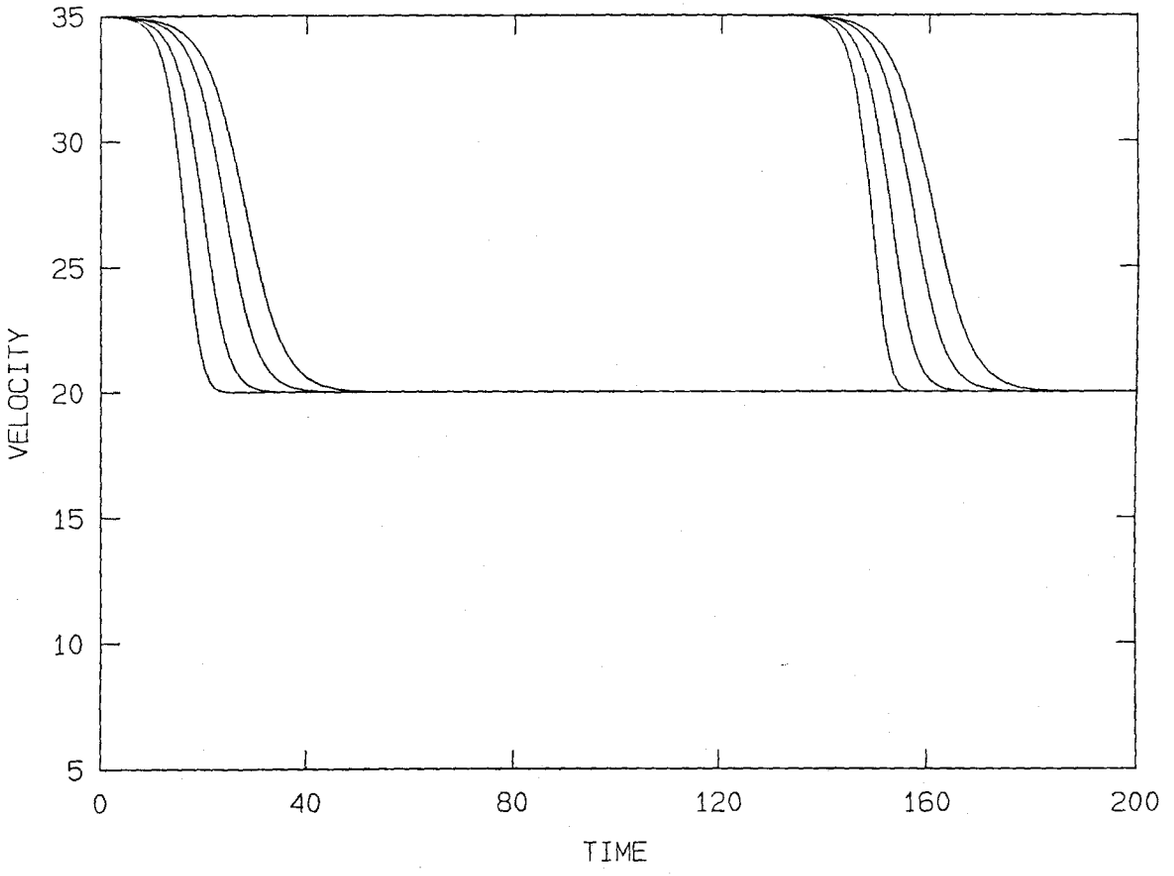

Figure 2.5: Velocity profiles of car numbers 50 and 100 for values of $\alpha_2 T < 1/2$. The steepest profile corresponds to $\alpha_2 T = .4$.

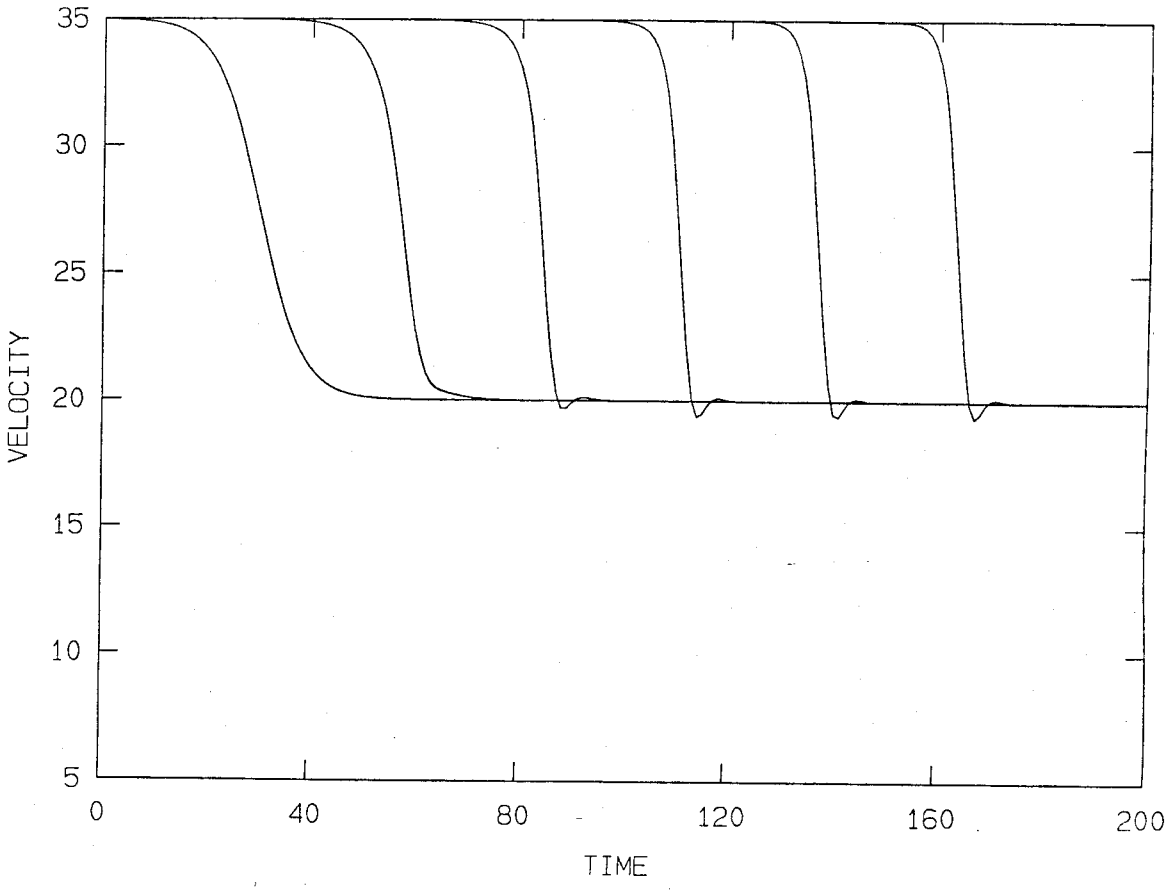

Figure 2.6: $\alpha_2 T = .5$, $T = 1.0$, cars 0 through 50.

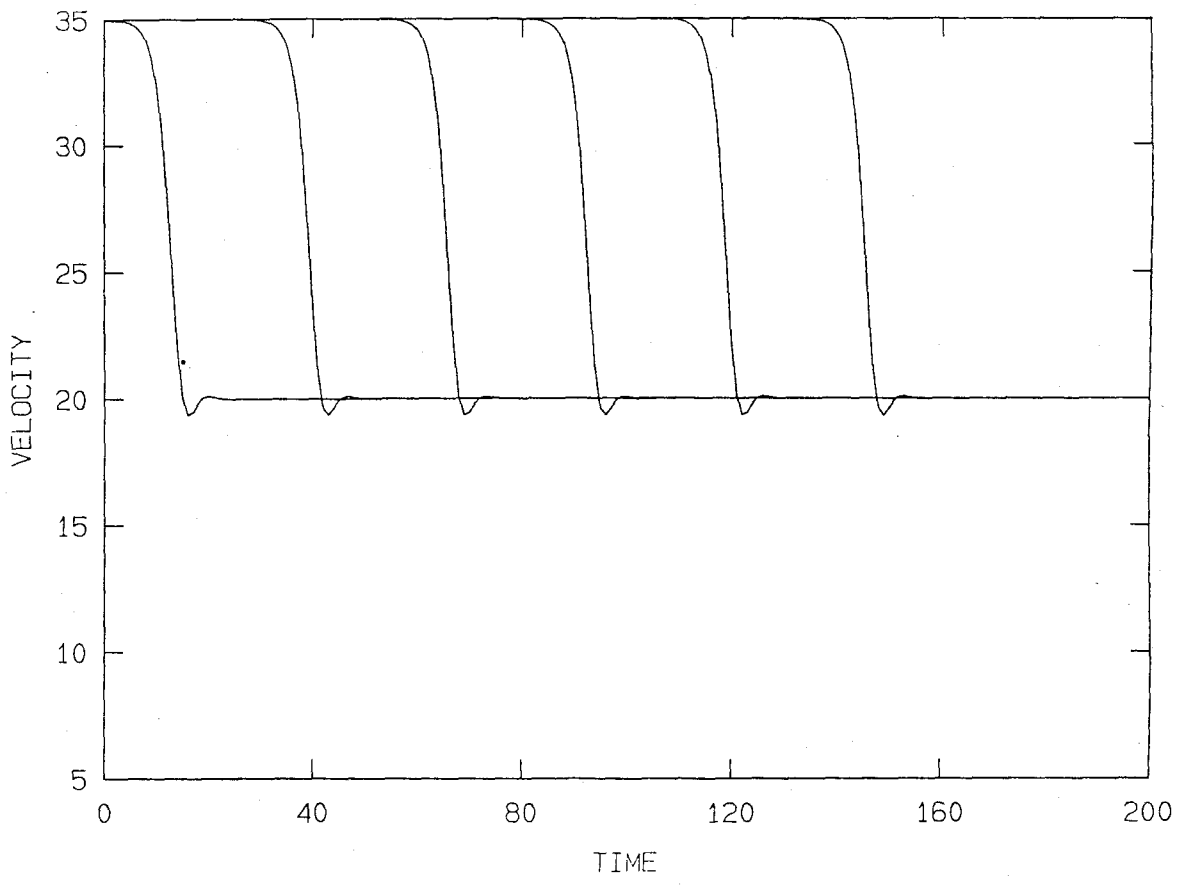

Figure 2.7: $\alpha_2 T = .5$, $T = 1.0$, cars 50 through 100

profile as the car in front of it at a time $\frac{1}{U}$ later. We see this steady profile solution for $\alpha_2 T < .56$ (figures (2.8) and (2.9)). We also see that as $\alpha_2 T$ increases, the amplitude of the oscillation increases.

When $\alpha_2 T = .56$, we no longer see steady profile solutions. The amplitude no longer stabilizes, but oscillates in n, see figures (2.10) through (2.15).

We call the amplitude of any one profile the amplitude of the largest oscillation. So far, the largest oscillation has been the first oscillation. For $\alpha_2 T = .56$, we see that the amplitude of the first oscillation decreases at times giving the other oscillations more weight. Figures (2.10) - (2.15) show clearly that the solution is no longer a steady profile solution. We run this case for many more cars and see that this shifting of weight of the oscillations continues until some of the cars have profiles in which the second oscillation is the dominant one rather than the first. We also see here that the amplitude is becoming quite large in comparison to the cases for $\alpha_2 T < .56$.

For greater values of $\alpha_2 T$, we see this eventual growth in the amplitude sooner and thus, we see a crash sooner. When the headway gets below a certain value, we call this a crash and the program is stopped. Figures (2.16) - (2.19) illustrate this growing solution for $\alpha_2 T = .57$.

We see that when $\alpha_2 T$ is not too large, there is growth in n but it is either bounded or the growth is so slow that it cannot be noticed. Eventually, for $\alpha_2 T$ too large, the oscillation continues to grow and becomes large enough to cause a crash. We note that the stability analysis for large time implies that we should see oscillatory solutions which decay in time and we do see this. Perhaps this is why we mainly see the first oscillation grow in n - the

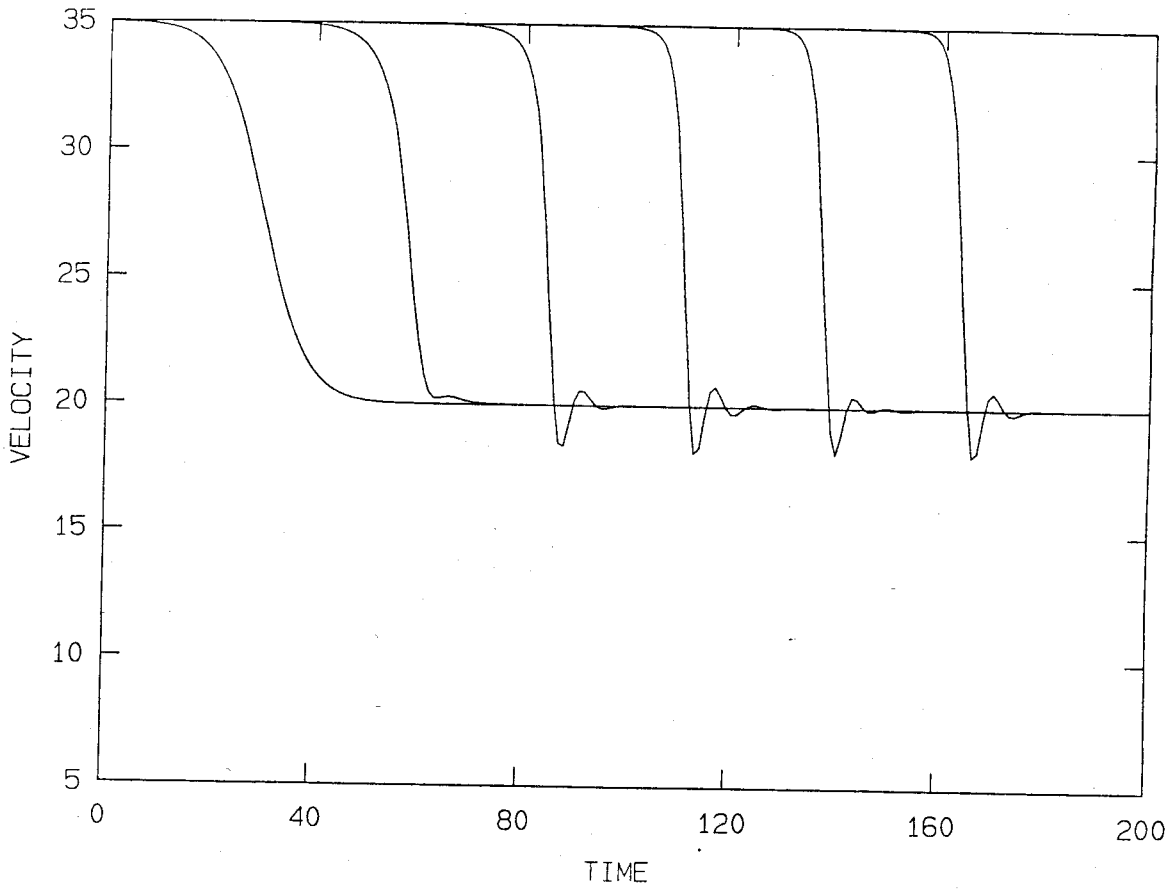

Figure 2.8: $\alpha_2 T = .55$, $T = 1.1$, cars 0 through 50.

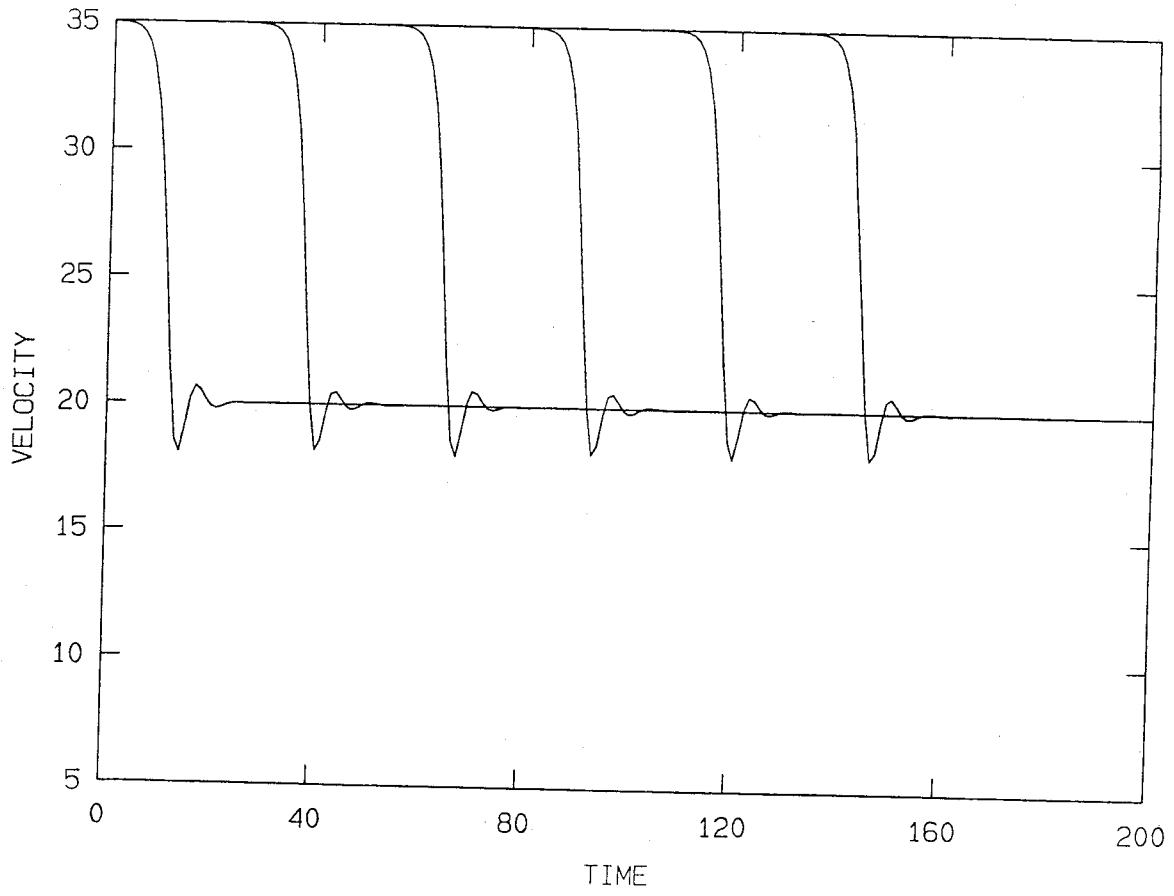

Figure 2.9: $\alpha_2 T = .55$, $T = 1.1$, cars 50 through 100.

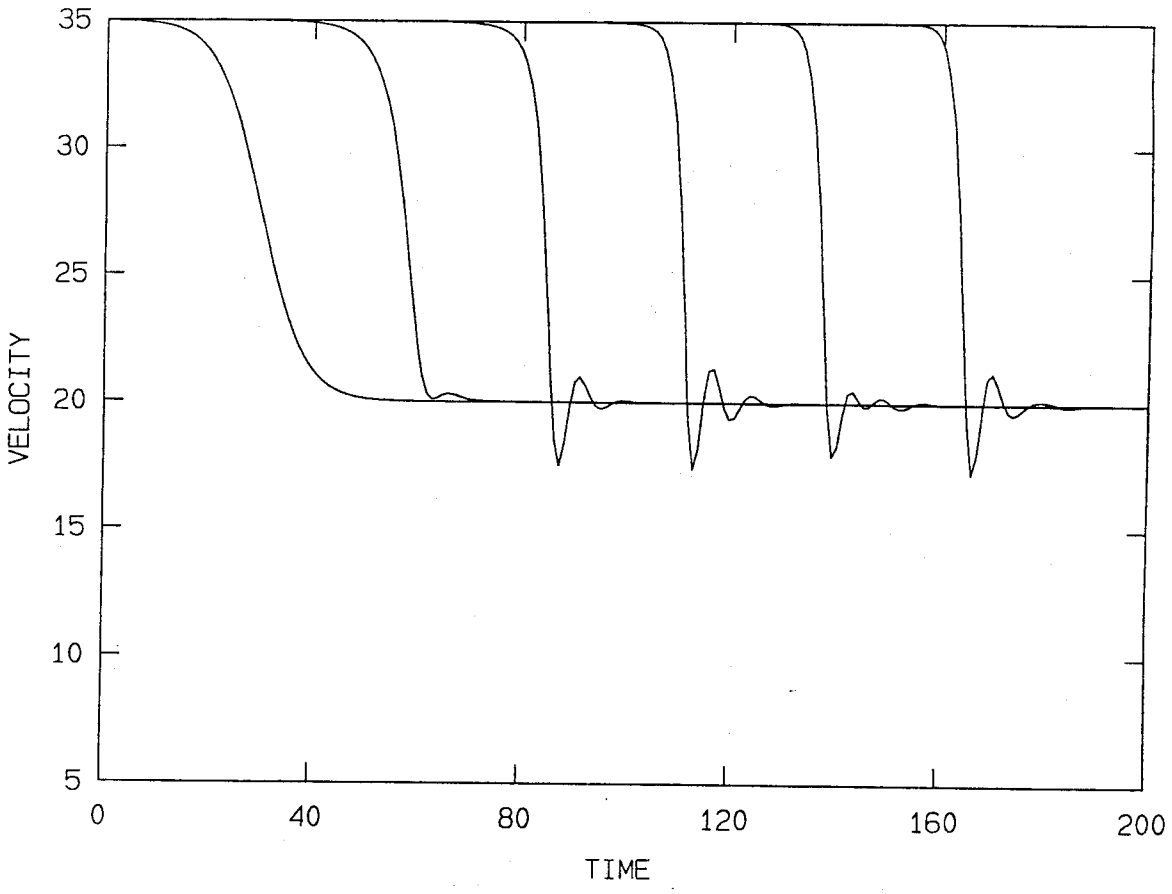

Figure 2.10: $\alpha_2 T = .56$, $T = 1.13$, cars 0 through 50.

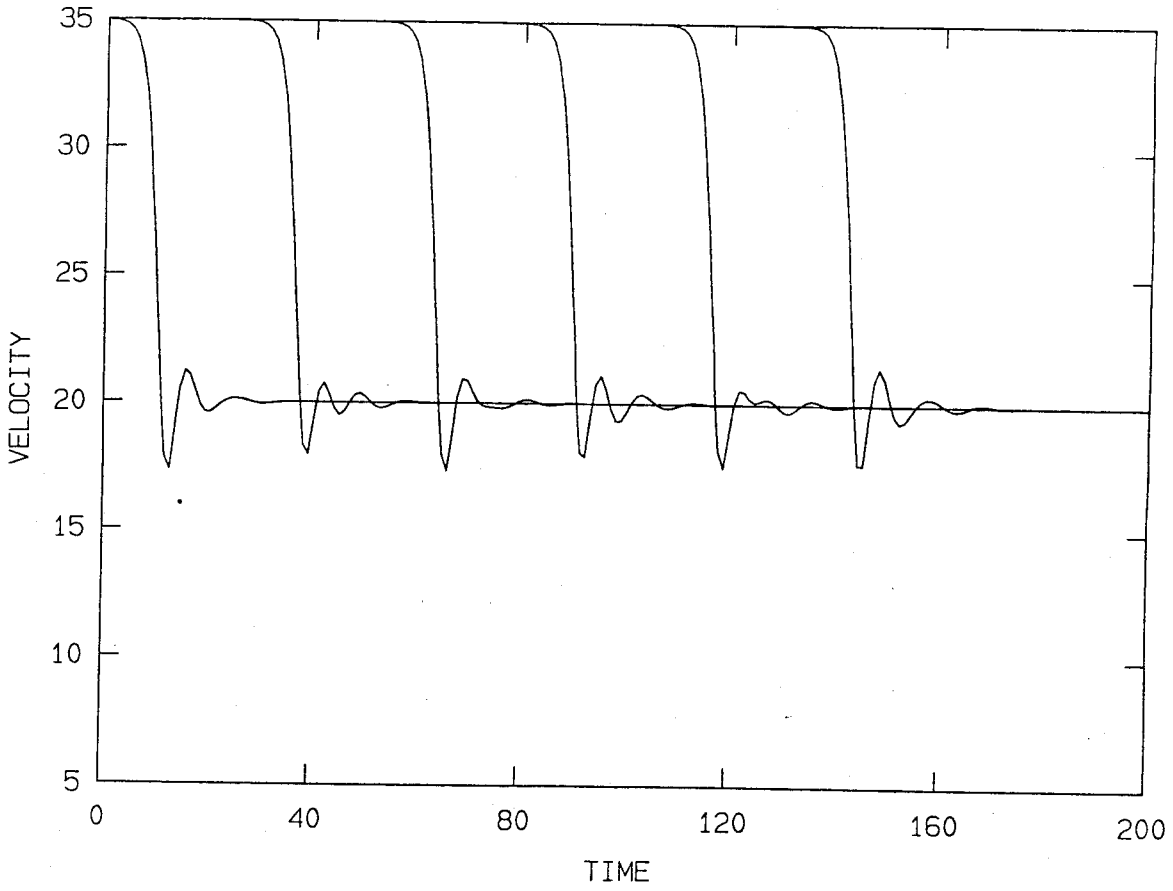

Figure 2.11: $\alpha_2 T = .56$, $T = 1.13$, cars 50 through 100.

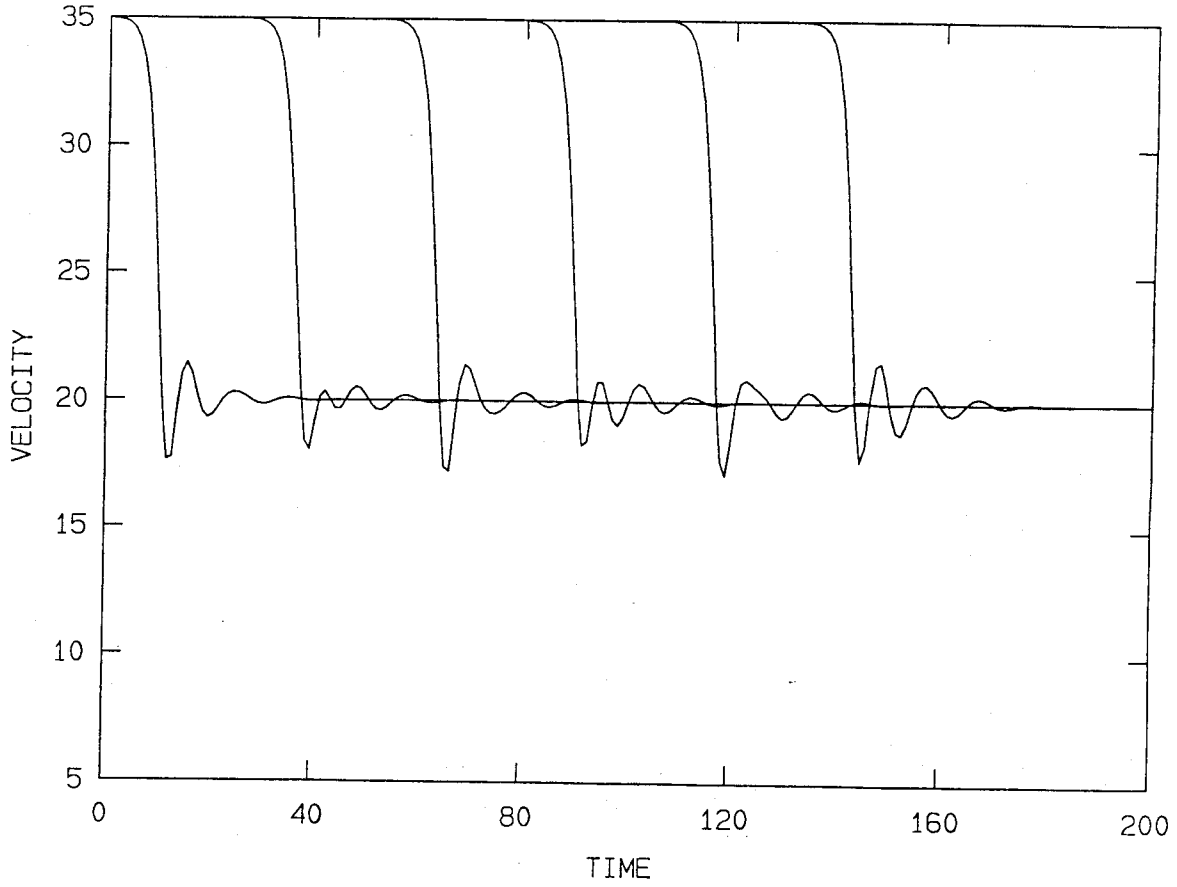

Figure 2.12: $\alpha_2 T = .56$, $T = 1.13$, cars 100 through 150.

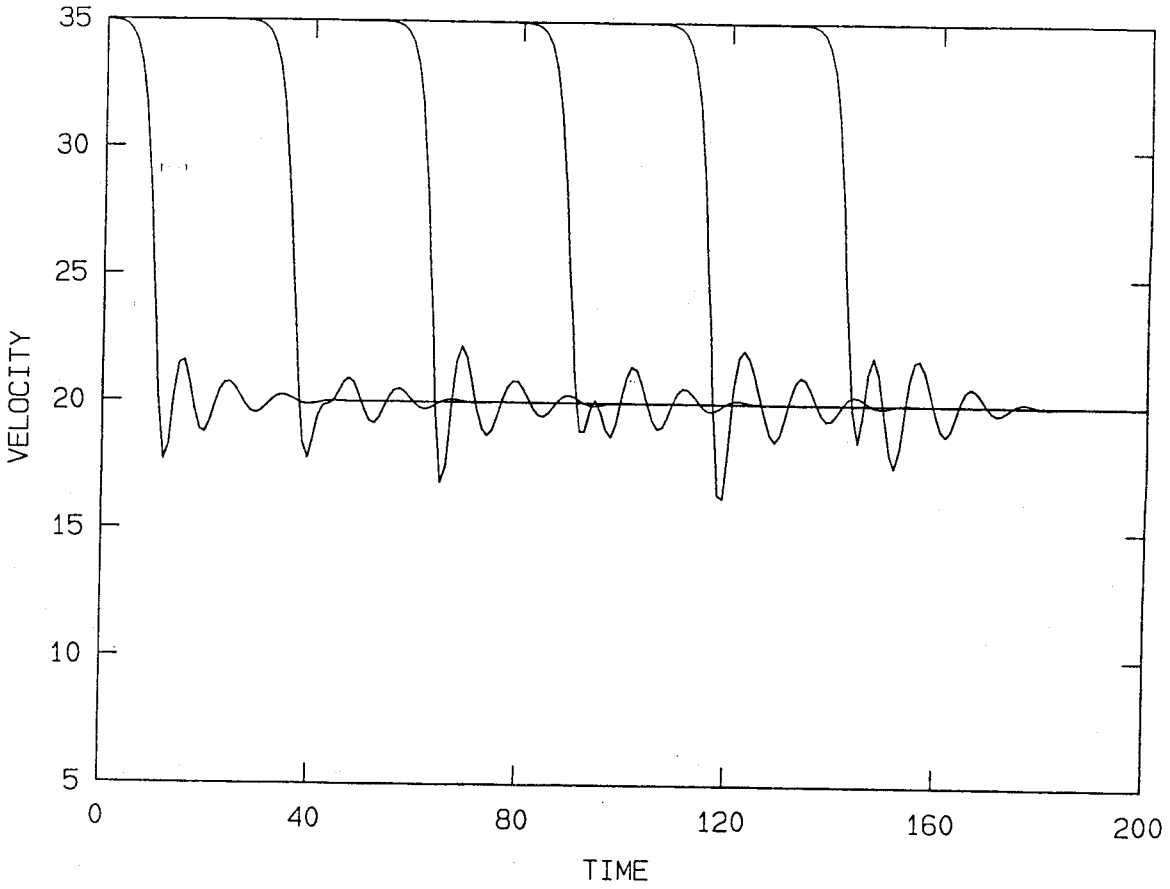

Figure 2.13: $\alpha_2 T = .56$, $T = 1.13$, cars 150 through 200.

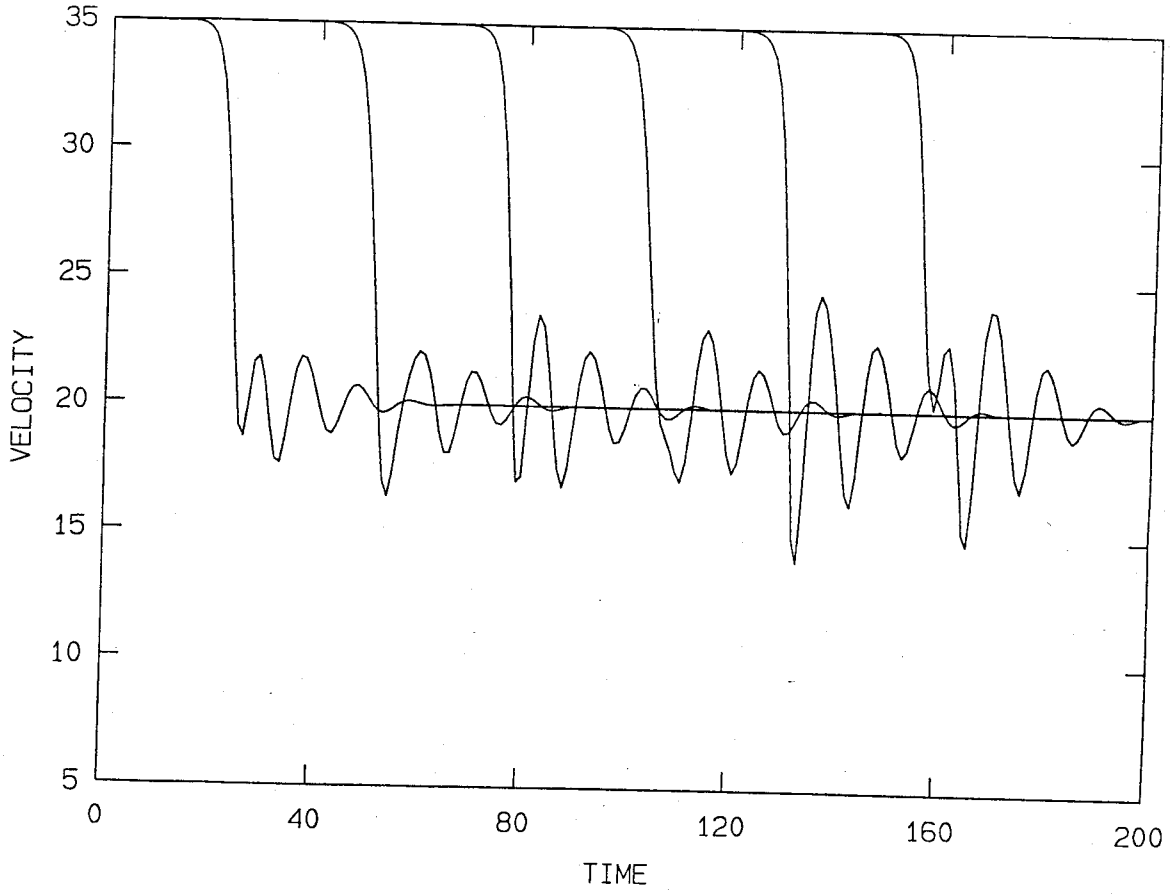

Figure 2.14: $\alpha_2 T = .56$, $T = 1.13$, cars 200 through 250.

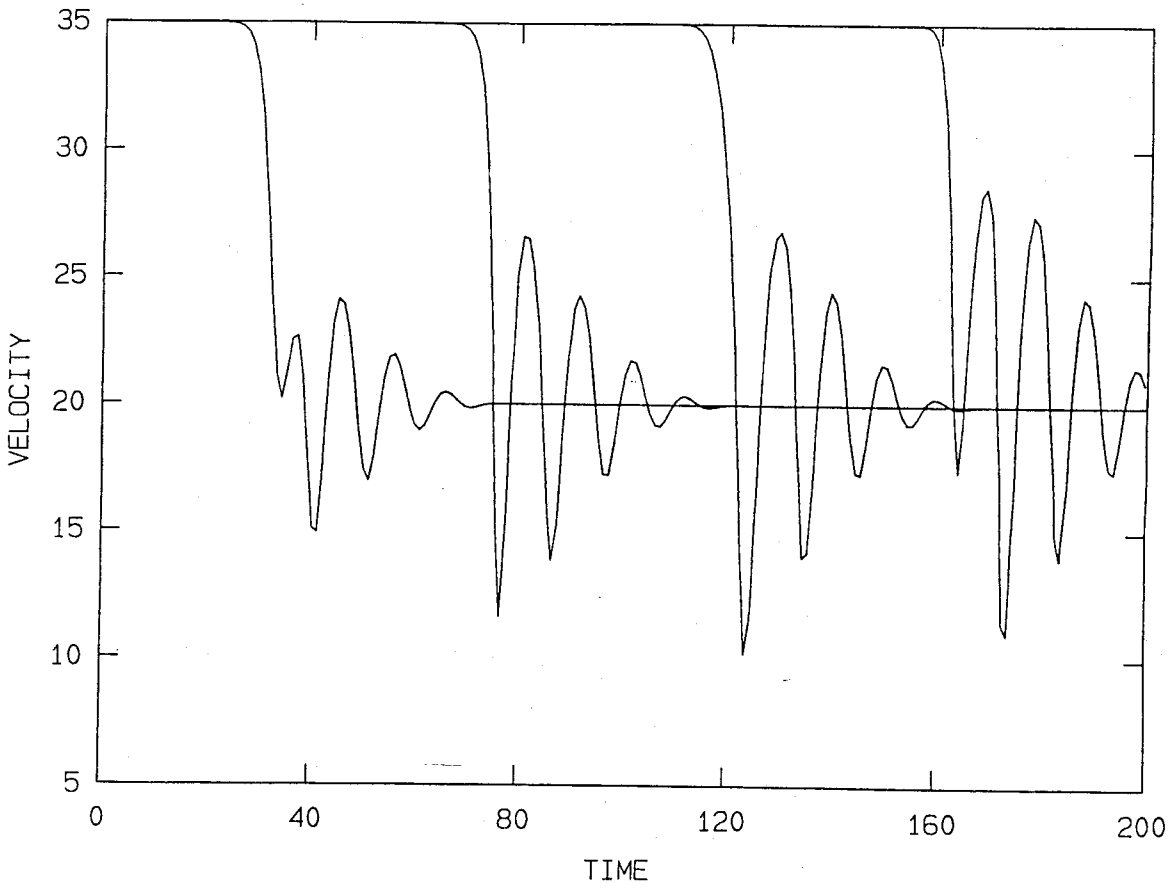

Figure 2.15: $\alpha_2 T = .56$, $T = 1.13$, cars 250 through 300.

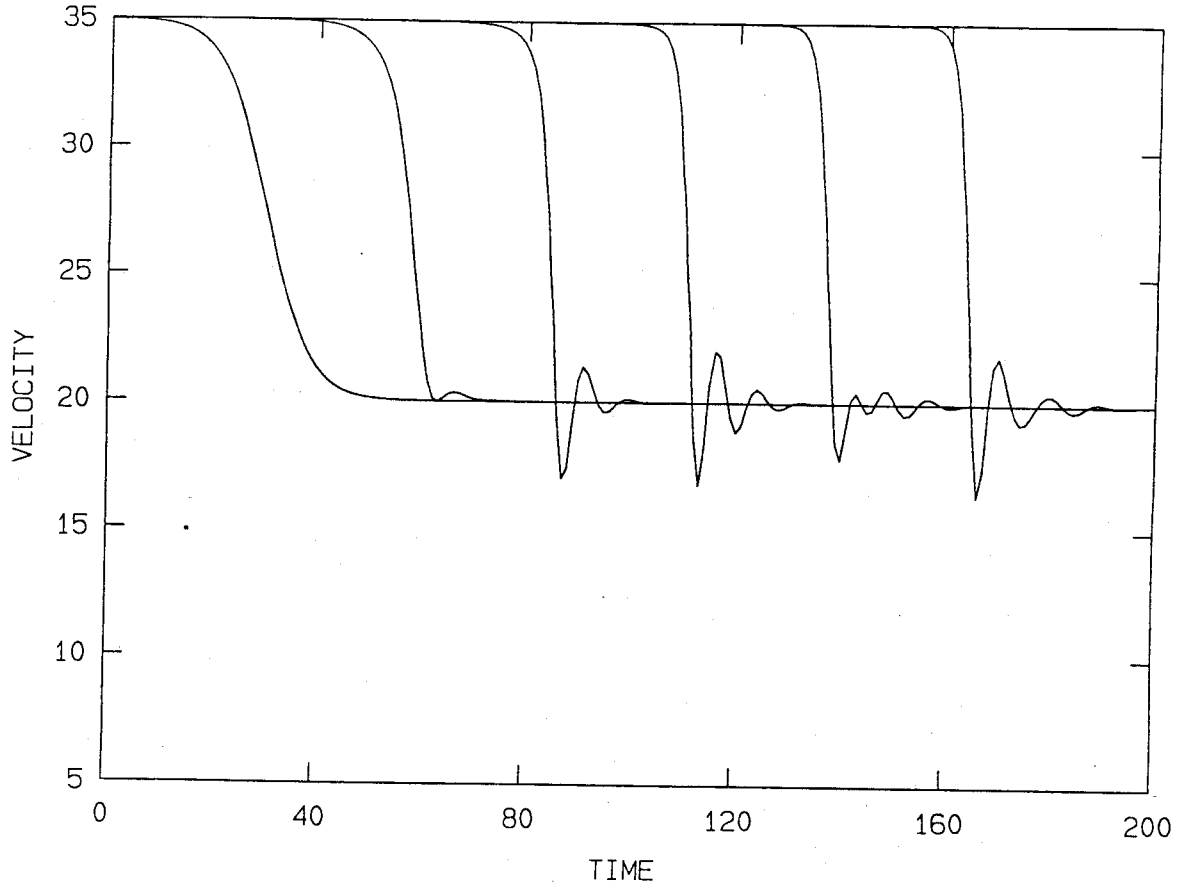

Figure 2.16: $\alpha_2 T = .57$, $T = 1.15$, cars 0 through 50.

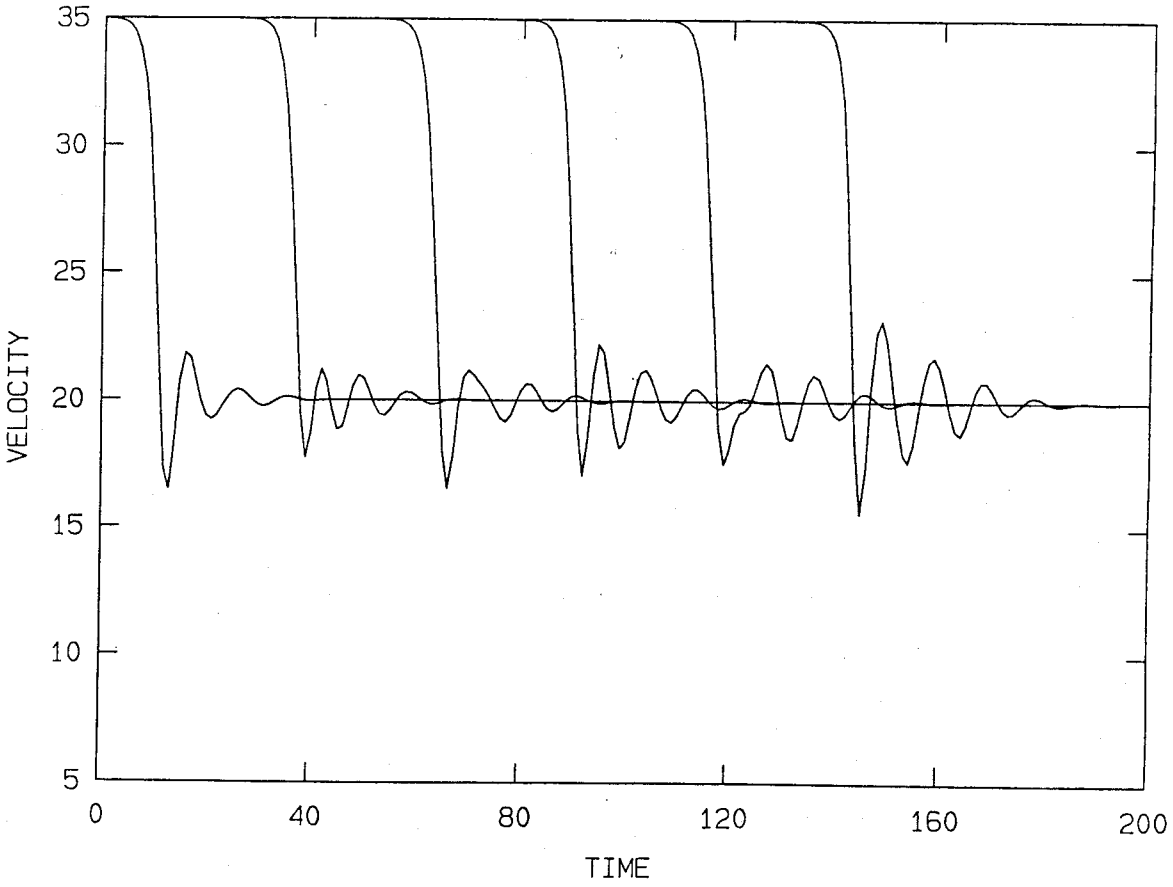

Figure 2.17: $\alpha_2 T = .57$, $T = 1.15$, cars 50 through 100.

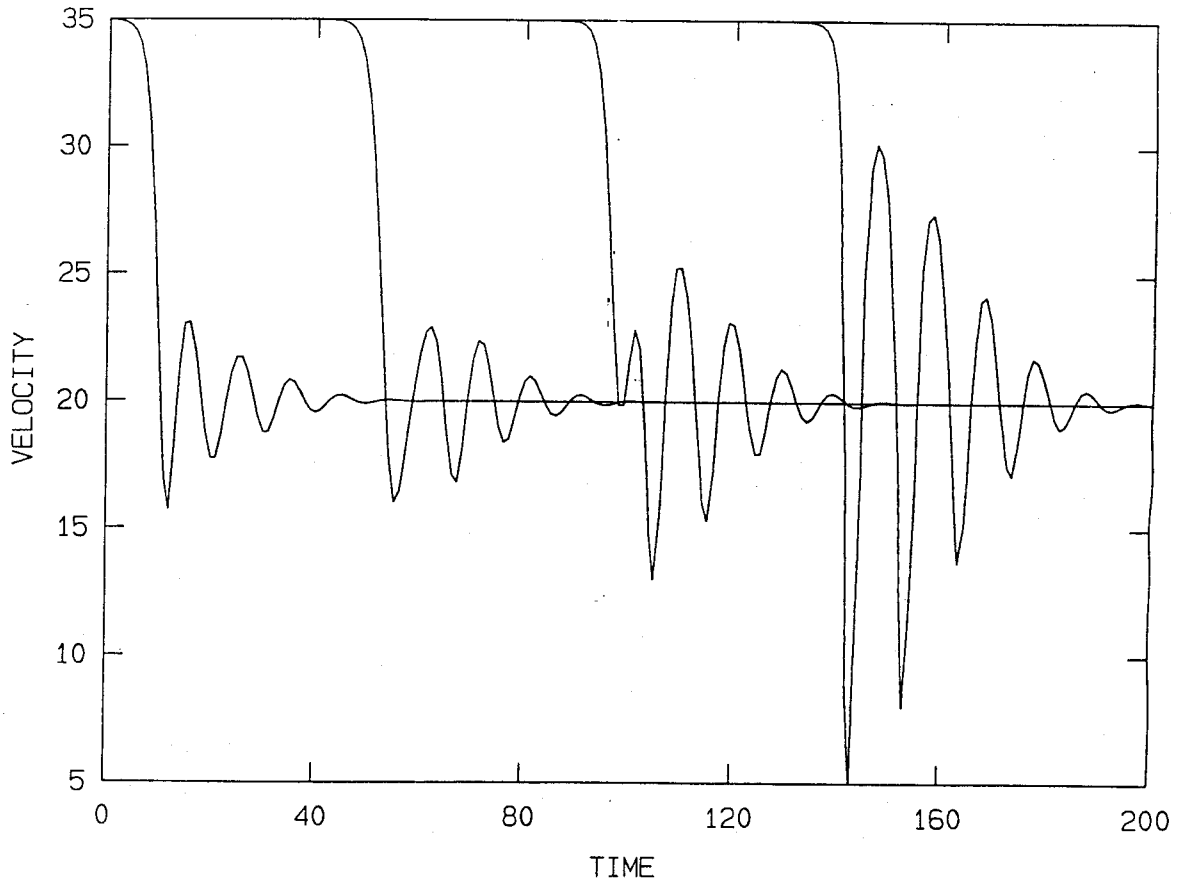

Figure 2.18: $\alpha_2 T = .57$, $T = 1.15$, cars 100 through 150.

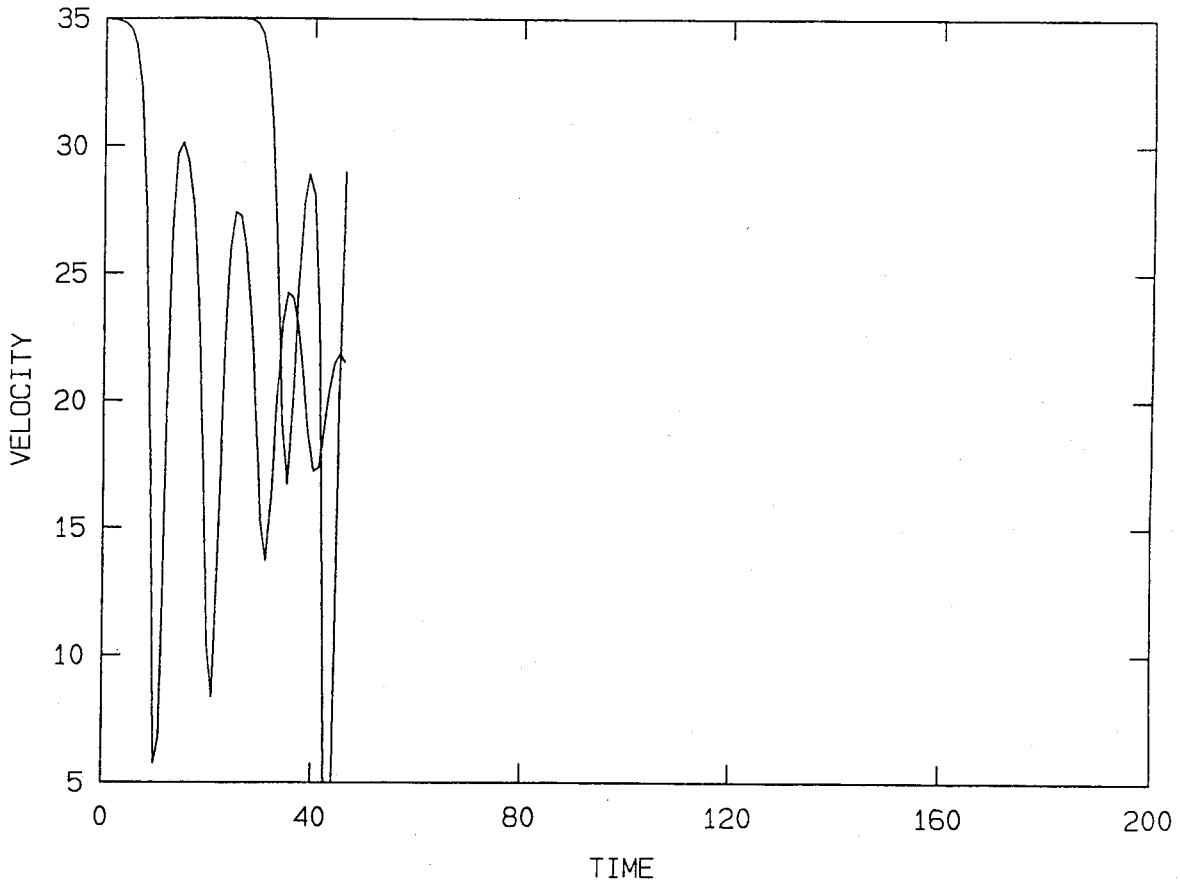

Figure 2.19: $\alpha_2 T = .57$, $T = 1.15$, cars 150 and 160.

growth in n must overcome the decay in time for the secondary oscillations to grow as n increases. We also check the shock speed U. This is checked from the distance between consecutive velocity profiles. This distance should be $\frac{1}{U}$ and we find that it fits the theory quite well.

Since we appear to have found traveling wave solutions, we look at the traveling wave problem to assess the types of solutions that are possible. We change variables to look at variations about a uniform state, v_0, h_0, by $x_n(t) = v_0 t - nh_0 + y_n(t)$ and look for traveling wave solutions by setting $\xi = Ut - n$, $g(\xi) = y_n(t)$ in equation (2.1) to obtain the equation:

$$v_0 + Ug'(\xi + UT) = G(g(\xi + 1) - g(\xi) + h_0).$$

We linearize the equation and normalize U and T by $\alpha = G'(h_0)$, $\frac{U}{\alpha} = W$ and $\alpha T = \tau$, to obtain

$$Wg'(\xi + W\tau) = g(\xi + 1) - g(\xi).$$

We look for solutions of the form $g(\xi) = e^{\lambda\xi}$ and find that λ must satisfy

$$W\lambda e^{\lambda W\tau} = e^{\lambda} - 1. \tag{2.4}$$

We let $f(\lambda) = W\lambda e^{\lambda W\tau}$ and $h(\lambda) = e^{\lambda} - 1$ and sketch the two sides of equation (2.4) in figure (2.20). Since the slope of f at the origin is W, the type of intersection we will have depends on whether W is less than or greater than one. We know that $U = \frac{v_2 - v_1}{h_2 - h_1}$ from section 2.2.2. Therefore, for the velocities we have chosen, we have that $W = \frac{U}{\alpha} = .7581$ which is less than one.

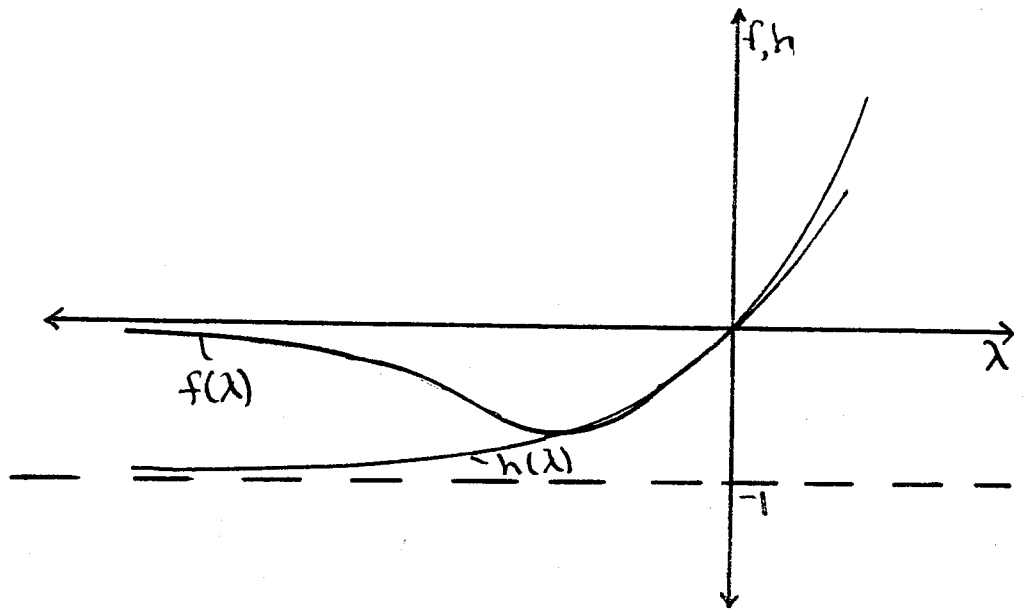

Figure 2.20: Sketch of the two sides of $W\lambda e^{\lambda W\tau} = e^{\lambda} - 1$ as functions of λ for $W < 1$.

For $W < 1$, we have three types of intersections. For the first type, we have two real roots, both negative. This corresponds to an exponentially decaying solutions for ξ increasing in the positive direction. The second type is no intersection at all, or purely complex roots. This corresponds to oscillatory solutions which decay or grow in ξ. The last possibility is that of a double root for λ negative. Given a value for W, we can find the value of $\tau = \tau^*$ such that we have a double root. For $\tau < \tau^*$, we have decaying solutions with no oscillations. For $\tau > \tau^*$, we have oscillatory solutions which either decay or grow. The numerical results indicate a solution which decays as t increases and hence, as ξ increases in the positive direction. Since the two real solutions are negative, our numerical results suggest that these correspond to small values of τ, $\tau < \tau^*$. Thus, for $\tau > \tau^*$, we expect that

there are complex solutions with negative real part which corresponds to the numerical results of decaying oscillations discussed earlier.

We proceed now to find the value of τ^* for which equation (2.4) has a double root. For a double root, we have that equation (2.4) and its derivative are satisfied. This leads to the pair of equations:

$$W\tau = \frac{1}{1-e^{-\lambda}} - \frac{1}{\lambda} \tag{2.5}$$

$$W\lambda e^{\lambda W\tau} = e^{\lambda} - 1. \tag{2.6}$$

Substituting the value of $W\tau$ from equation (2.5) into equation (2.6), leaves an equation in terms of λ alone:

$$We^{-1}\lambda e^{\frac{\lambda}{1-e^{-\lambda}}} = e^{\lambda} - 1.$$

We solve this for λ by Newton's Method and find $\lambda = -2.82$ and by substituting this into equation (2.5), we find $\tau^* = .38$. We see in figure (2.5), that for $\tau = .4$, there are no oscillations, but, for $\tau = .5$, in figure (2.6), we do have oscillations. Therefore, visible oscillations start for τ between .4 and .5. This theory we have presented suggests that oscillations begin for $\tau > .38$ and this is approximately what we see.

Chapter 3

A Revised Model

In chapter 2, we modeled the reaction time discretely. This implies that the driver waits exactly T seconds after some change in headway occurs before he/she adjusts the velocity. It seems plausible to consider a continuous reaction time. This leads to a model in which $v_n(t+T)$ is replaced by $v_n(t) + T\dot{v}_n(t)$. This is also the first two terms of the Taylor expansion of $v_n(t+T)$ for small T. This method of modeling reaction times is used in other contexts as well. As one example, the relaxation time in polymers is modeled this way. To illustrate how this models the reaction time continuously, we look at the equation

$$v_n(t) + T\dot{v}_n(t) = k.$$

The solution is

$$v_n(t) = k(1 - e^{-\frac{1}{T}t}) + Ae^{-\frac{1}{T}t},$$

where $v(0) = A$ and $v(\infty) = k$. The parameter T here gives the time that it takes for the velocity to be within, say $1/10$ of k and hence gives the reaction time continuously. Noting this and the slim range of αT for which we found

stable solutions to the car following equation in Chapter 2, we came to the view that the revised model:

$$v_n(t) + T\dot{v}_n(t) = G(x_{n-1} - x_n),$$

where G is the same as in the previous chapter, was a reasonable model to consider. We expect there to be similarities in the solution to this equation and in that of Chapter 2 since for T small, $v_n(t+T)$ is close to $v_n(t)+T\dot{v}_n(t)$.

3.1 Stability

Using this modified equation where

$$G(h) = v_f(1 - e^{-\frac{\lambda}{v_f}(h-L)}),$$

we find that the stability analysis for large n gives the same constraint that we obtained in Chapter 2. We let $x_n = v_0 t + y_n + x_n(0)$ as before. We then let $y_n(t) = e^{i\omega t} f^n$ and substitute this into the linearized equation:

$$\dot{y}_n(t) + T\ddot{y}_n(t) = \alpha[y_{n-1}(t) - y_n(t)]$$

to obtain

$$i\omega - T\omega^2 = \alpha(\frac{1}{f} - 1).$$

Solving for f, we have

$$f = \frac{\alpha}{\alpha + i\omega - T\omega^2}.$$

For stability, we require $|f| < 1$. This leads to the constraint

$$2\alpha T < 1 + T^2\omega^2$$

which, to be true for all ω requires that $\alpha T < 1/2$. When $\alpha T > 1/2$, there will be a range of ω where the solution will be unstable. This is so for $\omega \in (0, \omega^*)$, where

$$\omega^{*2} = \frac{2\alpha T - 1}{T^2}.$$

This says that long waves will be unstable.

3.2 Numerical Studies for Shock Waves

We compute the solution to the full nonlinear equation with the same initial conditions, velocities and motion of the lead car as in Chapter 2 and find very similar results. A difference in the computational method arises because we now have a second order differential equation. We integrate this with a Runga-Kutta method and only need the velocity and position at $t = 0$ to get started.

We first look at the case where $\alpha_2 T$ is less than $1/2$. For $\alpha_2 T = .1$, we see that the solution is almost identical to the solution in Chapter 2 for the same value of $\alpha_2 T$. As $\alpha_2 T$ increases, we see that the solutions of this chapter are consistently not as steep as the solutions of Chapter 2 and we see steady profile solutions here as well. Another feature that we notice is that for $\alpha_2 T = .4$, the solution has already begun to oscillate. This was not so in Chapter 2. If we repeat the analysis of section 2.2.3 — look for traveling waves, linearize the equation and look for solutions of the form $e^{\lambda \xi}$ — we find that the equation λ must satisfy is:

$$W\lambda + W^2 \tau \lambda^2 = e^{\lambda} - 1.$$

We find that the double zero occurs for $\lambda = -1.82$ and $\tau = .28$. We see oscillations for $\tau = .4$ and thus visible oscillations begin for τ between .3 and .4 and the theory appears to be consistent with our numerical findings. The cases for $\alpha_2 T < 1/2$ are plotted in figure (3.1) for $\alpha_2 T$ equal to .1, .2, .3 and .4.

We see here that, as in Chapter 2, the solution initially grows in n but stabilizes rather quickly. Figures (3.2) - (3.6) show several cases where the solution settles to a steady profile, as it did in Chapter 2. Analogously, we find that when $\alpha_2 T$ is too large, the solutions do not settle to a steady profile solution. At $\alpha_2 T = .61$, figures (3.7) - (3.10) clearly show that the profiles are not the same. The value of $\alpha_2 T$ which is too large to obtain steady profile solutions, $\alpha_2 T = .61$, is a higher value than in Chapter 2 and correspondingly, we find steady profile solutions with larger amplitudes than those of Chapter 2. We also see in figures (3.11) - (3.12), where $\alpha_2 T = .65$ that the amplitude grows quite quickly and the solution does eventually crash (this is not shown) just as in Chapter 2. We see that although the amplitude is growing in n, the velocity profiles also oscillate in n and allow for different peaks to take on the maximum value. Again, we check the shock speed U and find that it agrees with equation (2.3). One benefit of this version is that the cars do not crash as readily as in the model with discrete T.

3.3 Periodic Solution

We now investigate whether there exists a smooth periodic solution to the car following model of this chapter similar to the one constructed with shocks

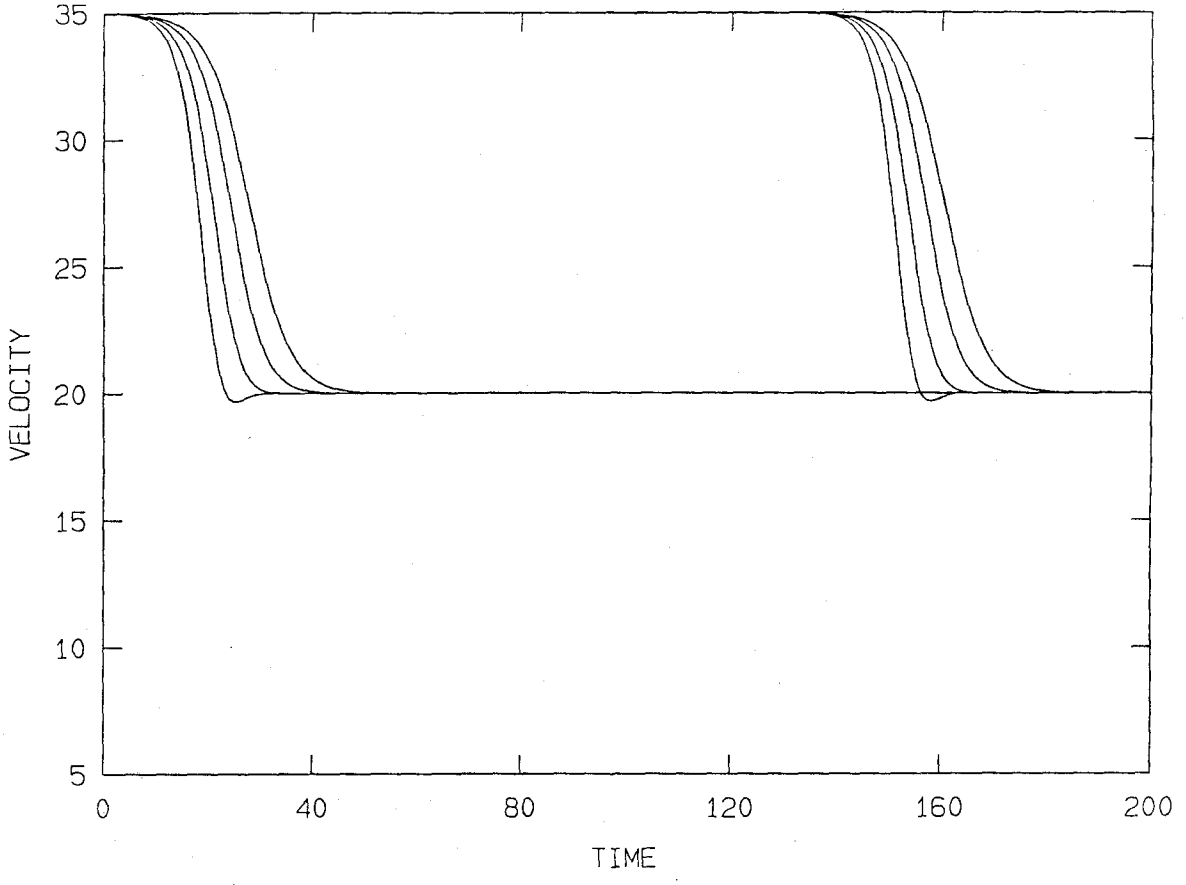

Figure 3.1: $\alpha_2 T < 1/2$

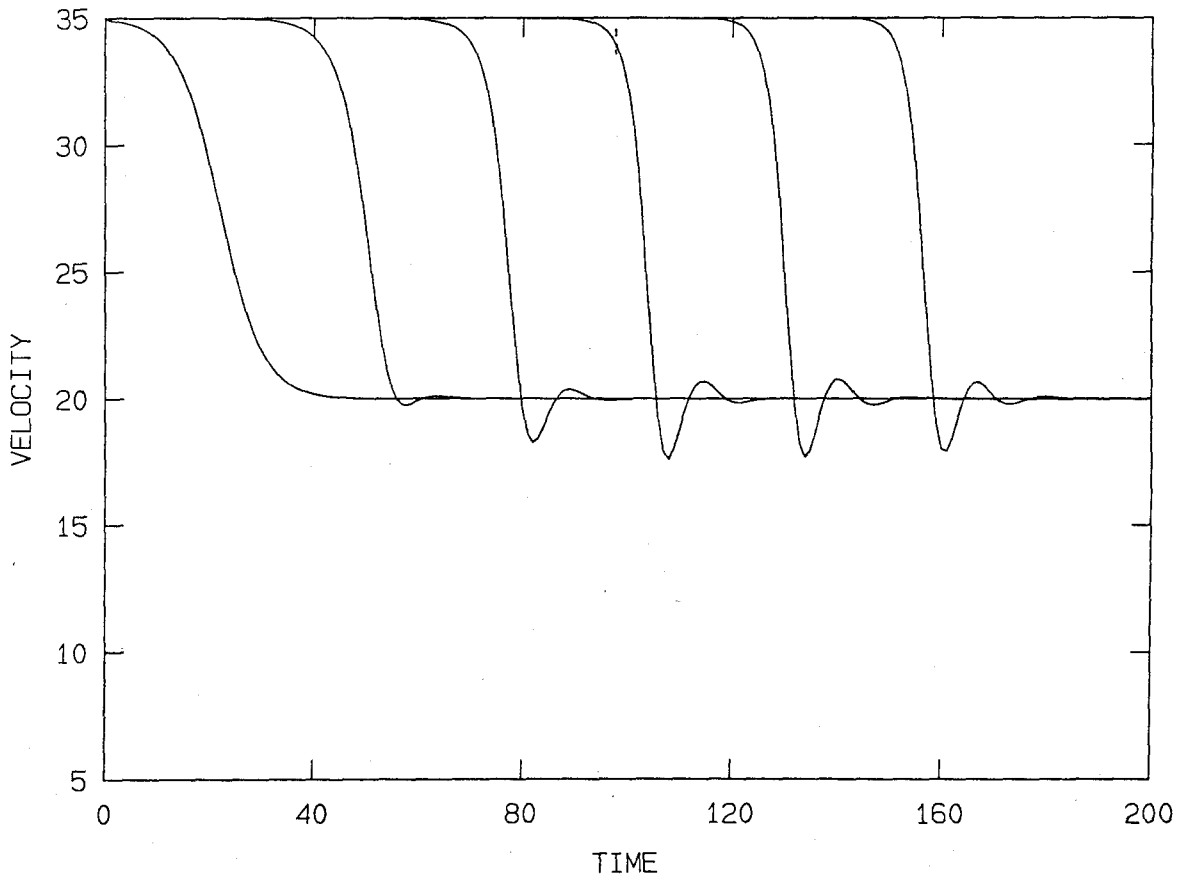

Figure 3.2: $\alpha_2 T = .53$, $T = 1.07$, cars 0 through 50.

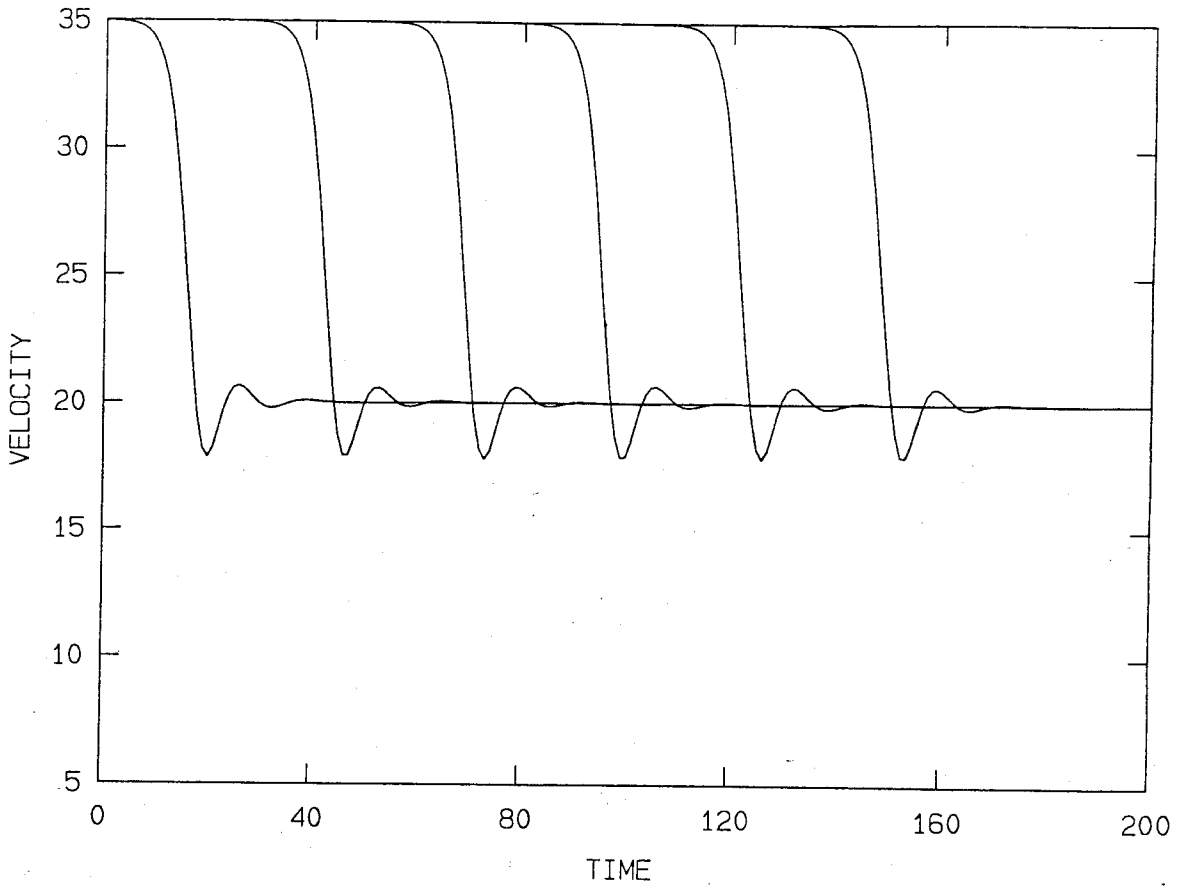

Figure 3.3: $\alpha_2 T = .53$, $T = 1.07$, cars 50 through 100.

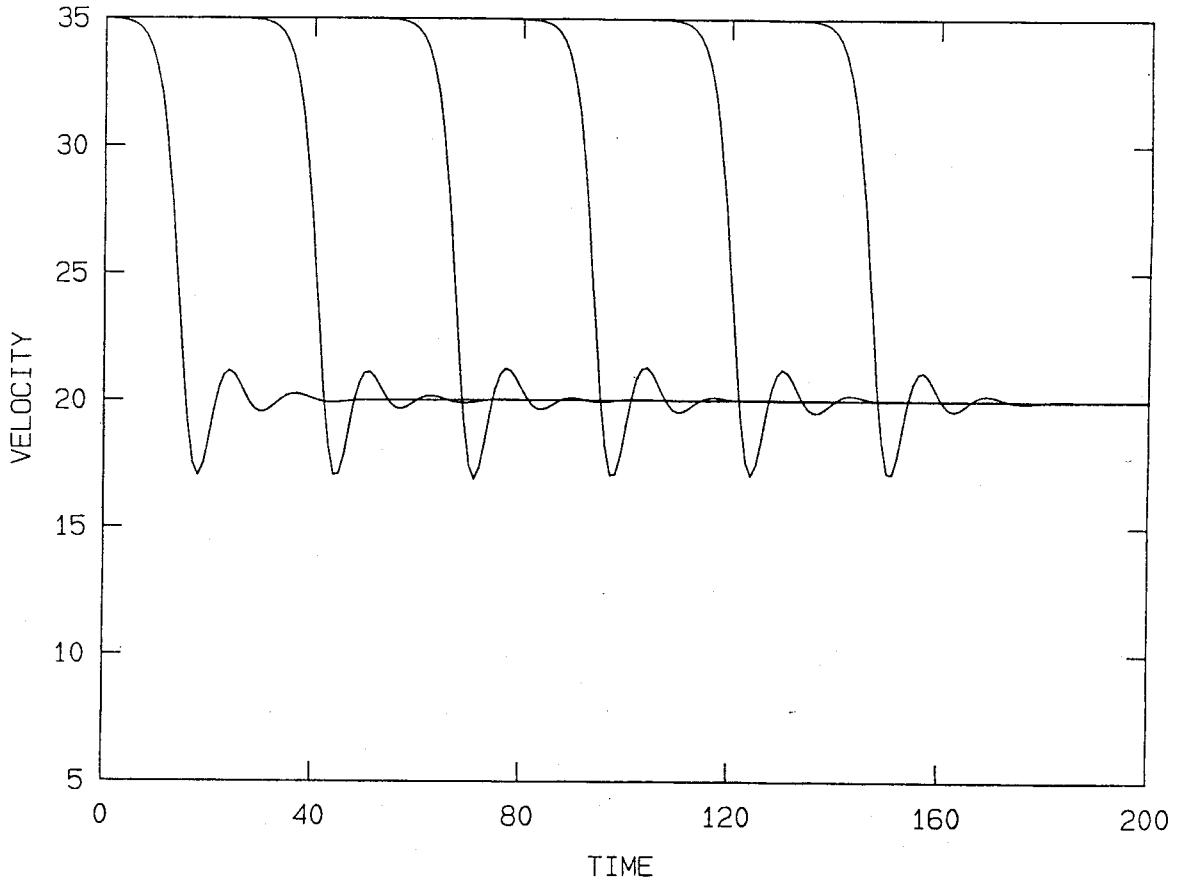

Figure 3.4: $\alpha_2 T = .57$, $T = 1.15$, cars 100 through 150.

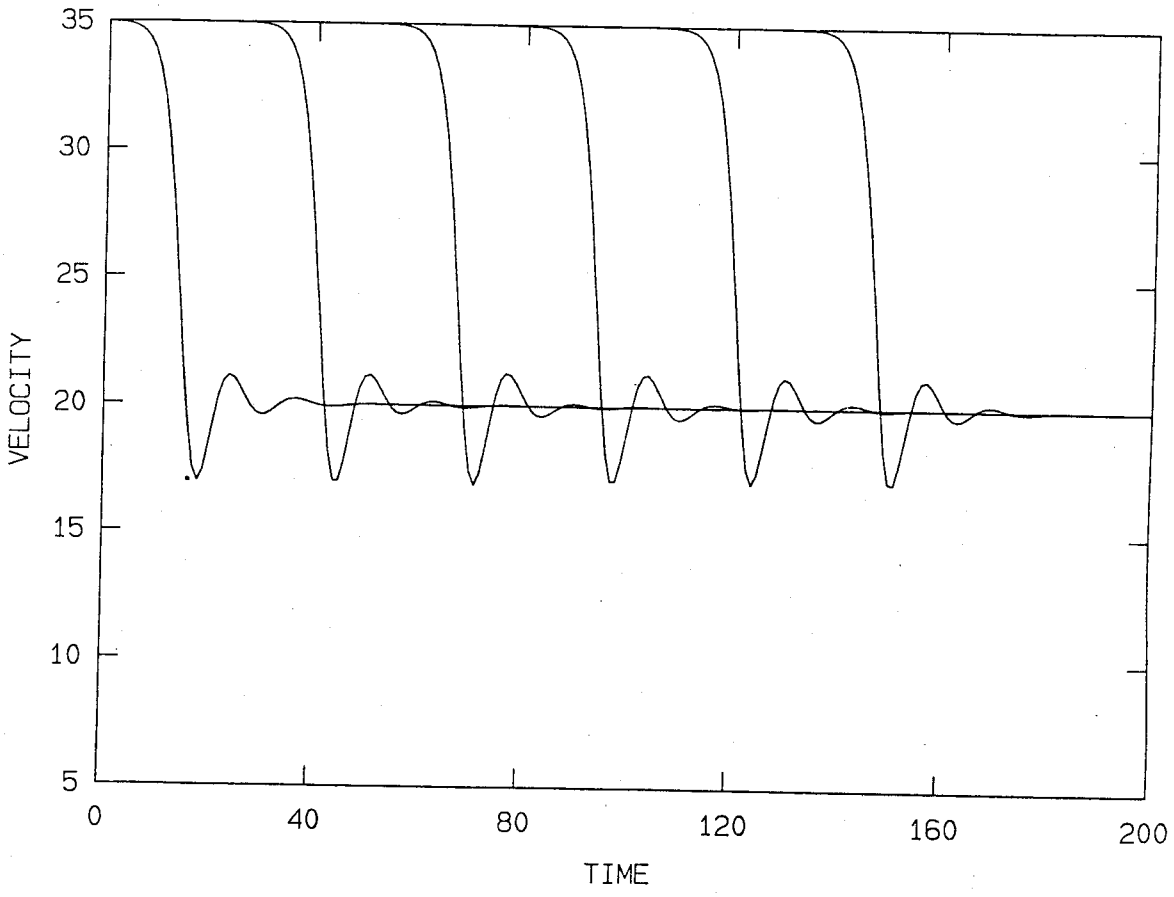

Figure 3.5: $\alpha_2 T = .57$, $T = 1.15$, cars 150 through 200.

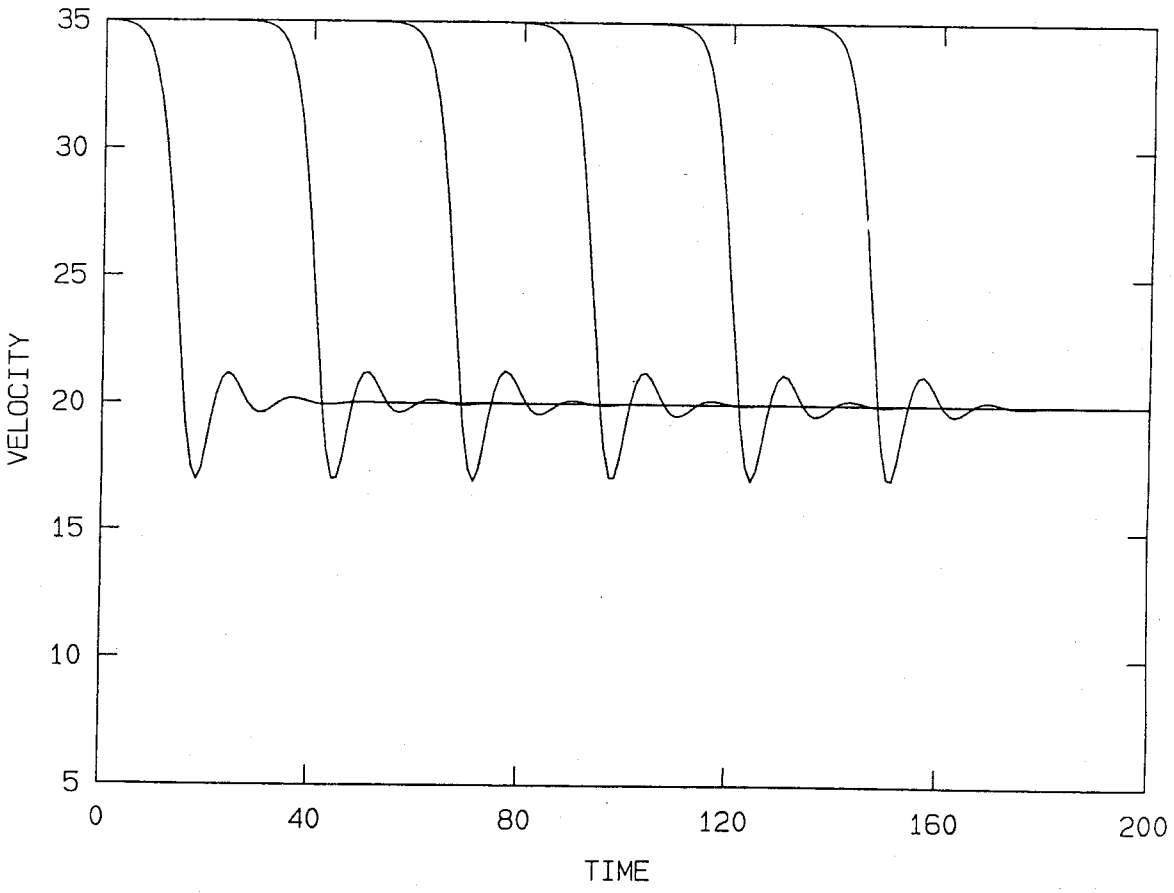

Figure 3.6: $\alpha_2 T = .57$, $T = 1.15$, cars 200 through 250.

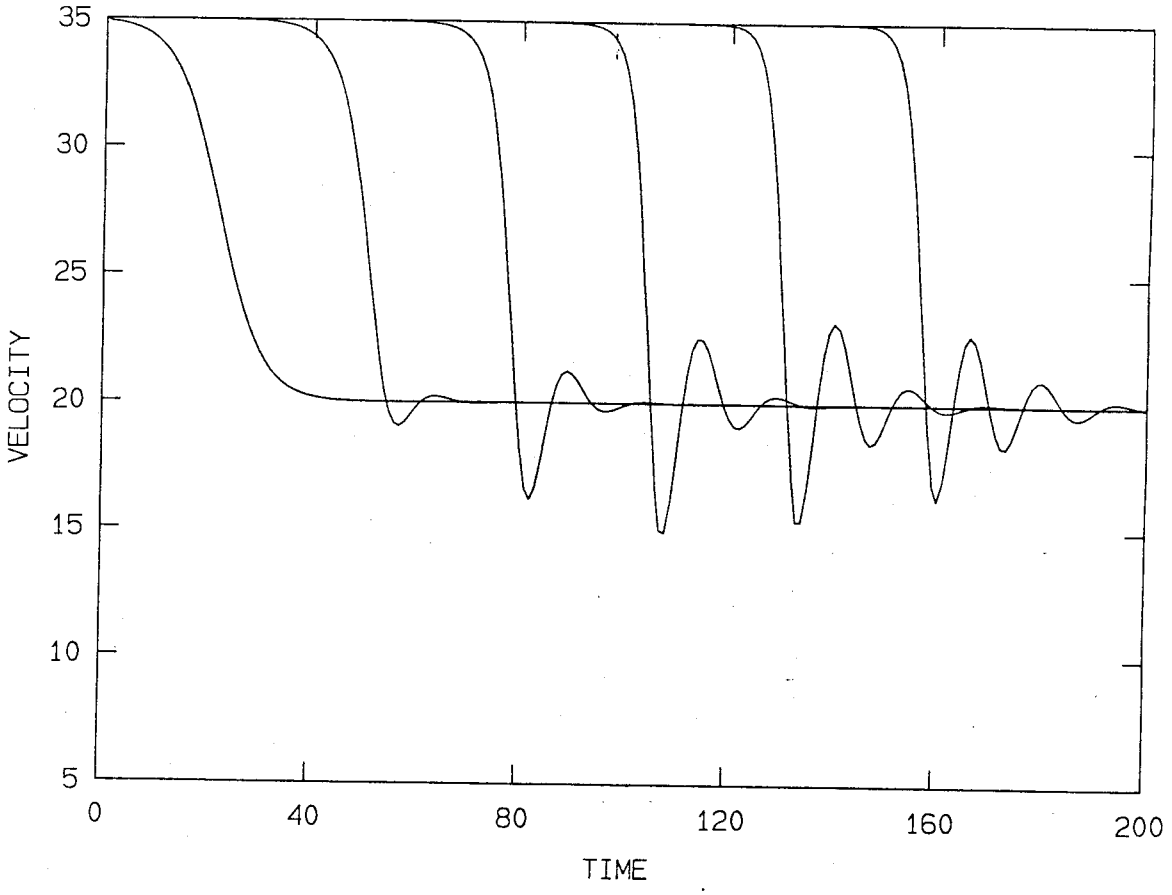

Figure 3.7: $\alpha_2 T = .61$, $T = 1.23$, cars 0 through 50.

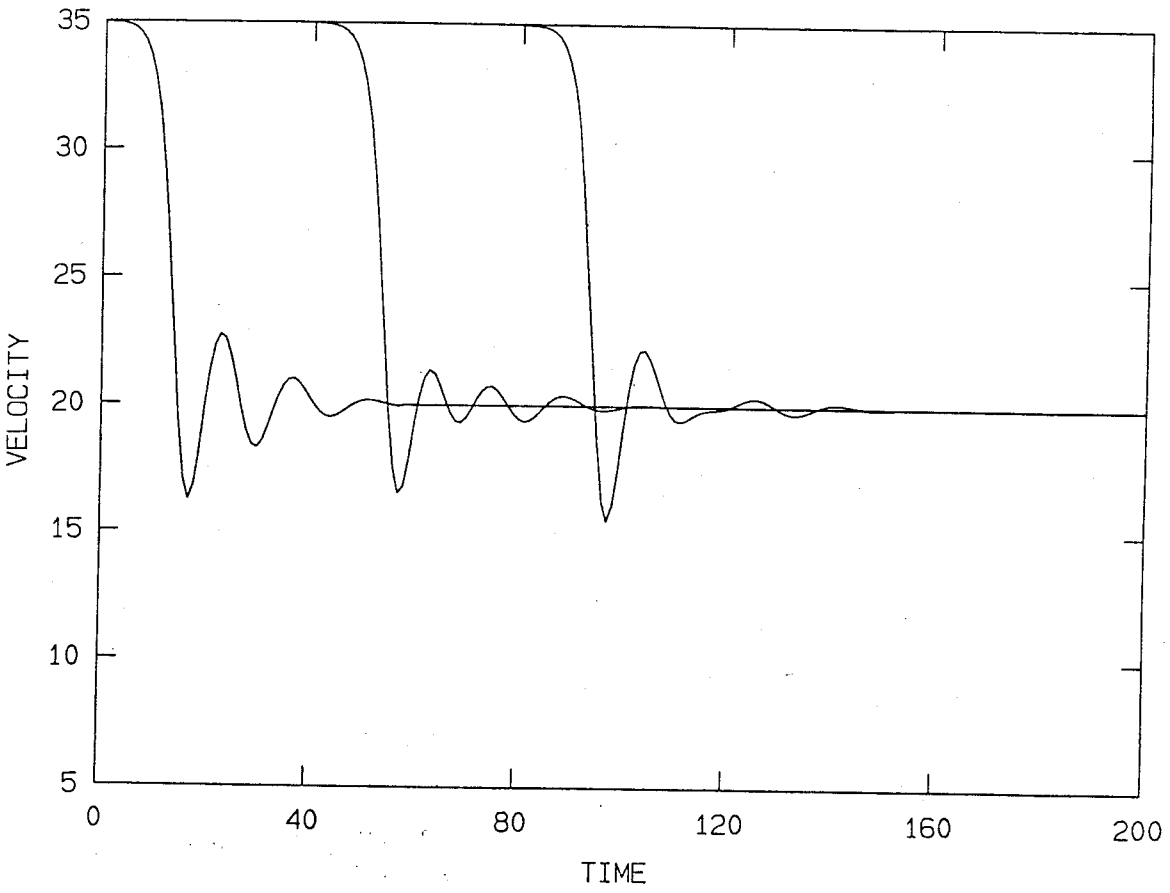

Figure 3.8: $\alpha_2 T = .61$, $T = 1.23$, cars 50 through 80.

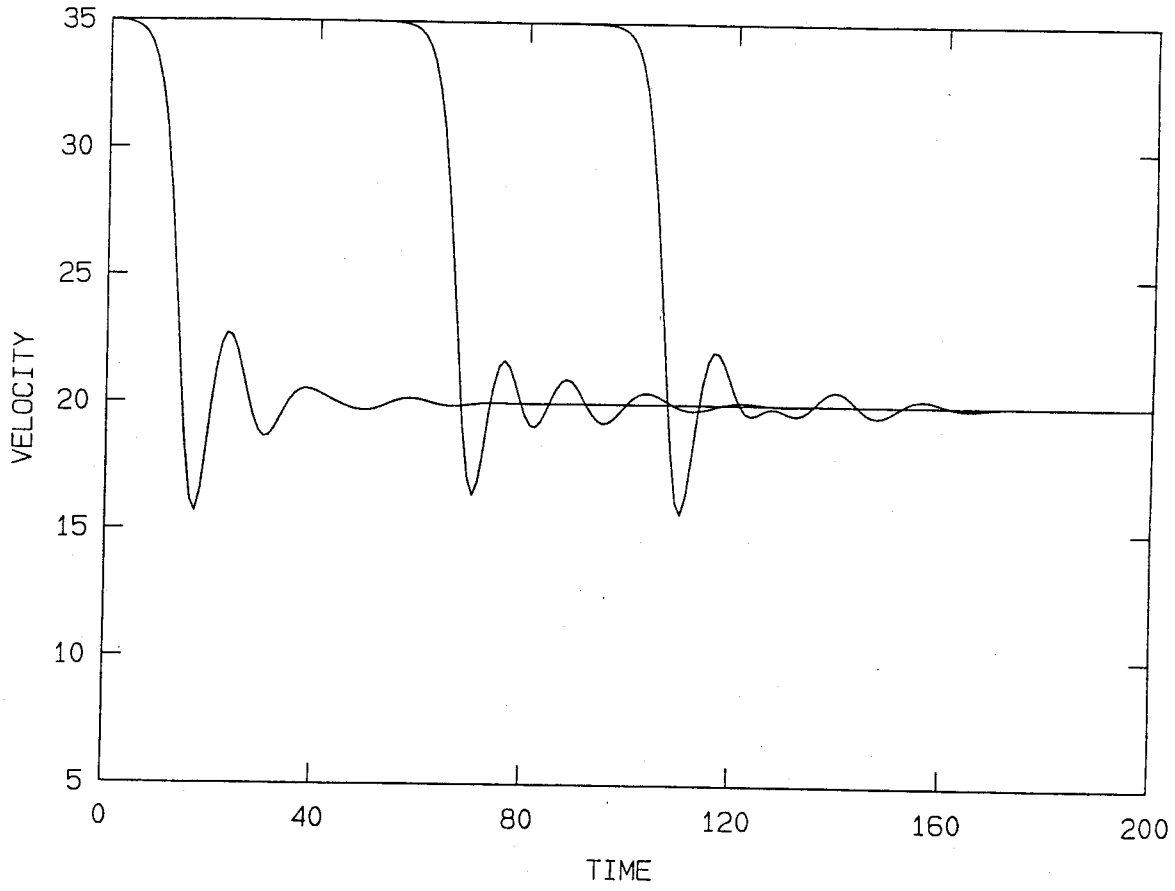

Figure 3.9: $\alpha_2 T = .61$, $T = 1.23$, cars 90 through 125.

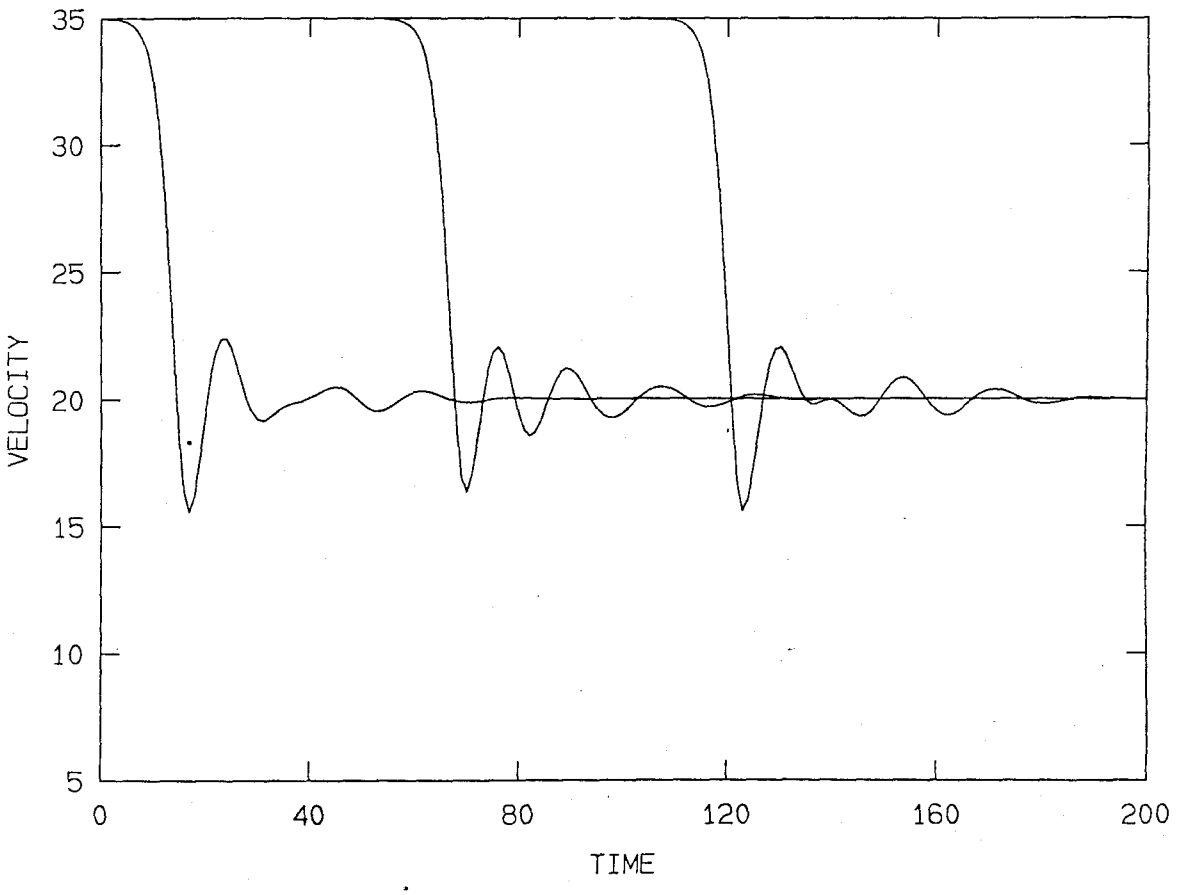

Figure 3.10: $\alpha_2 T = .61$, $T = 1.23$, cars 130 through 170.

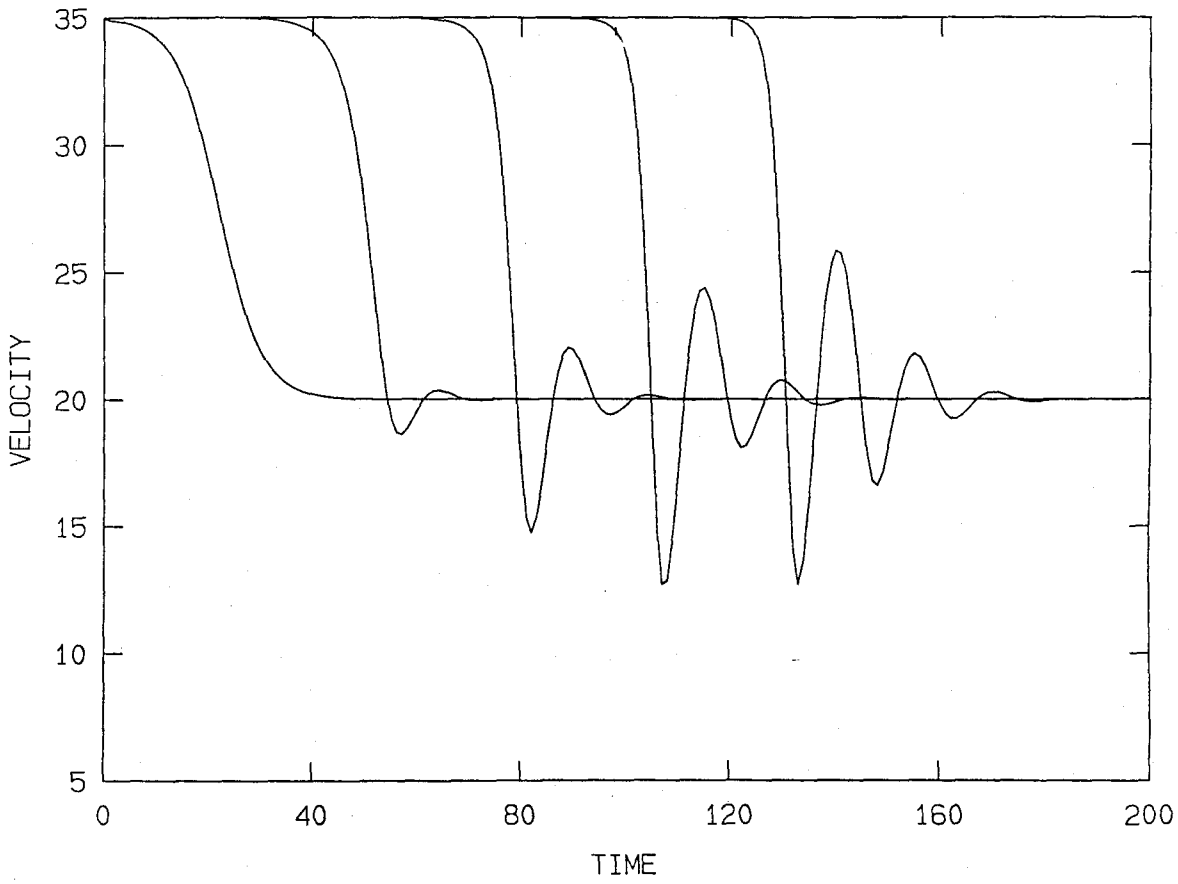

Figure 3.11: $\alpha_2 T = .65$, $T = 1.31$, cars 0 through 40.

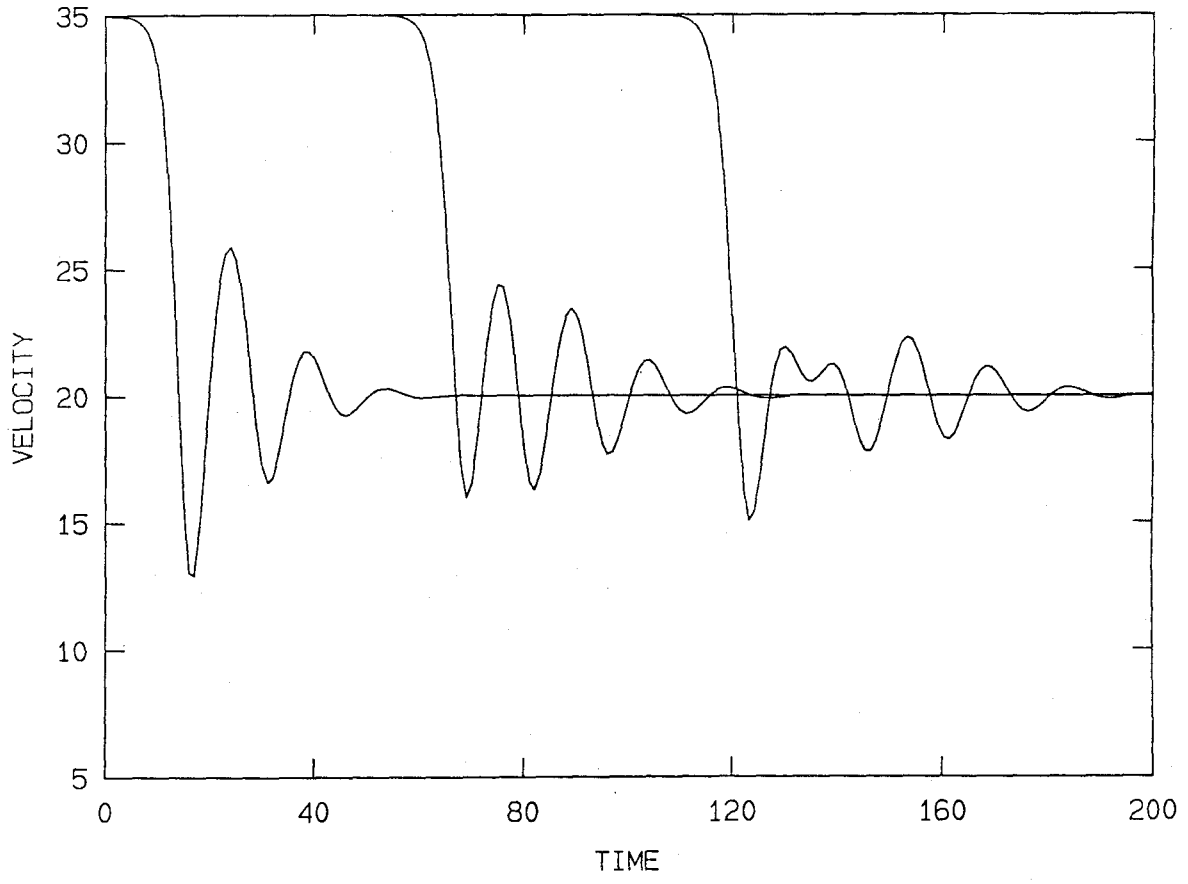

Figure 3.12: $\alpha_2 T = .65$, $T = 1.31$, cars 40 through 80.

from the continuous traffic equations of Chapter 1. We start by looking for a periodic solution to the linearized problem. We linearize about v_0 and h_0 as before and let $x_n = y_n - nh_0 + v_0 t$. The linearized equation is:

$$\dot{y}_n + T\ddot{y}_n = \alpha(y_{n-1} - y_n).$$

We look for steady profile waves by setting $\chi = \Omega t - \mu n$ and $y_n(t) = g(\chi)$ and find the equation for $g(\chi)$ is

$$\Omega g'(\chi) + \Omega^2 T g''(\chi) = \alpha[g(\chi + \mu) - g(\chi)].$$

We let $\omega = \frac{\Omega}{\alpha}$, and $\tau = \alpha T$, to normalize the equation and obtain

$$\omega g'(\chi) + \omega^2 \tau g''(\chi) = g(\chi + \mu) - g(\chi).$$

We now look for a solution of the form $g(\chi) = e^{i\chi}$, and obtain the relation

$$i\omega - \omega^2 \tau = e^{i\mu} - 1.$$

Separating real and imaginary parts, we have

$$\begin{aligned} \omega &= \sin\mu \\ \omega^2\tau &= 1 - \cos\mu. \end{aligned}$$

This determines ω and μ in terms of τ:

$$\begin{aligned} \omega &= \sin\mu \\ \cos\mu &= \frac{1-\tau}{\tau}. \end{aligned}$$

Thus, we do have a periodic solution to the linearized problem. Notice that for μ ro be real, τ must be greater than $\frac{1}{2}$, i.e., τ must be in the unstable region.

3.3.1 Perturbation Expansion

We use this linear solution as a starting point for a perturbation expansion where the small parameter is the amplitude of the waves. We expand g, μ and ω in the typical way:

$$\begin{aligned} g(\chi) &= \epsilon g_1 + \epsilon^2 g_2 + \cdots \\ \mu &= \mu_0 + \epsilon^2 \mu_2 + \cdots \\ \omega &= \omega_0 + \epsilon^2 \omega_2 + \cdots . \end{aligned}$$

When we apply the perturbation expansion to the equation, we find that there is a term on the right hand side of the equation at the second order which leads to solutions which are not periodic. This arises in other problems, such as water waves, as well. It is resolved by assuming a deviation from the mean velocity or headway of order ϵ^2. In our case, we will assume a deviation in both the mean headway and velocity and look at a particular case later on. Therefore, back in the original equation, we let

$$\begin{aligned} x_n(t) &= y_n(t) - n(h_0 + D) + (v_0 + C)t \\ \chi &= \Omega t - \mu n \\ y_n(t) &= g(\chi) \end{aligned}$$

and then obtain the modified equation

$$\frac{v_0}{\alpha} + \frac{C}{\alpha} + \omega g'(\chi) + \omega^2 \tau g''(\chi) = \frac{1}{\alpha} G[g(\chi + \mu) - g(\chi) + h_0 + D].$$

We again look for small amplitude waves by letting

$$\begin{aligned} g(\chi) &= \epsilon g_1 + \epsilon^2 g_2 + \cdots \\ \mu &= \mu_0 + \epsilon^2 \mu_2 + \cdots \\ \omega &= \omega_0 + \epsilon^2 \omega_2 + \cdots \\ C &= \epsilon^2 C_2 + \cdots \\ D &= \epsilon^2 D_2 + \cdots , \end{aligned}$$

and expand G about h_0 . When we do this, we find that we must also expand $g(\chi+\mu)$ about $\chi+\mu_0$. When this is included and we equate like powers of ϵ, we obtain:

$$\begin{aligned}
\epsilon^0: &\quad v_0 = G(h_0)\\
\epsilon^1: &\quad \omega_0 g_1' + \omega_0^2\tau g_1'' = [g_1(\chi+\mu_0) - g_1(\chi)]\\
\epsilon^2: &\quad \tfrac{C_2}{\alpha} + \omega_0 g_2' + \omega_0^2\tau g_2'' = [g_2(\chi+\mu_0) - g_2(\chi)]\\
&\qquad +\tfrac{1}{2\alpha}G''(h_0)[g_1(\chi+\mu_0) - g_1(\chi)]^2 + D_2\\
\epsilon^3: &\quad \omega_0 g_3' + \omega_0^2\tau g_3'' + \omega_2 g_1' + 2\omega_0\omega_2\tau g_1'' =\\
&\qquad [g_3(\chi+\mu_0) - g_3(\chi)]\\
&\qquad +\mu_2 g_1'(\chi+\mu_0) + 2D_2\tfrac{G''(h_0)}{2\alpha}[g_1(\chi+\mu_0) - g_1(\chi)]\\
&\qquad +2[g_1(\chi+\mu_0) - g_1(\chi)][g_2(\chi+\mu_0) - g_2(\chi)]\tfrac{G''(h_0)}{2\alpha}\\
&\qquad +\tfrac{G'''(h_0)}{6\alpha}[g_1(\chi+\mu_0) - g_1(\chi)]^3\\
&\qquad \vdots,
\end{aligned}$$

where we have used the relation $G'(h_0)=\alpha$. To simplify, we let $\frac{G''(h_0)}{2\alpha} = \alpha_2$ and $\frac{G'''(h_0)}{6\alpha} = \alpha_3$. Then, the equations can be written as:

$$\begin{aligned}
\epsilon^1: &\quad \omega_0 g_1' + \omega_0^2\tau g_1'' = g_1(\chi+\mu_0) - g_1(\chi)\\
\epsilon^2: &\quad \tfrac{C_2}{\alpha} + \omega_0 g_2' + \omega_0^2\tau g_2'' = g_2(\chi+\mu_0) - g_2(\chi) +\\
&\qquad \alpha_2[g_1(\chi+\mu_0) - g_1(\chi)]^2 + D_2\\
\epsilon^3: &\quad \omega_0 g_3' + \omega_0^2\tau g_3'' + \omega_2 g_1' + 2\omega_0\omega_2\tau g_1'' =\\
&\qquad g_3(\chi+\mu_0) - g_3(\chi) + \mu_2 g_1'(\chi+\mu_0) + 2\alpha_2 D_2[g_1(\chi+\mu_0) - g_1(\chi)] +\\
&\qquad 2\alpha_2[g_1(\chi+\mu_0) - g_1(\chi)][g_2(\chi+\mu_0) - g_2(\chi)] +\\
&\qquad \alpha_3[g_1(\chi+\mu_0) - g_1(\chi)]^3\\
&\qquad \vdots.
\end{aligned}$$

At order ϵ, we have the linearized problem that we solved previously and found that

$$\begin{aligned}
&g_1(\chi) = e^{i\chi} + e^{-i\chi} = 2\cos\chi\\
&\cos\mu_0 = \tfrac{1-\tau}{\tau}\\
&\omega_0 = \sin\mu_0.
\end{aligned}$$

At the next order, we have the equation

$$\frac{C_2}{\alpha} + \omega_0 g_2' + \omega_0^2\tau g_2'' =$$

$$g_2(\chi+\mu_0)-g_2(\chi)+\alpha_2[g_1(\chi+\mu_0)-g_1(\chi)]^2+D_2.$$

Looking at the terms on the right hand side, we see that the term

$$[g_1(\chi+\mu_0)-g_1(\chi)]^2=e^{2i\chi}(e^{i\mu_0}-1)^2+\overline{e^{2i\chi}(e^{i\mu_0}-1)^2}+4(1-\cos\mu_0),$$

where $\overline{x}$ means the complex conjugate of x, includes the constant term $4(1-\cos\mu_0)$. This must be balanced with $\frac{C_2}{\alpha}$ and D_2. Thus, we find that

$$\frac{C_2}{\alpha}=4(1-\cos\mu_0)\alpha_2+D_2.$$

We solve for g_2 by assuming the form $g_2=Ae^{2i\chi}+\overline{Ae^{2i\chi}}$ and determine that

$$A=\frac{\alpha_2}{2(1-\cos\mu_0)}(\cos\mu_0-1+i\sin\mu_0).$$

Or, writing the solution in terms of sines and cosines, we have

$$g_2(\chi)=-\alpha_2[\cos 2\chi+\frac{1}{\sqrt{2\tau-1}}\sin 2\chi].$$

The third order equation is:

$$\begin{aligned}
&\omega_0 g_3'+\omega_0^2 g_3''+\omega_2 g_1'+2\omega_0\omega_2\tau g_1''=\\
&\quad g_3(\chi+\mu_0)-g_3(\chi)+\mu_2 g_1'(\chi+\mu_0)+2\alpha_2 D_2[g_1(\chi+\mu_0)-g_1(\chi)]\\
&\quad +2\alpha_2[g_1(\chi+\mu_0)-g_1(\chi)][g_2(\chi+\mu_0)-g_2(\chi)]\\
&\quad +\alpha_3[g_1(\chi+\mu_0)-g_1(\chi)]^3.
\end{aligned}$$

We want g_3 to be periodic so we require all of the terms involving $e^{i\chi}$ and $e^{-i\chi}$ to balance. This means that the $e^{i\chi}$ and $e^{-i\chi}$ terms of $\omega_2 g_1'+2\omega_0\omega_2\tau g_1'$ must balance with those of

$$\begin{aligned}
&\mu_2 g_1'(\chi+\mu_0)+2\alpha_2 D_2[g_1(\chi+\mu_0)-g_1(\chi)]+\\
&\quad 2\alpha_2[g_1(\chi+\mu_0)-g_1(\chi)][g_2(\chi+\mu_0)-g_2(\chi)]\\
&\qquad +\alpha_3[g_1(\chi+\mu_0)-g_1(\chi)]^3.
\end{aligned}$$

When we require this, we obtain the complex relation:

$$
\begin{aligned}
&(i - 2\omega_0\tau)\omega_2 = \\
&\quad \mu_2 i e^{i\mu_0} + 2\alpha_2 D_2(e^{i\mu_0} - 1) \\
&\quad 2\alpha_2 A(e^{2i\mu_0} - 1)(e^{-i\mu_0} - 1) + \\
&\quad 3\alpha_3(e^{i\mu_0} - 1)^2(e^{-i\mu_0} - 1).
\end{aligned}
$$

Substituting the value for A and separating real and imaginary parts results in the two equations:

$$
\begin{aligned}
&\omega_2 - \mu_2 \cos\mu_0 = \\
&\quad \Im\{\mu_2 i e^{i\mu_0} + 2\alpha_2 D_2(e^{i\mu_0} - 1) + 2\alpha_2 A(e^{2i\mu_0} - 1)(e^{-i\mu_0} - 1) \\
&\quad +3\alpha_3(e^{i\mu_0} - 1)^2(e^{-i\mu_0} - 1)\} \\
&-2\omega_0\tau\omega_2 + \mu_2 \sin\mu_0 = \\
&\quad \Re\{\mu_2 i e^{i\mu_0} + 2\alpha_2 D_2(e^{i\mu_0} - 1) + 2\alpha_2 A(e^{2i\mu_0} - 1)(e^{-i\mu_0} - 1) \\
&\quad +3\alpha_3(e^{i\mu_0} - 1)^2(e^{-i\mu_0} - 1)\},
\end{aligned}
$$

which, after determining the real and imaginary parts of the left hand side yields:

$$\omega_2 - \mu_2 \cos\mu_0 = \sin\mu_0[2\alpha_2 D_2 + 4\alpha_2^2 \cos\mu_0 + 6\alpha_3(1 - \cos\mu_0)]$$

and

$$
\begin{aligned}
&-2\omega_0\tau\omega_2 + \mu_2 \sin\mu_0 = \\
&\quad (\cos\mu_0 - 1)[2\alpha_2 D_2 + 4\alpha_2^2(1 + \cos\mu_0) + 6\alpha_3(1 - \cos\mu_0)].
\end{aligned}
$$

Solving for μ_2 and ω_2 and using the relation that $\alpha_2 = -\frac{1}{2}\frac{\lambda}{v_f}$ and $\alpha_3 = \frac{1}{6}(\frac{\lambda}{v_f})^2$, we obtain

$$\mu_2 = 2\alpha_2 D_2 \frac{2\tau\omega_0 \sin\mu_0 + \cos\mu_0 - 1}{\sin\mu_0 - 2\tau\omega_0 \cos\mu_0}.$$

Or, in terms of τ,

$$\mu_2 = \frac{2\alpha_2 D_2}{\sqrt{2\tau - 1}}$$

and

$$\omega_2 = \frac{2\alpha_2 D_2}{\sqrt{2\tau - 1}} + \alpha_2^2 \frac{\sqrt{2\tau - 1}}{\tau}.$$

Finally, for the first few terms of the expansion, we have that

$$\begin{aligned}
g(\chi) &= 2\epsilon \cos\chi - \alpha_2 \epsilon^2 [\cos 2\chi + \tfrac{1}{\sqrt{2\tau-1}} \sin 2\chi] + \bigcirc(\epsilon^3) \\
C &= \epsilon^2 \alpha [4(1 - \cos\mu_0)\alpha_2 + D_2] + \bigcirc(\epsilon^4) \\
\mu &= \mu_0 + \epsilon^2 \tfrac{2\alpha_2 D_2}{\sqrt{2\tau-1}} + \bigcirc(\epsilon^4) \\
\omega &= \sin\mu_0 + \epsilon^2 [\tfrac{2\alpha_2 D_2}{\sqrt{2\tau-1}} + 4\alpha_2^2 \tfrac{\sqrt{2\tau-1}}{\tau}] + \bigcirc(\epsilon^4)
\end{aligned}$$

where μ_0 is defined in terms of τ by $\cos\mu_0 = \frac{1-\tau}{\tau}$ and D is arbitrary. In terms of our original variables, we have:

$$\begin{aligned}
h_n(t) &= g(\chi + \mu) - g(\chi) + h_0 + D \\
v_n(t) &= \alpha\omega g'(\chi) + v_0 + C.
\end{aligned}$$

The headway, $h_n(t)$ and the velocity, $v_n(t)$ are periodic, oscillating about $h_0 + D$ and $v_0 + C$ respectively. The frequency in time is

$$\Omega = \alpha\omega = \alpha \sin\mu_0 + \bigcirc(\epsilon^2)$$

and the period is then $\frac{2\pi}{\Omega}$ which to first order is $\frac{2\pi}{\alpha \sin\mu_0}$. Thus, the closer μ_0 is to 0, the longer the period, and this will occur when τ is near $1/2$.

These perturbation results are expected to be good only for small amplitude ϵ. Small amplitude depends on the ratio of succesive terms. Thus, ϵ small means that

$$\frac{\epsilon^2 |g_2|_{max}}{\epsilon |g_1|_{max}} \ll 1,$$

which gives the condition

$$\frac{\lambda}{4v_f}(1+\frac{1}{\sqrt{2\tau-1}})\epsilon \ll 1.$$

We can view the solution with a shift of mean velocity alone (case $D=0$), or a shift of the mean headway alone (case $C=0$), or a shift of both the headway and the velocity, where the shifts are related by

$$C = \alpha[4(1-\cos\mu_0)\alpha_2 + D_2]\epsilon^2 + \cdots.$$

If we choose to look at this as a shift in mean velocity alone, then we have $D=0$ and this results in

$$\mu = \mu_0 + \bigcirc(\epsilon^4)$$
$$\omega = \sin\mu_0[1+(\tfrac{\lambda}{v_f}\epsilon)^2] + \bigcirc(\epsilon^4).$$

To order ϵ^2, μ does not change and the mean velocity is then

$$v_0 - 2\alpha\frac{\lambda}{v_f}(1-\cos\mu_0)\epsilon^2$$

which is smaller than that predicted by linear theory.

3.3.2 Comparison to Ordinary Differential Equations

We could look at this problem in another way. We use the ideas of limit cycles for differential equations without a delay and apply them to our differential-delay equation. For reasons that will become apparent later, we change the independent variable slightly and look for steady profile waves by letting $\xi = Vt - n$, $(\xi = \frac{x}{\mu})$. With everything else the same as before, the equation becomes

$$v_0 + C + Vg'(\xi) + TV^2g''(\xi) = G[g(\xi+1) - g(\xi) + h_0 + D]. \qquad (3.1)$$

Following the ideas of the Hopf Bifurcation theorem, we choose a bifurcation parameter. We take that as $W = \frac{V}{\alpha}$. The critical W is that value where the linearized problem gives an exact periodic solution. Paralleling the ideas for limit cycles, the small parameter which we consider is the distance from the critical, $W - W_0$. For second order differential equations, we know that in most cases we will get a limit cycle on one side or the other of W_0, that is $W < W_0$ or $W > W_0$. To see which side of W_0 to expect limit cycles, we note from our perturbation expansion that $W - W_0 = \epsilon^2 W_2 = \epsilon^2 \frac{(\omega_2 \mu_0 - \omega_0 \mu_2)}{\mu_0^2}$ which, in terms of μ_0 and τ is

$$W - W_0 = \epsilon^2 [\frac{2\alpha_2 D_2}{\mu_0 \sqrt{2\tau - 1}}(1 - W_0) + 4\alpha_2^2 W_0]. \tag{3.2}$$

The sign of W_2 gives which side of W_0 we find the limit cycle. Consistent with the case for differential equations, we find that the amplitude of the periodic solution is proportional to $|W - W_0|^{1/2}$. Thus, the further W is from the critical, the larger the amplitude. In the perturbation expansion, we had that the amplitude was ϵ. In terms of W, we have that the amplitude is determined by

$$\epsilon^2 = \frac{1}{W_2}(W - W_0) + \bigcirc(\epsilon^4).$$

If we had defined ϵ as $\sqrt{|W - W_0|}$, then the perturbation expansion determines the amplitude of g_1, $a\epsilon$ in terms of the other parameters τ and μ_0. We would obtain the amplitude instead of ω_2, which was obtained in the perturbation expansion done earlier. The Hopf theory for ordinary differential equations also tells us that we will find limit cycles for W in a limited region about W_0. That is $b < W < W_0$ for the case where limit cycles are found

for $W < W_0$ or $W_0 < W < c$ for the case where limit cycles are found for $W > W_0$. Assuming that these ideas carry over for our differential-delay equation, we expect there to be a limit on how large the amplitude can be such that we still have a periodic solution.

3.3.3 Singular Points of the Equation

The equation which we will compute the solution to is a modified version of equation (3.1). Since C and D are not known in advance, we set them equal to 0. We non-dimensionalize the equation by setting $f(\xi) = \frac{\lambda}{v_f} g(\xi)$ and set $W = \frac{V}{\alpha}$ and $\tau = \alpha T$, as before. Using this change of variables and the relations, $v_0 = G(h_0)$ and $\alpha = G'(h_0)$, we obtain the equation

$$W f'(\xi) + W^2 \tau f''(\xi) = 1 - e^{-(f(\xi+1)-f(\xi))}. \tag{3.3}$$

We would like to look at a phase diagram for this equation, however, in its present form, it is not clear how to do this. From the perturbation, we found that f' is periodic and f is not. This suggests that the phase space in which we will see periodic orbits is not the usual f versus f', but f' versus f''. We set $u = f'$ and $v = f''$ and obtain the pair of equations in u and v:

$$\begin{aligned} u' &= v \\ v' &= \tfrac{1}{W^2\tau}\{-Wv + [1 - Wu - W^2\tau v][u(\xi+1) - u(\xi)]\}. \end{aligned}$$

The singular points of the equation are at $v = 0$ and $[1 - Wu][u(\xi+1) - u(\xi)] = 0$, which leads to $u = \frac{1}{W}$ and $u = const = S$. Checking $u = \frac{1}{W}$ in equation (3.3), we find that $u = \frac{1}{W}$ leads to $W = 0$ which is not a feasible solution. We check $u = S$ in equation (3.3) and find that S must satisfy

$$WS = 1 - e^{-S}.$$

There are two solutions to this, $S = 0$ and one positive solution for $W < 1$. Thus, the two singular points of the equation are $u = 0$, $v = 0$ and $u = S$, $v = 0$. Both of these points correspond to uniform states. The point $u = 0$, $v = 0$ corresponds to the uniform state $v = v_0$, $h = h_0$, and the point $u = S$, $v = 0$ corresponds to $v = v_0 + \alpha W \frac{v_1}{\lambda} S$, $h = h_0 + \frac{v_1}{\lambda} S$.

We first look at the point $u = 0$, $v = 0$. We linearize equation (3.3) about this point by setting $f = \eta$. The linear equation has solutions of the form $\eta = e^{\beta\xi}$ where β satisfies

$$W\beta + W^2\tau\beta^2 = e^{\beta} - 1. \tag{3.4}$$

We know that there are purely periodic solutions for W exactly equal to W_0 with $\beta = i\mu_0$. When W is not exactly equal to W_0, we expect to find complex solutions with the real part non-zero. The sign of the real part tells us in which direction in ξ the phase plane will have outgoing spirals. We expect the outgoing spirals to lead to limit cycles.

Since we know there is a pure imaginary root at $\beta = i\mu_0$ for $W = W_0$, we perturb about this solution and look for a root, $\beta = \epsilon + i\mu_0$, for $W = W_0 - \gamma$. On substituting these into equation (3.4), expanding for small ϵ and keeping only order ϵ terms and larger, we find that the real part of β is

$$\Re(\beta) = A^2\{\frac{W_0 - \gamma}{W_0}(\frac{1-\tau}{\tau} - \gamma) - 1\}$$

where A^2 is a positive constant.

Since the sign of this depends on whether W is less than or greater than W_0, we look back at the perturbation solution to determine which side of W_0 we find periodic solutions. Equation (3.2) gives the value of W_2 in terms of

α, τ and W_0. We see that it also depends on D_2. In order to find the sign of W_2, we must know the the value of D_2 - the shift in the mean headway. When we look for periodic solutions numerically, having set $C = D = 0$, a term proportional to ξ will arise in the solution, f. Thus, we choose D such that $Ct - Dn$ is proportional to ξ. This fixes D_2 and determines the value of W_2:

$$W_2 = -4\alpha_2^2 W_0$$

which is negative. Thus, for periodic solutions, we require $W < W_0$.

To determine whether the real part of β is positive or negative, the fact that $W < W_0$ tells us that γ is positive and hence, $\frac{W_0-\gamma}{W_0} < 1$. Since $\frac{1-\tau}{\tau} \leq 1$, $\frac{1-\tau}{\tau} - \gamma < 1$ and hence, the real part of β is negative. Therefore, the point $u = 0$, $v = 0$ is an outward winding spiral for $\xi < 0$ provided $W < W_0$.

For the other singular point, $u = S$, $v = 0$, we linearize and set $\eta = e^{\beta\xi}$ to obtain

$$W\beta + W^2\tau\beta^2 = e^{-S}[e^{\beta} - 1].$$

If we graph the two sides of this equation as functions of β, we find that the slope of the parabola at the origin is W, which in terms of S is $W = \frac{1-e^{-S}}{S}$. The slope of the exponential at the origin is e^{-S}. Since $e^S > 1 + S$, we see that $W > e^{-S}$. Therefore, there are two real roots of this equation, one positive and one negative and the point $u = S$, $v = 0$ is a saddle point.

3.3.4 Numerical Studies of the Periodic Solution

The equation we will compute solutions to is equation (3.3). The right side of this equation is a function of $f(\xi+1)-f(\xi)$, the left side only involves $f(\xi)$

and its derivatives. In order to solve for $f(\xi)$ as an initial value problem, we must know $f(\xi+1)$. This means that we must let ξ increase in the negative direction rather than the positive direction. The analysis of the singular points implies an unstable spiral for ξ increasing in the negative direction and therefore, this is the direction we expect to find limit cycles.

We start at the point $u=\epsilon$, $v=0$, close to the spiral point. Setting $u=\epsilon$ implies that $f=\epsilon\xi$. Since we must give the values of $f(\xi)$ for ξ in the interval $[0,1]$, we set $f=\epsilon\xi$ in this interval. We integrate this numerically using a fourth order Runga-Kutta scheme where the equation is written as

$$\begin{aligned} u &= f'(\xi) \\ u' &= f''(\xi) = \tfrac{1}{\tau W^2}\{1-e^{-[F(\xi)-f(\xi)]}-Wu\} \end{aligned}$$

and $F(\xi)=f(\xi+1)$ is known at each new step. The Runga-Kutta scheme requires the values of F at the step which was just computed, ξ_{prev}, one step later, $\xi_{prev}+\Delta\xi$, and at the half step between these two, $\xi_{prev}+\frac{\Delta\xi}{2}$. The values, $F(\xi_{prev})$ and $F(\xi_{prev}+\Delta\xi)$, are either given in the initial conditions or are the result of a calculation done earlier. We must approximate $F(\xi_{prev}+\frac{1}{2}\Delta\xi)$ and we do this by taking the average value over one step:

$$F(\xi_{prev}+\frac{1}{2}\Delta\xi)=\frac{1}{2}[F(\xi_{prev})+F(\xi_{prev}+\Delta\xi)].$$

We find limit cycles, as expected. Figure (3.13) shows the solution winding out to the limit cycle. Depending on the starting value ϵ_f, and on the distance that W is from the critical, we obtain curves in the phase plane which either wind out to the limit cycle or wind in to the limit cycle. We find that for τ near $1/2$, we are very limited in our choice of W. It must be very close to W_0 to get periodic solutions. If it is too far from W_0, the solution grows

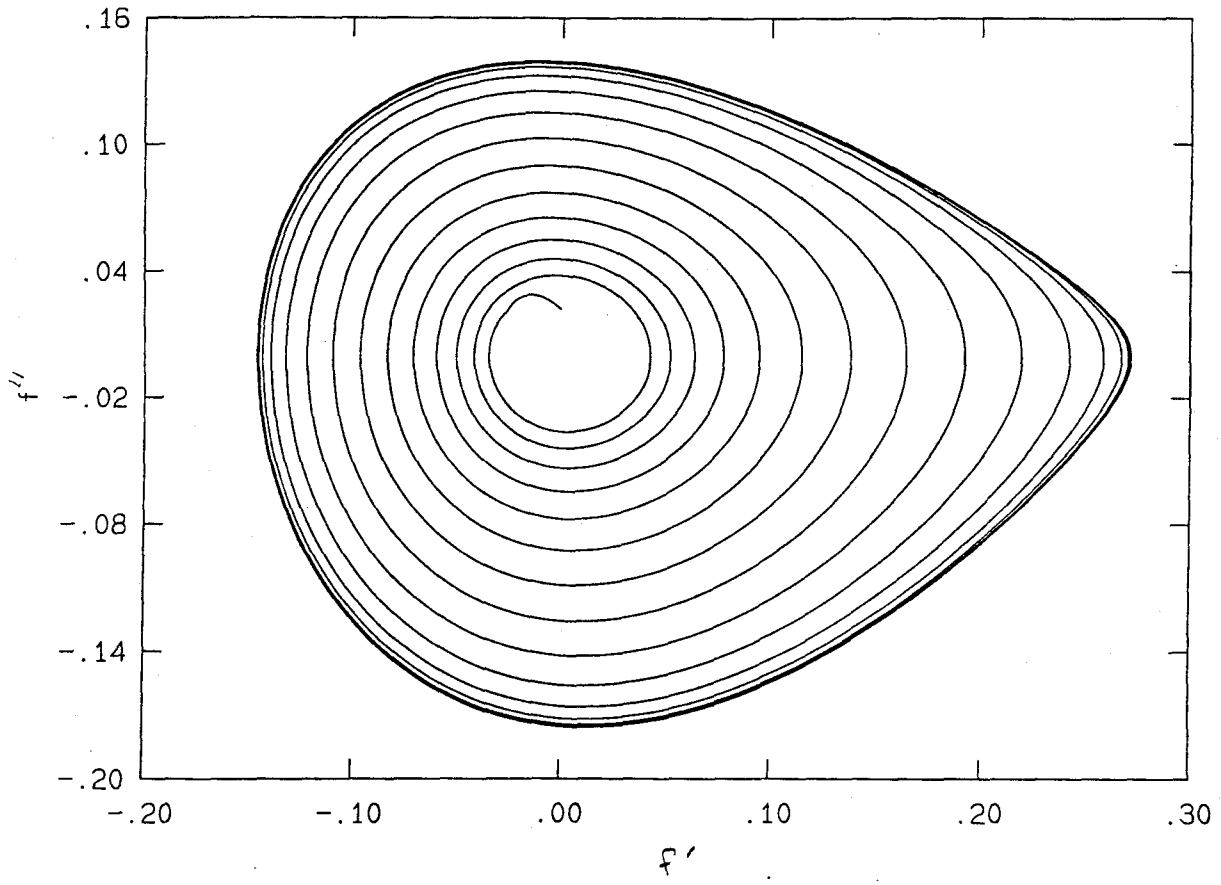

Figure 3.13: Limit cycle for $W = .865$ and $\tau = .61$.

infinitely and there is no periodic solution. As τ decreases towards $1/2$, the period becomes longer, consistent with the perturbation prediction. But as τ increases, the range of acceptable values for W becomes larger. This means that one way of obtaining relatively long waves, requires that the amplitude be small and to obtain larger amplitudes, we must have larger values of τ.

Comparison of Various W for Fixed τ

We first look at the numerical calculations for a fixed value of τ and vary W away from W_0. The phase diagrams for all of the various selected values for W are shown in figure (3.14) with the values W and $W_0 - W$ given in table (3.1). The largest curve corresponds to the largest $W_0 - W$ and

Table 3.1: The values for τ, W, and $W_0 - W$ for the case of fixed τ and various W.

τ	W	$W_0 - W$
.57	.9082	.008503
	.91	.006703
	.913	.003703
	.916	.000703

the smallest corresponds to W closest to W_0. For the case $\tau = .57$, the amplitude decreases as $W_0 - W$ decreases, which is what we expect from the perturbation analysis. The phase diagram also shows that as $W_0 - W \to 0$, the solution becomes more symmetric. The solution curve for the largest value of $W_0 - W$ has its maximum value of f' closest to the saddle point. Table (3.2) shows how the distance from the maximum to the saddle point

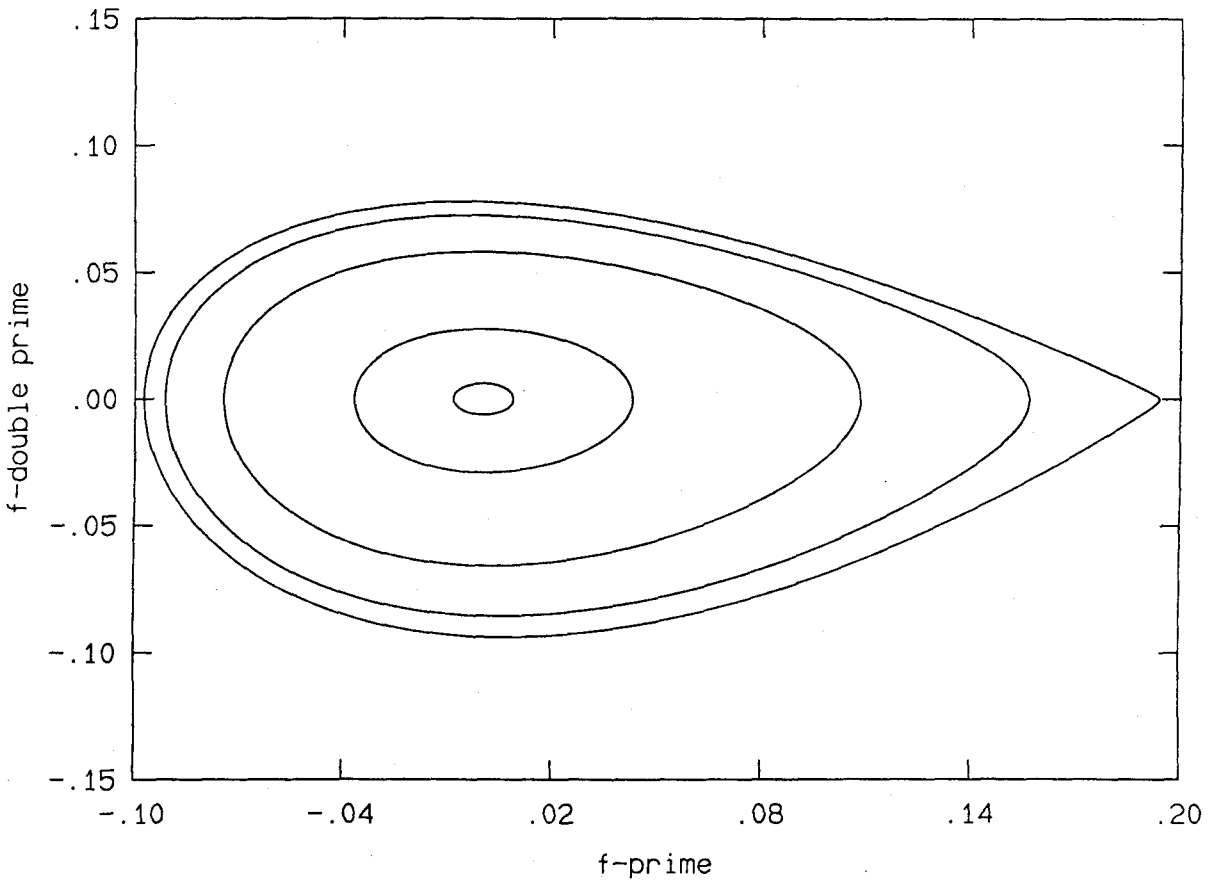

Figure 3.14: Phase diagrams for $\tau = .57$ and various values of W.

Table 3.2: Comparison of the maximum value of $f'(\xi)$ with the value of f' at the saddle point for the case of fixed τ and various W.

W	saddle point	maximum of f'	distance from the saddle point
.9082	.1959	.1938	.0021
.91	.1917	.1565	.0352
.913	.1849	.1085	.0764
.916	.1781	.0430	.1351

increases as $W_0 - W$ decreases. Since the location of the saddle point depends on W, it will be at a different place for each value of W.

We look now at the profiles for the velocity perturbations, $f'(\xi)$, figures (3.15) - (3.18). We see that the period decreases as the distance from the critical decreases. The perturbation expansion predicts that the amplitude will decrease with $W_0 - W$ since $\epsilon \propto \sqrt{W_0 - W}$. We compare the perturbation amplitude given by $2\mu_0\sqrt{\frac{W_0 - W}{W_0}}$ with the amplitudes given by the numerical calculation in table (3.3). We see that the agreement is good for $W_0 - W$

Table 3.3: Comparison of the amplitudes of the numerical solution, A_N with the amplitudes of the perturbation solution, A_p for the case of fixed τ and various W.

W	A_N	A_p	relative error $\frac{A_N - A_p}{A_N}$
.9082	.1456	.1379	5.0%
.91	.1239	.1225	1.0%
.913	.0915	.0910	0.5%
.916	.0397	.0397	0.1%

small and gets worse as $W_0 - W$ increases. For values of W closer to W_0

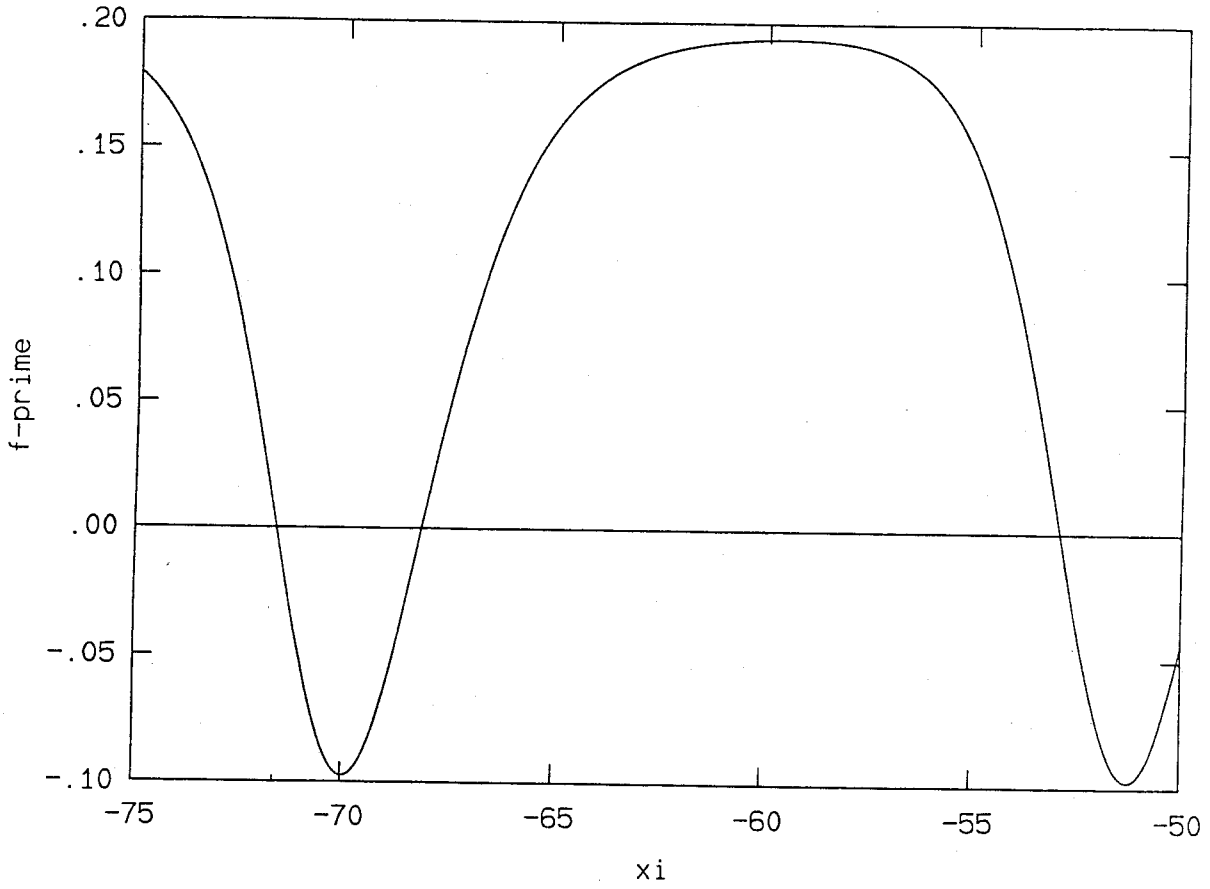

Figure 3.15: The velocity perturbation for $\tau = .57$, $W = .9082$

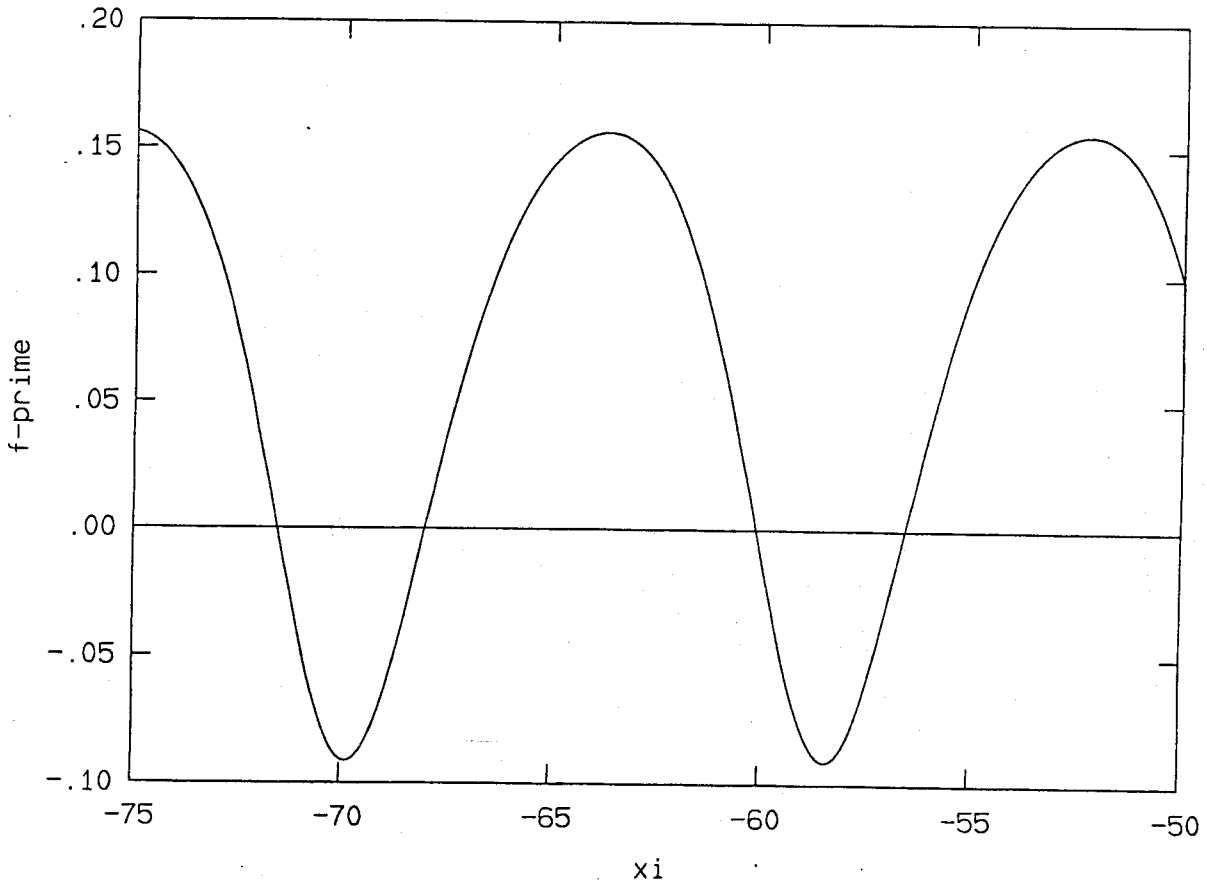

Figure 3.16: The velocity perturbation for $\tau = .57$, $W = .91$

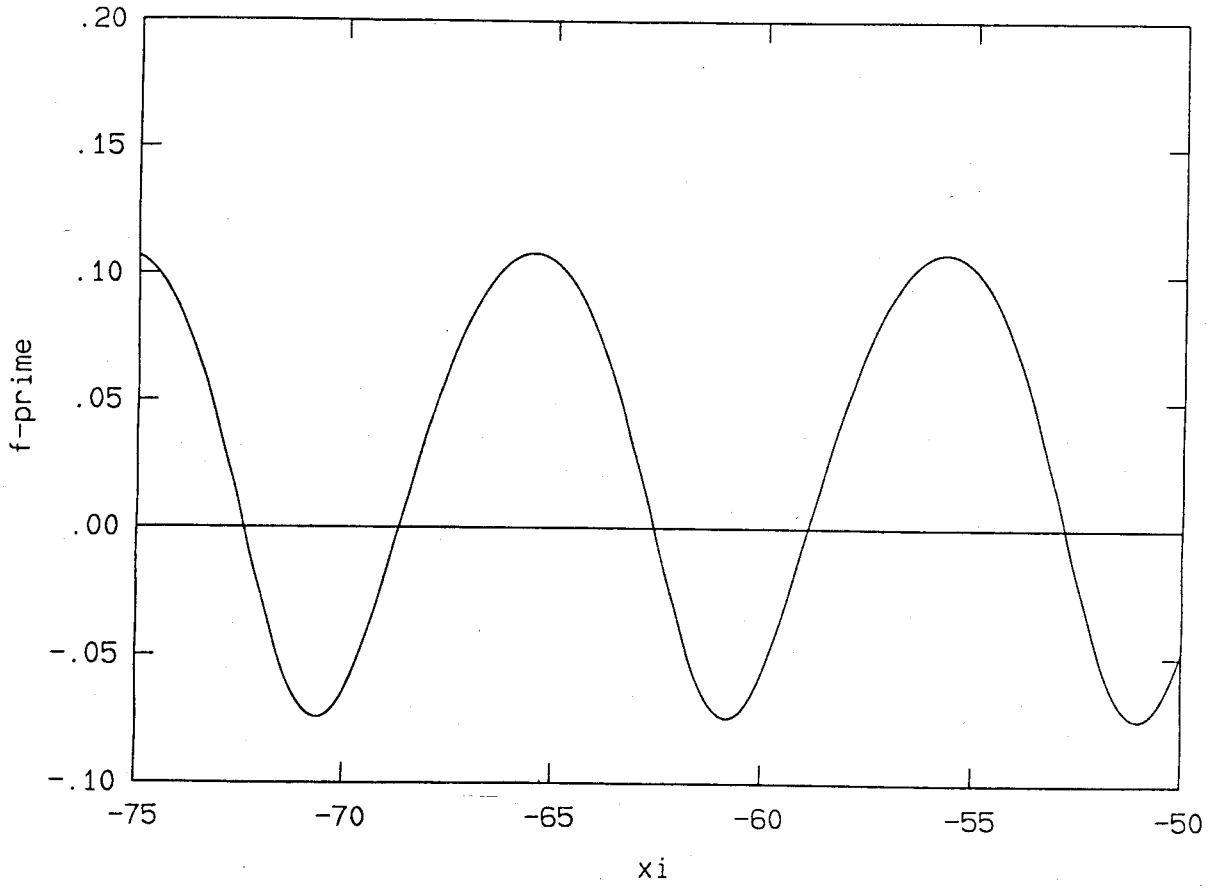

Figure 3.17: The velocity perturbation for $\tau = .57$, $W = .913$

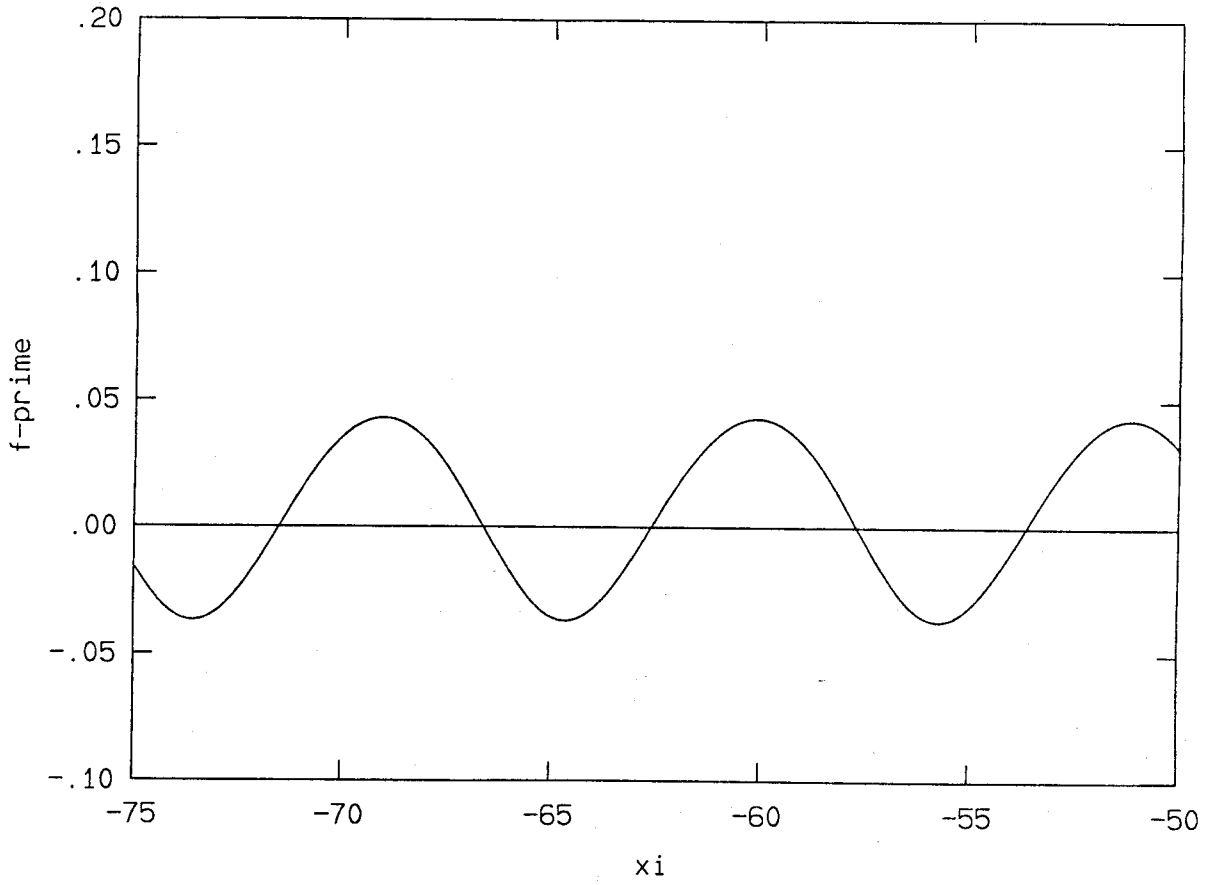

Figure 3.18: The velocity perturbation for $\tau = .57$, $W = .916$

than we show here, we found that the the relative error in the solution was quite large. This is because the solution is winding out to the limit cycle very tightly and thus, it is very difficult to tell when the solution has arrived at the limit cycle. The linear theory implies periodic solutions of arbitrary amplitude for $W = W_0$ and an outward spiral for $W < W_0$. The closer W is to W_0, the more tightly the solution will wind out. Thus, this tight winding to the limit cycle is consistant with the linear theory.

Looking at the period of the perturbation expansion, $\frac{2\pi}{\mu}$, with

$$\mu = \mu_0 - 2\frac{W_0 - W}{W_0}\frac{\sin\mu_0}{1 - W_0},$$

we see that it also decreases with $W_0 - W$. The difference from μ_0 , however, is not as pronounced in the perturbation as it is in the numerical calculations. Table (3.4) has the details of this comparison.

Table 3.4: Comparison of the period of the perturbation solution, $P_p = \frac{2\pi}{\mu}$, with the period of the computed solution, P_N, for the case of fixed τ and various W. Two terms are taken in the expansion for μ.

W	P_N	P_p	relative error $\frac{P_N - P_p}{P_N}$
.9082	18.75	11.03	41.0%
.91	11.52	10.46	9.0%
.913	9.79	9.63	1.6%
.916	8.95	8.93	0.2%

We look now at the shape of the velocity profiles and see that the largest value for $W_0 - W$ gives a shape which is very wide on top and narrow on the bottom and which also has the smallest percentage of its total amplitude

Table 3.5: The maximum and minimum values of $f'(\xi)$ and the percentage of the total amplitude (2A) which is negative for the case of fixed τ and various W. The percentage which is negative is $\frac{|min|}{max-min}$.

W	maximum	minimum	% negative
.9082	.1938	-.0974	33%
.91	.1565	-.0913	37%
.913	.1085	-.0745	41%
.916	.0430	-.0368	46%

less than zero, see table (3.5). As $W_0 - W$ decreases, the mean value of $f'(\xi)$ moves down towards zero, that is, the curves become more symmetric about zero. We compare the curves corresponding to $W = .916$ and $W = .9082$ to the perturbation solution in more detail. Figures (3.20) and (3.19) show the 2-term perturbation solution as the solid curve and the numerical solution as the dotted one and see that we have good agreement for $W = .916$ and the solution is very different from the perturbation for $W = .9082$.

We compare the computed mean values of the numerical solutions to those predicted by the perturbation expansion in table (3.6). The mean is

Table 3.6: Comparison of the mean value of $f'(\xi)$ from the numerical calculation, M_N, with the mean value from the perturbation expansion, M_p for the case of fixed τ and various W.

W	M_N	M_p	% difference = $\frac{M_N - M_p}{M_N}$
.9082	.1127	.0547	51%
.91	.0568	.0431	24%
.913	.0266	.0238	10%
.916	.0046	.0045	2%

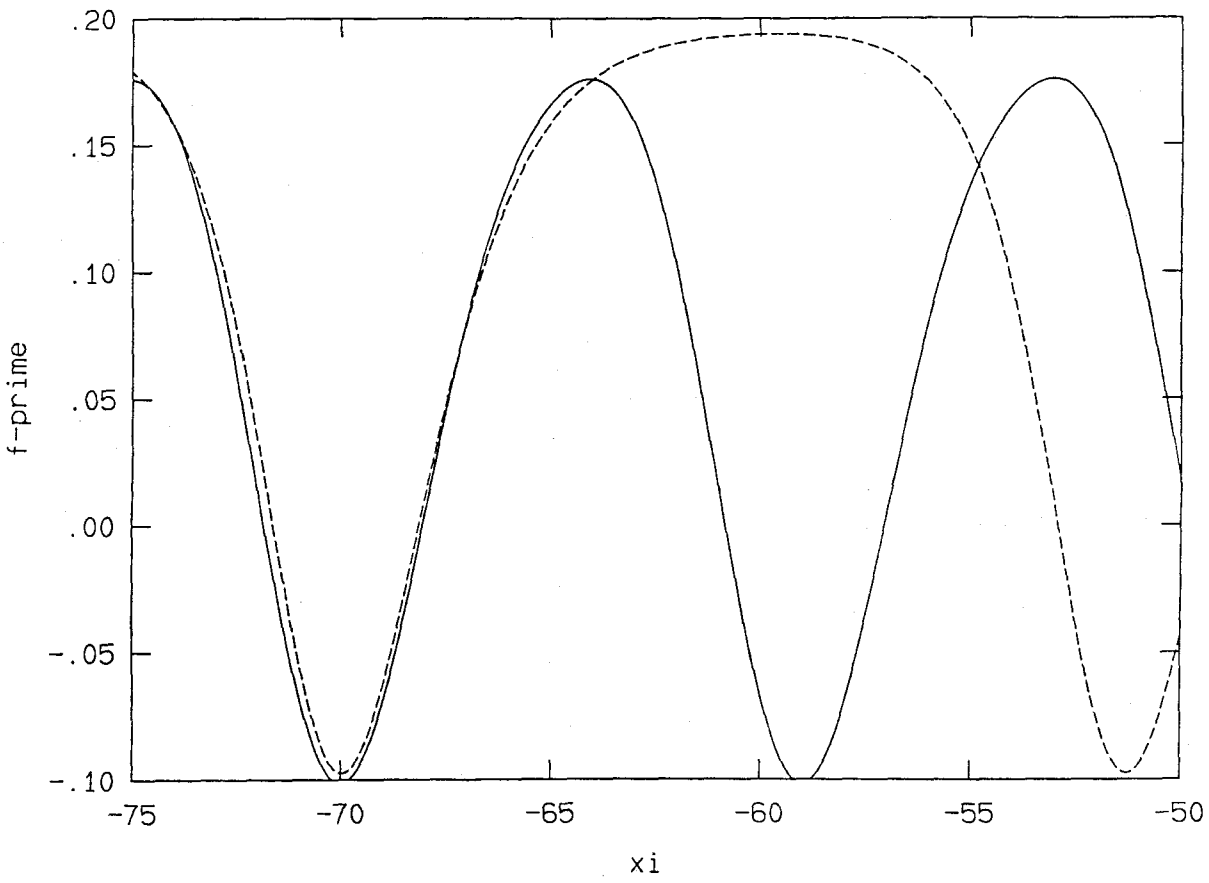

Figure 3.19: Comparison of the perturbation solution with the numerical solution for $\tau = .57$, $W = .9082$.

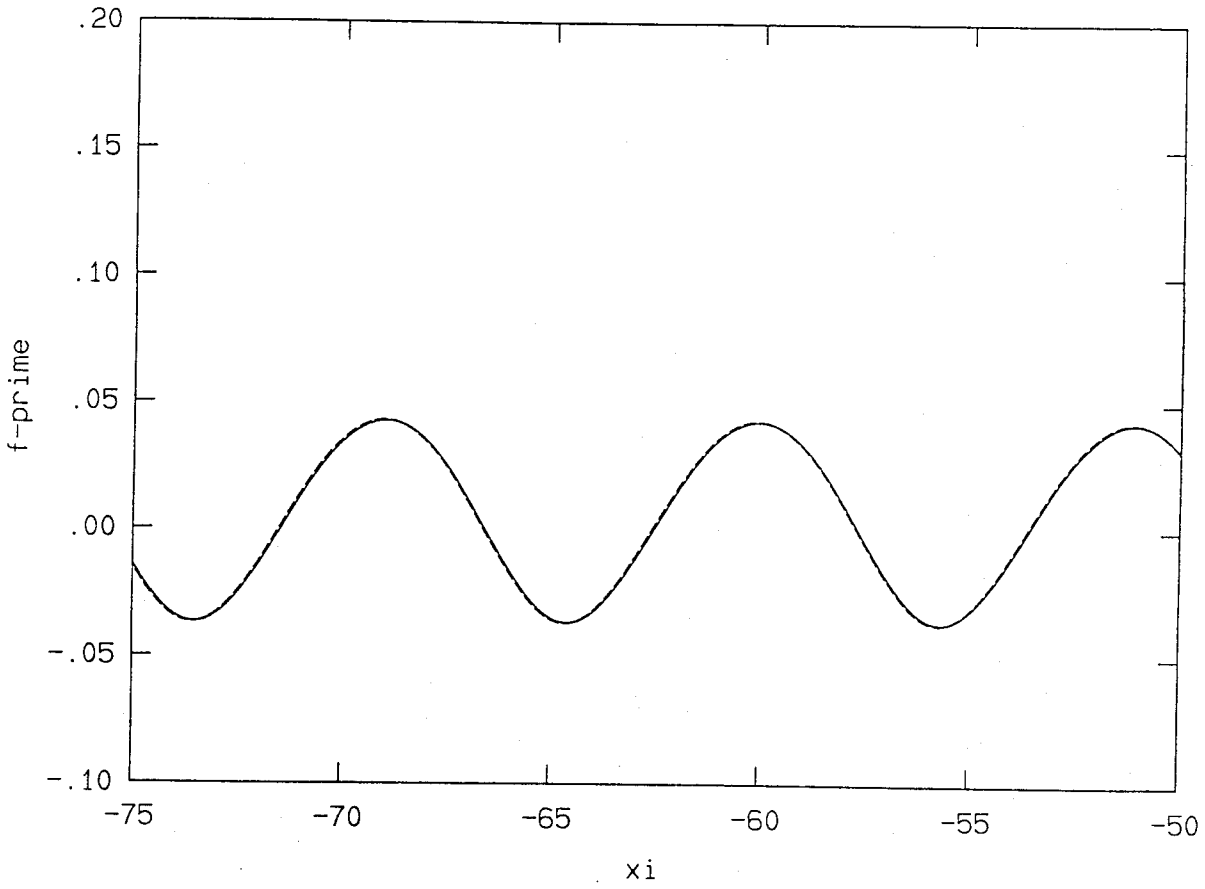

Figure 3.20: Comparison of the perturbation solution with the numerical solution for $\tau = .57$, $W = .916$.

computed by

$$M = \frac{1}{P}\int_a^{a+P} f'(\xi)d\xi = \frac{f(a+P) - f(a)}{P}$$

where P is the period. The function f is known from the numerical calculation and we find the period from $f'(\xi)$ which we know to be periodic ($f(\xi)$ is not). The perturbation prediction of the mean,

$$M_p = 2\frac{W_0 - W}{W_0}\frac{1 - \cos\mu_0}{1 - W_0},$$

is consistently smaller than the mean of the numerical calculations. For $W_0 - W$ at its largest value, the perturbation predicts a mean which is about half of the numerical mean. This case, however, is for a reasonably large value of ϵ and the shape is quite different from that of the 2-term perturbation expansion, as is seen in figure (3.19).

We see that qualitatively, the numerical calculations are in agreement with the predictions of the perturbation expansion, but when $W_0 - W$ is the largest that we have computed, the actual numbers do not agree so well. The amplitude, however, is getting quite large and we would not expect the perturbation expansion to do as well. The numerical solutions do, however, give us some information that the perturbation cannot. They tell us that for large amplitudes, the mean is tending towards the other steady state solution, the value at the saddle point, and that the curves are not sinusoidal for large ϵ.

Going back to the physical variable, v, we have that

$$v_n(t) = v_0 + \alpha W\frac{v_f}{\lambda}f'(\xi)$$

so that the amplitude of the velocity is $A_v = (v_f - v_0)WA_f$. For $v_0 = 20ft/sec$ and $v_f = 54ft/sec$, we see that this value varies from $A_v = 4.5ft/sec$ for $W = .9082$, to $A_v = .13ft/sec$ for $W = .9167$. Also, since the variable $\xi = \alpha Wt - n$, the period in ξ is related to the period in time by $P_t = \frac{1}{\alpha W} P_\xi$. Therefore, for $\lambda = .79/sec$, the period in time ranges from 41.29 sec for $W = .9082$ to 19.64 sec for $W = .916$. In terms of the number of cars, the period in ξ is the same as the period in n and thus ranges from 18 cars to 9 cars.

Maximum Amplitude Solutions for Various τ

We look at the numerical calculations another way now. We compare the solutions of the maximum amplitude for various τ. The maximum was determined from the value of W furthest from W_0 that gave a limit cycle. Values of W further from W_0 gave solutions which diverged. Since the phase portraits are very close to the saddle point for each τ, these solutions are close to the maximum possible amplitude. We vary τ from just above $1/2$, $\tau = .51$, up to $\tau = .6667$ which was an arbitrarily chosen stopping point. In each case we have varied W as far away from W_0 as was possible before the solution diverged.

We find that for the smallest value of τ, closest to $1/2$, this maximum amplitude was the smallest. As τ increases, the maximum amplitude for each τ increases. We know from the perturbation theory that the amplitude depends on the difference $W_0 - W$. Correspondingly, we find that we can choose W further from W_0 as τ increases and thus, we get larger amplitudes. Figure (3.21) shows the phase portraits for these various cases with table

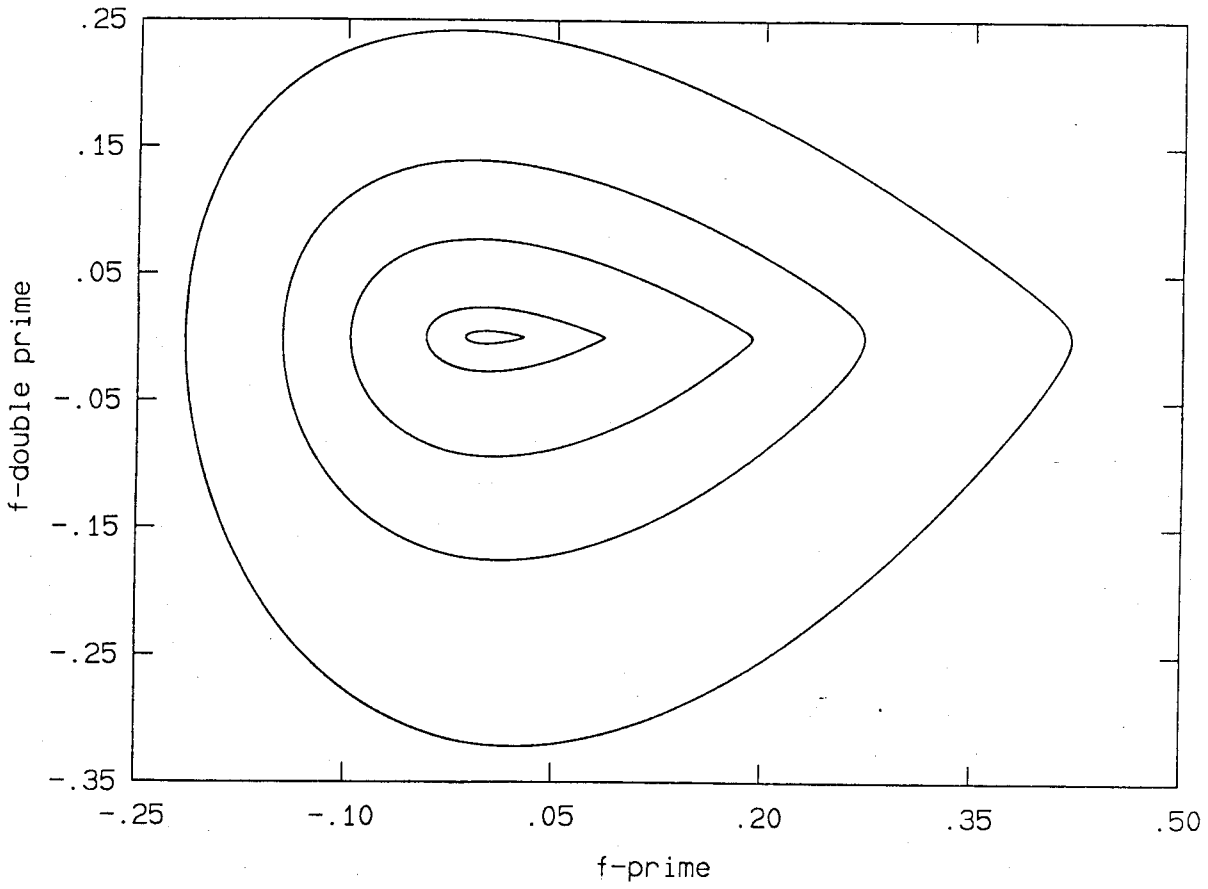

Figure 3.21: Final phase portraits for the case of maximum amplitudes for various τ.

(3.7) giving the values of τ, W and W_0 that were used. The largest solution

Table 3.7: The values of τ, W and W_0 for the case of maximum amplitude for various τ.

τ	W	W_0
.6667	.8100	.8270
.61	.8650	.8766
.57	.9082	.9167
.53	.9583	.9620
.51	.9855	.9869

Table 3.8: Comparison of the amplitudes of the perturbation solution, A_p with the amplitudes of the numerical solutions, A_N for the case of maximum amplitudes for various τ.

τ	A_N	A_p	% difference = $\frac{A_N - A_p}{A_N}$
.6667	.3182	.3000	5.7%
.61	.2090	.2019	3.4%
.57	.1456	.1379	4.5%
.53	.0605	.0594	1.9%
.51	.0209	.0211	-1.0%

is the solution for $\tau = .6667$ and the smallest corresponds to $\tau = .51$. Table (3.8) has the values of the amplitudes. We see that there are limit cycles for $W < W_0$ but $W > b$. The numerical solutions suggest that b depends on τ in such a way that the smaller τ gets, the closer b is to W_0. We see that the limiting condition on the amplitude to the right of zero is the saddle point. The location of the saddle point is an upper bound on $f'(\xi)$. Table (3.9) shows how close the maximum of f' is to the saddle point. Perhaps

Table 3.9: Comparison of the saddle point with the maximum value of $f'(\xi)$ for the case of maximum amplitude for various τ.

τ	saddle point	maximum of $f'(\xi)$	distance from the saddle point
.6667	. 4374	.4210	.0074
.61	.2974	.2722	.0253
.57	.1959	.1938	.0021
.53	.0858	.0786	.0072
.51	.0293	.0272	.0021

an explanation for the significantly smaller amplitudes for τ near $1/2$, is that for τ near $1/2$, $W_0 \sim 1$, and the saddle point, S, is near 0. Therefore, provided that we must choose W near W_0, we cannot expect to see a very large amplitude since S will be near 0.

Looking at the velocity profiles, figures (3.22) - (3.26), it is clear that the greatest amplitude comes from the largest value of τ as was seen from the phase diagram. We compare the values of the amplitude for the different values of τ in table (3.8). We also compare the numerical value of the amplitude to the perturbation expansion. Because we are looking at the largest amplitudes for each value of τ, we do not expect our numerical solution to compare very well with the perturbation theory.

We look now at the shape of the velocity profiles. They are significantly different from the 2-term expansion, this was seen in figure (3.19) of the previous set of figures. We see that all of the shapes have in common that they are wider on top than on bottom. We also see that the curve extends further above zero than below zero. For the cases shown here, the amount

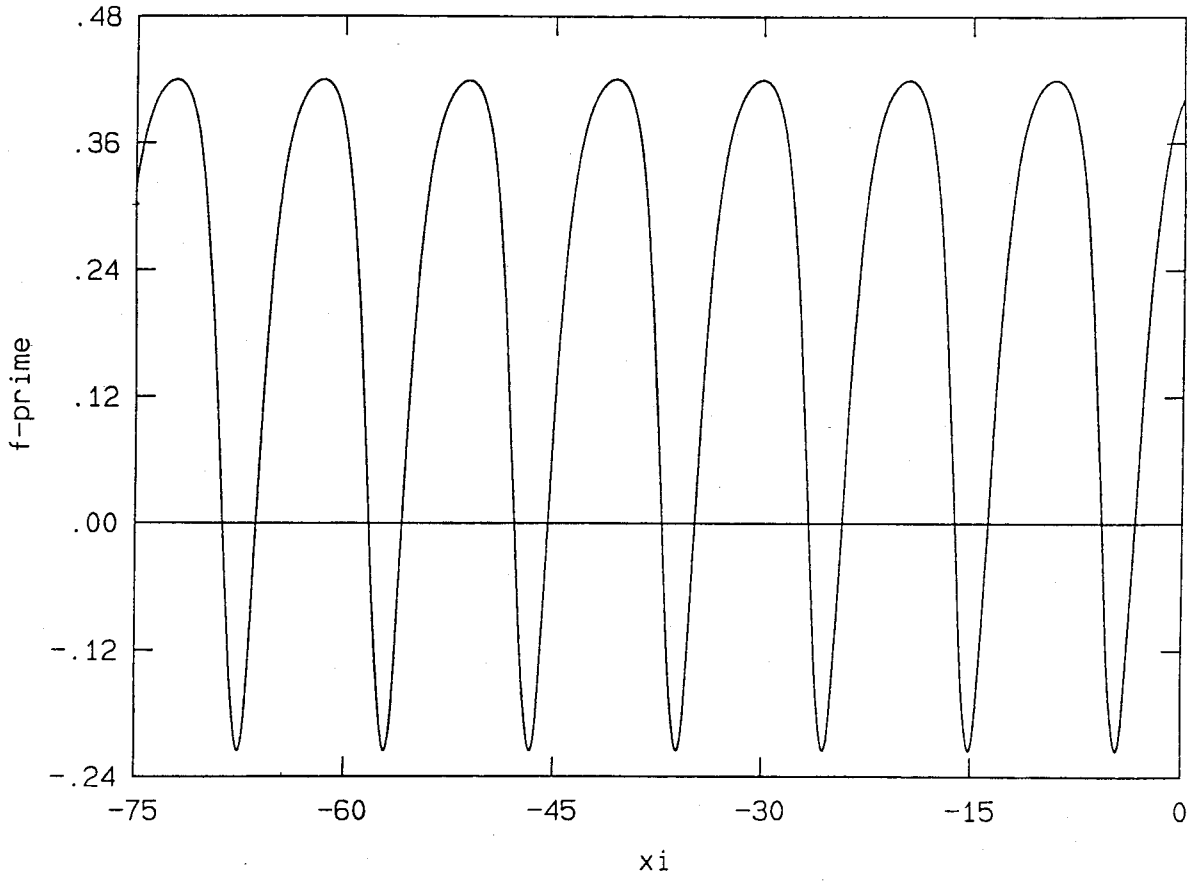

Figure 3.22: Velocity perturbation for $\tau = .6667$, $W = .81$.

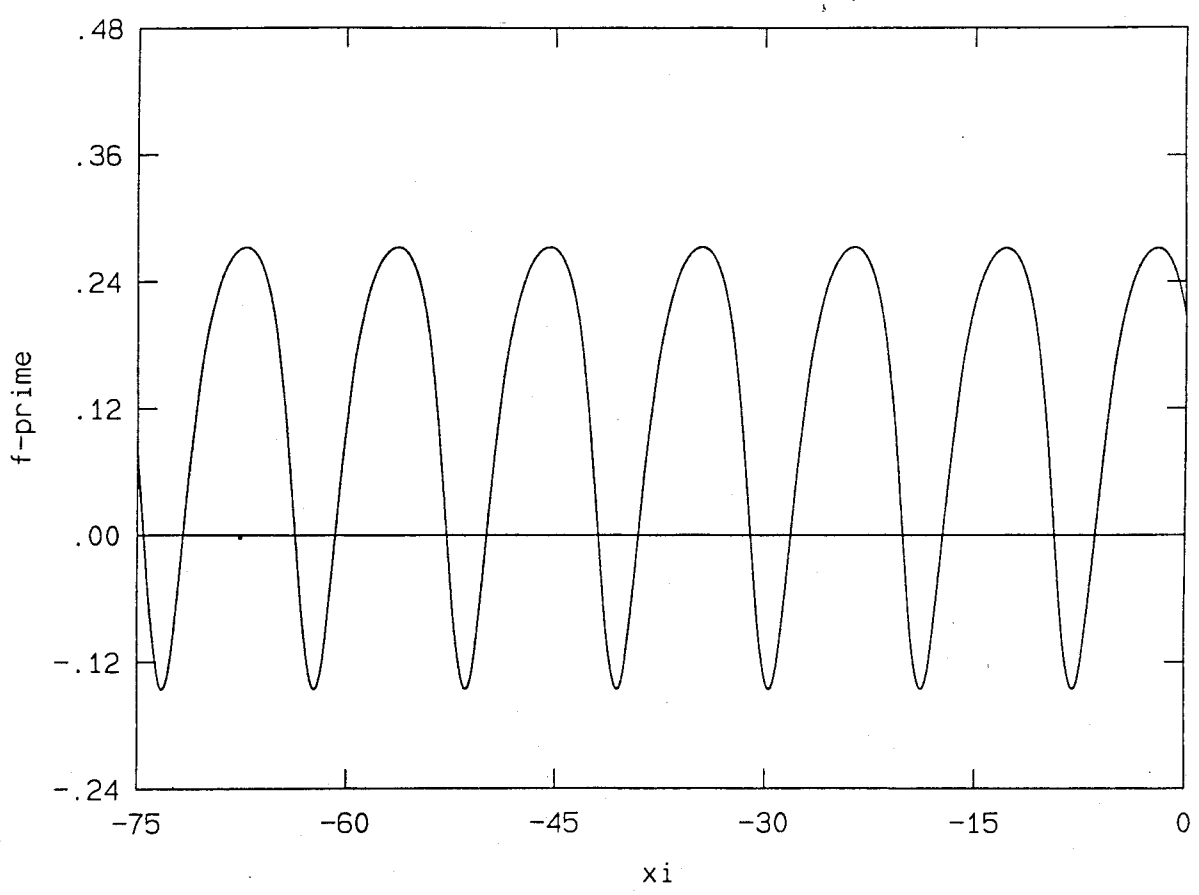

Figure 3.23: Velocity perturbation for $\tau = .61$, $W = .865$.

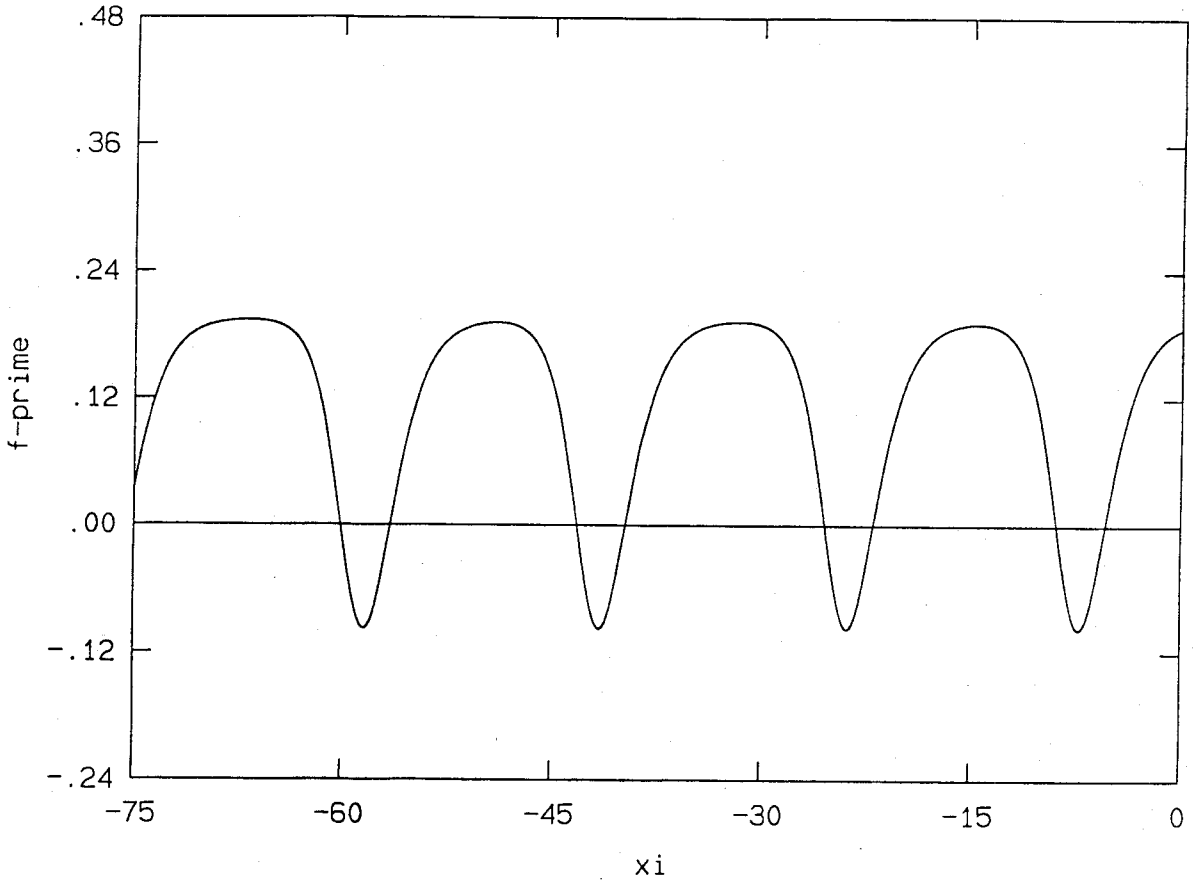

Figure 3.24: Velocity perturbation for $\tau = .57$, $W = .9082$.

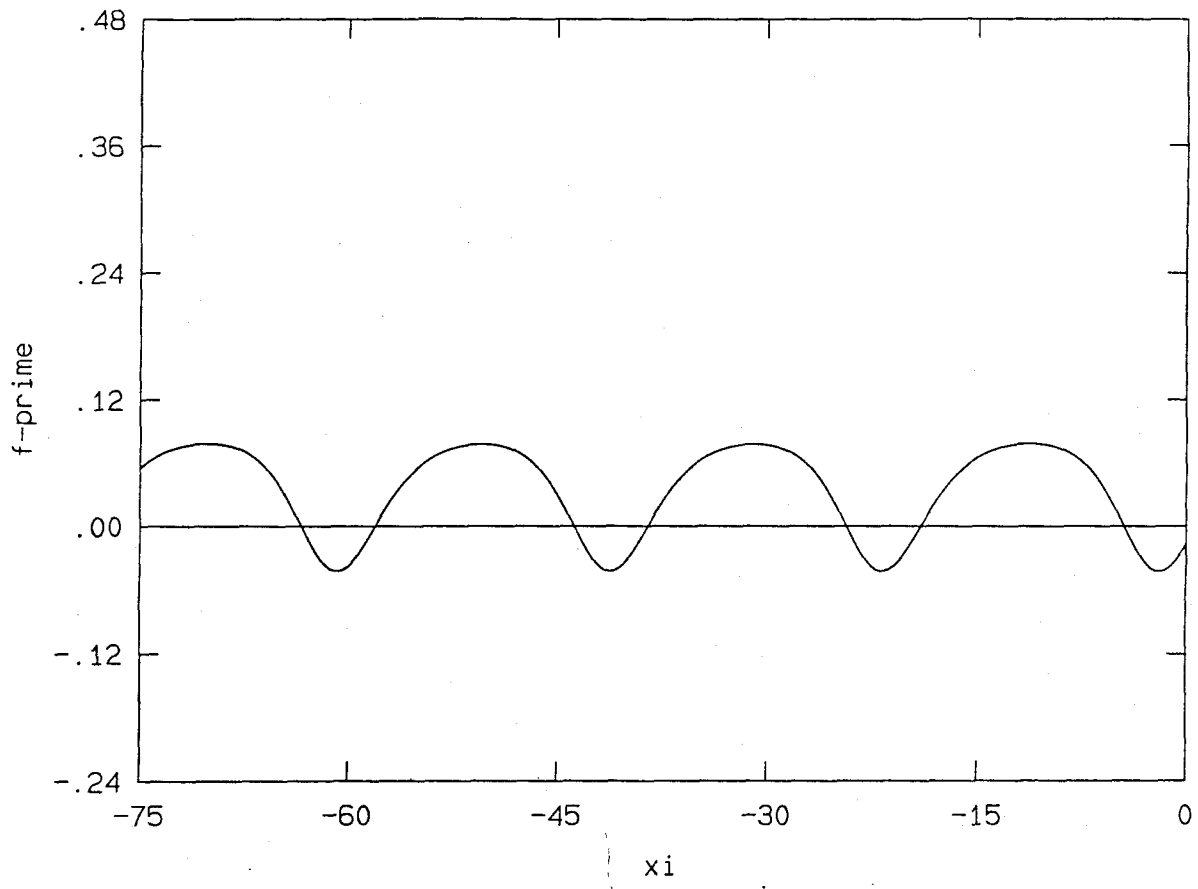

Figure 3.25: Velocity perturbation for $\tau = .53$, $W = .9583$.

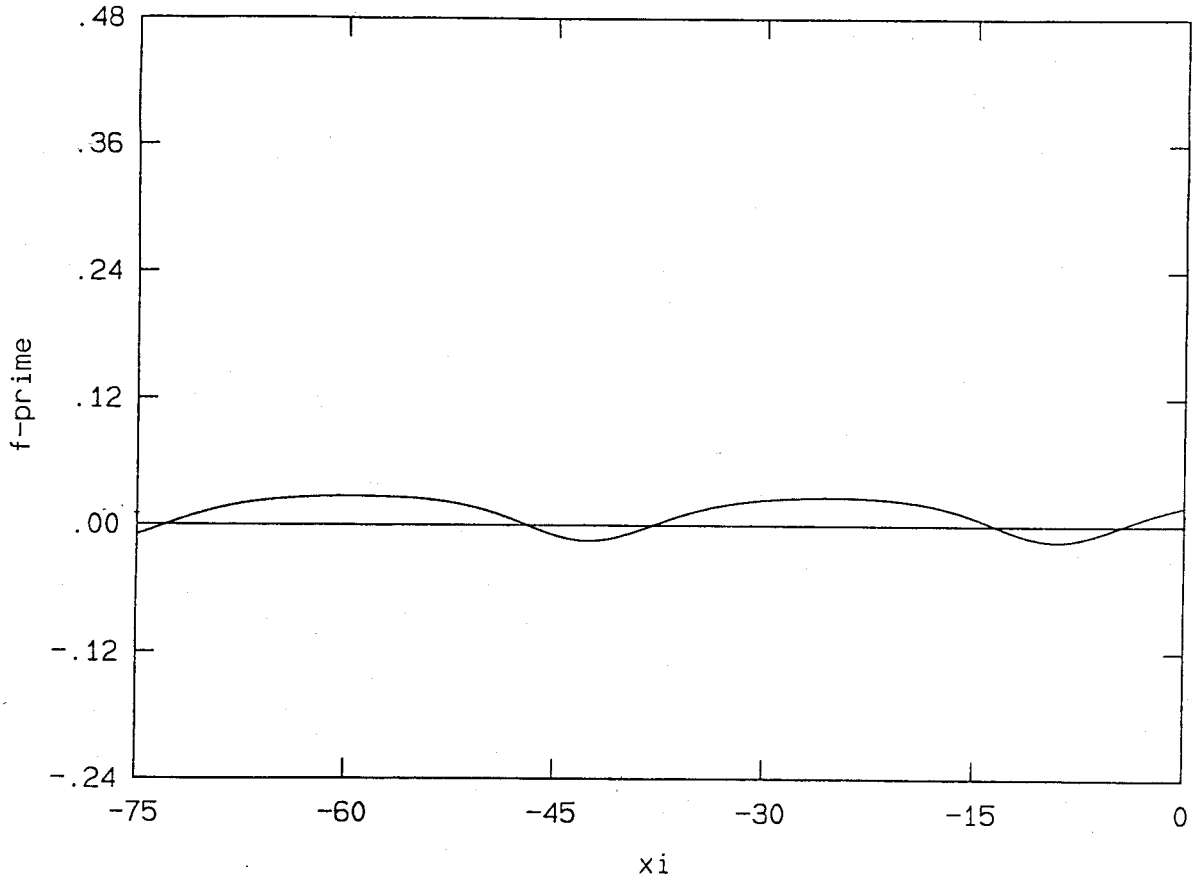

Figure 3.26: Velocity perturbation for $\tau = .51$, $W = .9855$.

of the curve below zero is between 33 and 35% of the distance from the maximum to the minimum. Table (3.10) shows this. This fact and the fact

Table 3.10: The maximum and minimum values of $f'(\xi)$ and the percentage of the total amplitude (2A) which is less than 0 for the case of maximum amplitudes for various τ.

τ	maximum	minimum	% less than 0 = $\frac{\lvert min \rvert}{max-min}$
.6667	.4210	-.2155	33%
.61	.2722	-.1459	35%
.57	.1938	-.0974	33%
.53	.0786	-.0424	35%
.51	.0272	-.0145	35%

that the curves are wider on top contribute to the mean value of $f'(\xi)$ being adjusted significantly above zero. This new mean was also predicted by the perturbation expansion. The perturbation expansion predicts a mean value for $f'(\xi)$ of

$$\frac{\lambda}{v_f}\epsilon^2 M_2 = 2\frac{W_0 - W}{W_0}\frac{1-\cos\mu_0}{1-W_0}.$$

In table (3.11), we compare the mean values of the numerical solution with those of the perturbation solution and we see that the numerical solution has a mean much higher than that of the perturbation expansion.

Qualitatively, at this point, we are in agreement with the results of the perturbation expansion, however, since we are looking at the extreme values of W for each τ, the actual numbers do not agree very well. From our analysis of the stationary points, we know that $f'(\xi) = S$ corresponds to a new mean flow different from v_0. We see that the maximum value of each of

Table 3.11: Comparison of the mean value of f' from the perturbation solution, M_p with the mean of the numerical solution, M_N for the case of maximum amplitudes for various τ.

τ	M_N	M_p	relative error $\frac{M_N - M_p}{M_N}$
.6667	.2103	.1186	44%
.61	.1184	.0774	35%
.57	.1127	.0547	51%
.53	.0343	.0227	34%
.51	.0122	.0085	31%

these curves is close to its corresponding value of S (table(3.9)). As we move further away from W_0, towards b, we see that the mean value of the function is moving up towards S. It would seem then, that if we could continue computing for greater values of $W_0 - W$, we would see the mean value of $f'(\xi)$ tending towards S with the top portion of the velocity curve getting wider and the bottom getting narrower. This is difficult to compute since we are approaching the saddle point. This means that we are getting close to the curve which heads directly into the saddle point. On one side of this curve we have a solution which diverges. Therefore, as we approach this curve, numerical errors can bump us onto the diverging solution curve. Typically, in ordinary differential equations, as the limit cycle nears the saddle point, the period increases and the limiting case which goes through the saddle point is a soliton, a curve which takes an infinite amount of time to return back to the saddle point. It is possible that our solutions do this also, but we do not see the periods diverging drastically from the perturbation solution. That is, we may see them twice the period of the perturbation solution, but no larger.

The periods are recorded and compared with the period of the perturbation solution in table (3.12). We can get periodic solutions of arbitrary period by

Table 3.12: Comparison of the periods of the numerical calculation, P_N with the periods of the perturbation solution, P_p for maximum amplitudes for various τ.

τ	P_N	P_p	relative error $\frac{P_N - P_p}{P_N}$
.6667	10.51	7.46	29%
.61	10.91	8.82	19%
.57	18.75	11.03	41%
.53	19.94	16.21	19%
.51	34.93	28.40	19%

varying τ. The choice of τ however, will limit the resulting amplitude.

Again, we relate these back to the physical variable, the velocity, and keep v_0 fixed at $20 ft/sec$. We have then that the amplitude of the velocity ranges from $A_v = 8.76 ft/sec$ for $\tau = .6667$, $W = .81$ to $A_v = .7 ft/sec$ for $\tau = .51$ and $W = .9855$. The period in time ranges from 70.89 sec for $\tau = .51$, $W = .9855$, to 25.95 sec for $\tau = .6667$, and $W = .81$.

Chapter 4

Periodic Solution for Discrete Time Lag

We now add the perturbation theory for the equation with a discrete time lag considered in Chapter 2. As in the case with the continuous reaction time, there will be a velocity shift. So we introduce perturbations by:

$$x_n(t) = y_n(t) - (h_0 + \tilde{D})n - (v_0 + \tilde{C})t$$
$$v_n(t) = \dot{y}_n - (v_0 + \tilde{C}),$$

where $\tilde{C}$ and $\tilde{D}$ accomodate changes in the mean velocity and headway. As in Chapter 3, we let $\chi = \Omega t - \mu n$ and $g(\chi) = y_n(t)$. We non-dimensionalize Ω and T with α by letting $\Omega = \alpha\omega$ and $\alpha T = \tau$ and normalize the equation as we did in Chapter 3 to obtain:

$$\omega f'(\chi + \omega\tau) + \frac{C}{\alpha} = 1 - e^{-[f(\chi+\mu)-f(\chi)+D]}.$$

The changes, C and D are second order, so the linear problem that we consider is:

$$\omega f'(\chi + \omega\tau) = f(\chi + \mu) - f(\chi).$$

The periodic solution is $f(\chi) = e^{i\chi}$ where ω satisfies:

$$\omega i e^{i\omega\tau} = e^{i\mu} - 1.$$

Separating real and imaginary parts, we find that

$$\omega = \frac{\mu}{2\tau}$$

and μ satisfies

$$\sin\frac{\mu}{2} = (\frac{\mu}{2})\frac{1}{2\tau}.$$

Thus, there is a periodic solution to the linear problem. We now go to the perturbation scheme to improve on this.

4.1 Perturbation Expansion for Small Amplitude Waves

We look for small amplitude waves using expansions

$$\begin{aligned} f &= \epsilon f_1 + \epsilon^2 f_2 + \cdots \\ \omega &= \omega_0 + \epsilon^2\omega_2 + \cdots \\ \mu &= \mu_0 + \epsilon^2\mu_2 + \cdots \\ C &= \epsilon^2 C_2 + \cdots \\ D &= \epsilon^2 D_2 + \cdots. \end{aligned}$$

After expanding $f'(\chi + \omega\tau)$, $f(\chi + \mu)$, and the exponential for small ϵ and equating like powers of ϵ, we find

$$\begin{aligned}
\epsilon^1: \quad & \omega_0 f_1'(\chi + \omega_0\tau) = f_1(\chi + \mu_0) - f_1(\chi) \\
\epsilon^2: \quad & \omega_0 f_2'(\chi + \omega_0\tau) + \tfrac{C_2}{\alpha} = f_2(\chi + \mu_0) - f_2(\chi) + D_2 \\
& \quad -\tfrac{1}{2}[f_1(\chi + \mu_0) - f_1(\chi)]^2 \\
\epsilon^3: \quad & \omega_0 f_3'(\chi + \omega_0\tau) + \omega_0\omega_2\tau f_1''(\chi + \omega_0\tau) + \omega_2 f_1'(\chi + \omega_0) = \\
& \quad f_3(\chi + \mu_0) - f_3(\chi) + \mu_2 f_1'(\chi + \mu_0) \\
& \quad -[f_1(\chi + \mu_0) - f_1(\chi)][f_2(\chi + \mu_0) - f_2(\chi)] \\
& \quad -D_2[f_1(\chi + \mu_0) - f_1(\chi)] + \tfrac{1}{6}[f_1(\chi + \mu_0) - f_1(\chi)]^3 \\
& \qquad \vdots
\end{aligned}$$

Here, f_1 is the linear solution of the last section with ω_0 and μ_0 determined by $\sin\frac{\mu_0}{2} = (\frac{\mu_0}{2})\frac{1}{2\tau}$ and $\omega = \frac{\mu_0}{2\tau}$. With $\omega_0\tau = \frac{\mu_0}{2}$, the equations take a more symetric form in the variable $\phi = \chi + \frac{\mu_0}{2}$. We then take the first order solution to be $f_1 = e^{i\phi} + e^{-i\phi} = 2\cos\phi$. In the order ϵ^2 equation, we see that the term

$$[f_1(\phi + \frac{\mu_0}{2}) - f_1(\phi - \frac{\mu_0}{2})]^2 = -4\sin^2\frac{\mu_0}{2}(e^{2i\phi} + e^{-2i\phi}) + 8\sin^2\frac{\mu_0}{2}$$

includes a constant term. We use C_2 and D_2 to eliminate this and get the relation:

$$\frac{C_2}{\alpha} = D_2 - 4\sin^2\frac{\mu_0}{2}.$$

This leaves us with the equation

$$\omega_0 f_1'(\phi) = [f_2(\phi + \frac{\mu_0}{2}) - f_2(\phi - \frac{\mu_0}{2})] - \frac{1}{2}(e^{i\frac{\mu_0}{2}} - e^{-i\frac{\mu_0}{2}})^2(e^{2i\phi} + e^{-2i\phi}).$$

To solve this, we let $f_2 = Ae^{2i\phi} + \tilde{A}e^{-2i\phi}$. We find that

$$A = \frac{1}{2i}\frac{\sin\frac{\mu_0}{2}}{1 - \cos\frac{\mu_0}{2}}$$

and that

$$f_2(\phi) = \frac{\sin\frac{\mu_0}{2}}{1 - \cos\frac{\mu_0}{2}}\sin 2\phi.$$

The third order equation is

$$\begin{aligned}
&\omega_0 f_3'(\phi) + \omega_0\omega_2\tau f_1''(\phi) + \omega_2 f_1'(\phi) = \\
&\quad f_3(\phi + \tfrac{\mu_0}{2}) - f_3(\phi - \tfrac{\mu_0}{2}) + \mu_2 f_1'(\phi + \tfrac{\mu_0}{2}) \\
&\quad -[f_1(\phi + \tfrac{\mu_0}{2}) - f_1(\phi - \tfrac{\mu_0}{2})][f_2(\phi + \tfrac{\mu_0}{2}) - f_2(\phi - \tfrac{\mu_0}{2})] \\
&\quad -D_2[f_1(\phi + \tfrac{\mu_0}{2}) - f_1(\phi - \tfrac{\mu_0}{2})] + \tfrac{1}{6}[f_1(\phi + \tfrac{\mu_0}{2}) - f_1(\phi - \tfrac{\mu_0}{2})]^3.
\end{aligned}$$

We must balance the terms involving $e^{i\phi}$ and $e^{-i\phi}$. We find that equating the $e^{i\phi}$ terms, we have the equation

$$\begin{aligned}
-\omega_2\omega_0\tau + \omega_2 i = \mu_2 i e^{i\frac{\mu_0}{2}} + 4i\frac{\sin^3\frac{\mu_0}{2}\cos\frac{\mu_0}{2}}{1-\cos\frac{\mu_0}{2}} \\
-2iD_2\sin\tfrac{\mu_0}{2} + 4i\sin^3\tfrac{\mu_0}{2}.
\end{aligned}$$

Equating the real parts, we obtain

$$\omega_0\omega_2\tau = \mu_2 \sin\frac{\mu_0}{2}$$

which is equivalent to

$$\mu_2 = 2\tau\omega_2.$$

Equating the imaginary parts yields

$$\omega_2(1 - 2\tau\cos\frac{\mu_0}{2}) = 4\frac{\sin^3\frac{\mu_0}{2}\cos\frac{\mu_0}{2}}{1-\cos\frac{\mu_0}{2}} + 4\sin^3\frac{\mu_0}{2} - 2D_2\sin\frac{\mu_0}{2}.$$

After some algebra, this can be rewritten as

$$\omega_2 = 4\frac{\sin\frac{\mu_0}{2}}{1-2\tau\cos\frac{\mu_0}{2}}(1+\cos\frac{\mu_0}{2} - \frac{D_2}{2})$$

and from this, we find that

$$\mu_2 = 8\tau\frac{\sin\frac{\mu_0}{2}}{1-2\tau\cos\frac{\mu_0}{2}}(1-2\tau\cos\frac{\mu_0}{2}).$$

Thus, to third order in our perturbation expansion, we do have a periodic solution:

$$\begin{aligned}
f(\phi) &= 2\epsilon\cos\phi + \epsilon^2\tfrac{\sin\frac{\mu_0}{2}}{1-\cos\frac{\mu_0}{2}}\sin 2\phi + \bigcirc(\epsilon^3)\\
\mu &= \mu_0 + \epsilon^2\tfrac{8\tau\sin\frac{\mu_0}{2}}{1-2\tau\cos\frac{\mu_0}{2}}(1+\cos\tfrac{\mu_0}{2} - \tfrac{D_2}{2}) + \bigcirc(\epsilon^4)\\
\omega &= \tfrac{\mu_0}{2\tau} + \epsilon^2\tfrac{\mu_2}{2\tau} + \bigcirc(\epsilon^4)\\
\tfrac{C}{\alpha} &= \epsilon^2(D_2 - 4\sin^2\tfrac{\mu_0}{2}) + \bigcirc(\epsilon^4)
\end{aligned}$$

where D is arbitrary and μ_0 is determined from $\sin\frac{\mu_0}{2} = \frac{\mu_0}{2}\frac{1}{2\tau}$.

We cannot compute the solution to this equation in the same way that we did in Chapter 3. The problem is that we now have two delays. If we give the information needed on the appropriate intervals to get started and try to compute this as an initial value problem, we see that as ϕ is increased or

decreased, the solution will be obtained at a point inside the interval where the initial data was given and possibly give conflicting information. Also, in terms of the parameter $W = \frac{\omega}{\mu}$, we see that $W = W_0$ to second order:

$$W = \frac{1}{2\tau} + \bigcirc(\epsilon^4).$$

Thus, if W_4, say, is non-zero, to find limit cycles, W must be closer to W_0 than it was in Chapter 3 for the same value of ϵ. It is possible that there are no limit cycles at all for this problem but periodic solutions only for $W \equiv W_0$ and for no other values of W. To determine this, one would need to show this was true for all orders in the perturbation. There are, in fact, periodic solutions for $W \equiv W_0$, obtained by G.B. Whitham earlier this year. Thus, periodic solutions are possible but it is not clear that they will be found in the form of limit cycles.

Chapter 5

Periodic Solutions to a Continuous Traffic Flow Model

We know from Chapter 1 that there is a periodic solution to the continuous traffic flow equations studied there supplemented by discontinuous shocks. We would like to get a smooth periodic solution to some modified continuous equations. For the roll waves problem of shallow water theory, Needham and Merkin found periodic solutions by adding on a higher derivative term, as is a standard approach to smoothing out discontinuous shocks. To get some idea of what kind of higher order term to add on to the equations from Chapter 1, we relate this set of continuous traffic flow equations,

$$\begin{aligned} &\rho_t + (v\rho)_x = 0 \\ &v_t + vv_x = -\tfrac{1}{\tau}[v - V(\rho) + \tfrac{\nu}{\rho}\rho_x], \end{aligned} \tag{5.1}$$

to the car following model,

$$v_n(t) + T\dot{v}_n(t) = G(x_{n-1}(t) - x_n(t)). \tag{5.2}$$

5.1 Derivation of Additional Terms

Since car following models are naturally given in Lagrangian coordinates, (the cars are analogous to particles in fluid dynamics and n is the label) we first convert the continuous traffic equations, equations 5.1, to Lagrangian form. We do this by introducing $x = x(a,t)$ and $v = v(a,t)$ where a is a label identifying individual cars ('particles'). We have the relations:

$$(\frac{\partial}{\partial t})|_a = \frac{\partial}{\partial t} + v\frac{\partial}{\partial x}$$

and

$$\frac{\partial}{\partial a} = x_a\frac{\partial}{\partial x}.$$

From these relations, the first of equations (5.1) becomes

$$(\frac{\partial \rho}{\partial t})|_a + \frac{\rho}{x_a}x_{ta} = 0 \tag{5.3}$$

or equivalently,

$$(\rho x_a)_t = 0;$$

this can also be established directly from the car following variables. This says that ρx_a is constant, say $\frac{1}{b}$. Solving for x_a and substituting this into equation (5.3), we have

$$(\frac{\partial \rho}{\partial t})|_a + b\rho^2\frac{\partial v}{\partial a} = 0.$$

Setting $\rho = \frac{1}{h}$ in this equation we have

$$\frac{\partial h}{\partial t} - b\frac{\partial v}{\partial a} = 0. \tag{5.4}$$

When the substitutions

$$\frac{\partial v}{\partial t} + v\frac{\partial v}{\partial x} = (\frac{\partial v}{\partial t})|_a$$

and

$$x_a = \frac{1}{\rho b}$$

are made in the second of equations (5.1), we have the equation

$$\tau(\frac{\partial v}{\partial t})|_a + v = V(\rho) - \frac{\nu}{\rho}\rho_x,$$

which in terms of h is:

$$\tau\frac{\partial v}{\partial t} + v = G(h) + \frac{\nu}{h^2}bh_a,$$

where $V(\rho) = G(h)$. If we take $\tau = T$ and $\nu = -\frac{1}{2}V'(\rho)$ we have $\nu = \frac{h^2}{2}G'(h)$ and the equations become

$$\begin{aligned} v + Tv_t &= G(h) + \tfrac{1}{2}bh_aG'(h) \\ h_t - bv_a &= 0. \end{aligned} \tag{5.5}$$

We now see how these compare with the discrete model, (5.2). The car following model could be written as a differential-delay equation rather than a differential-difference equation, (the differencing in x is replaced by a delay). This is done by setting $x_n(t) = X(-bn, t)$, where $-bn$ is, say, the position of the n^{th} car in some uniform initial state. If we let the variable, $a = -bn$, then $x_{n-1}(t) - x_n(t) = X(a + b, t) - X(a, t)$, and the equation becomes

$$v(a,t) + T\frac{\partial v}{\partial t} = G(X(a + b, t) - X(a, t)).$$

We note that expanding $X(a + b, t)$ for b small results in the equation

$$v(a,t) + T\frac{\partial v}{\partial t} = G(bX_a(a,t) + \frac{1}{2}b^2X_{aa}(a,t) + \cdots),$$

where b is small in comparison with the distance a long line of cars occupies. To compare with (5.5), we introduce $bX_a(a,t) = h$. Since $v = X_t(a,t)$, we have the identity

$$h_t - bv_a = 0.$$

This agrees with equation (5.4). We expand G for b small and obtain the equation

$$v(a,t) + T\frac{\partial v}{\partial t} = G(h) + \frac{1}{2}bh_aG'(h) + b^2[\frac{1}{8}h_a^2G''(h) + \frac{1}{6}h_{aa}G'(h)] + \cdots.$$

The left side of the equation is the same as the left side of the Lagrangian version of the continuous equation. The first two terms of the right side of this equation match up with the continuous equation also. Therefore, if we want to add higher derivative terms to the continuous equations, a good candidate would be the term

$$b^2[\frac{1}{8}h_a^2G''(h) + \frac{1}{6}h_{aa}G'(h)].$$

This choice should compare well with the periodic solutions to the car following equation studied in Chapter 3. This approach links the coefficients of the derivatives explicitly to the discrete model. These coefficients could be freed of this connection to include the same effects but in a more general model.

5.2 Steady Profile Wave Equation

We now study the continuous equations

$$\begin{aligned} &h_t - bv_a = 0 \\ &v + Tv_t = G(h) + \tfrac{1}{2}bh_aG'(h) + b^2[\tfrac{1}{8}h_a^2G''(h) + \tfrac{1}{6}h_{aa}G'(h)], \end{aligned}$$

with Newell's G:

$$G(h) = v_f(1 - e^{\frac{\lambda}{v_f}(h-L)}).$$

Relating these variables to those of the car following equation, we have

$$\begin{aligned} v(a,t) &= v_n(t) \\ h(a,t) &\approx x_{n-1}(t) - x_n(t). \end{aligned}$$

We let $a = b\hat{a}$ in order to eliminate b and obtain the equations

$$\begin{aligned} &h_t - v_{\hat{a}} = 0 \\ &v + Tv_t = G(h) + \tfrac{1}{2}h_{\hat{a}}G'(h) + \tfrac{1}{8}h_{\hat{a}}^2G''(h) + \tfrac{1}{6}h_{\hat{a}\hat{a}}G'(h). \end{aligned} \tag{5.6}$$

We look for steady profile waves by setting $\xi = Ut + \hat{a}$. The first equation of (5.6) becomes

$$Uh_\xi - v_\xi = 0$$

which, when integrated becomes

$$v - Uh = B = const. \tag{5.7}$$

The second equation of (5.6) becomes

$$v + TUv_\xi = G(h) + \frac{G'(h)}{2}h_\xi + \frac{1}{8}G''(h)h_\xi^2 + \frac{1}{6}G'(h)h_{\xi\xi}. \tag{5.8}$$

Solving (5.7) for v in terms of h and substituting this into (5.8), we have

$$\frac{1}{6}G'(h)h_{\xi\xi} = -\frac{1}{8}G''(h)h_\xi^2 + [U^2T - \frac{G'(h)}{2}]h_\xi + B + Uh - G(h). \tag{5.9}$$

We write this as

$$\tilde{P}(h)h_{\xi\xi} = \tilde{Q}(h)h_\xi^2 + \tilde{R}(h)h_\xi + \tilde{S}(h)$$

where $\tilde{P}$, $\tilde{Q}$, $\tilde{R}$ and $\tilde{S}$ are the corresponding coefficients in equation (5.9).

5.3 Singular Points and Stability

We expect from Chapter 3 that there will be a limit cycle around the point $h = h_0$, $v = v_0$. We first look at the linearized problem. This will give the critical wave speed. Analysis of the singular points determines whether or not we have an unstable spiral as a candidate for a limit cycle. The other singular point will give a possible bound on the amplitude. We normalize the equation by setting $\eta = \frac{\lambda}{v_f}(h - h_0)$ and fix B from the uniform state as $B = Uh_0 + v_0$. For $\tilde{S}(h)$, we then have

$$\tilde{S}(h) = U(h - h_0) - [G(h) - G(h_0)].$$

We introduce $h = \frac{v_f}{\lambda}\eta + h_0$ and note that

$$G(h) = v_f(1 - e^{-\frac{\lambda}{v_f}(h-L)}) = v_f(1 - \frac{\alpha}{\lambda}e^{-\eta})$$

where $\alpha = G'(h_0)$. We also let $W = \frac{U}{\alpha}$ and $\tau = \alpha T$ so that finally in (5.9), we have

$$P(\eta)\eta_{\xi\xi} = Q(\eta)\eta_\xi^2 + R(\eta)\eta_\xi + S(\eta) \tag{5.10}$$

where

$$\begin{aligned} P(\eta) &= \tfrac{1}{6}e^{-\eta} \\ Q(\eta) &= \tfrac{1}{8}e^{-\eta} \\ R(\eta) &= W^2\tau - \tfrac{1}{2}e^{-\eta} \\ S(\eta) &= W\eta - (1 - e^{-\eta}). \end{aligned}$$

We now consider the singular points of the full nonlinear equation, equation (5.10). We first set $f = \eta_\xi$, $f_\xi = \eta_{\xi\xi}$ and obtain the system of equations

$$\begin{aligned} \tfrac{df}{d\xi} &= \tfrac{Q(\eta)f^2 + R(\eta)f + S(\eta)}{P(\eta)} \\ \tfrac{d\eta}{d\xi} &= f. \end{aligned}$$

The singular point are at $f = 0$, $S(\eta) = 0$. Setting $S(\eta) = 0$, we have

$$W\eta = 1 - e^{-\eta}.$$

$S(\eta)$ has two zeros, one at $\eta = 0$ corresponding to $h = h_0$, and one other point. If $W < 1$, the intersection is for $\eta > 0$. If $W > 1$, the intersection is for $\eta < 0$.

The linear equation about the point (0,0) is

$$\frac{1}{6}\eta_{\xi\xi} = (W^2\tau - \frac{1}{2})\eta_\xi + (W-1)\eta.$$

It has solutions of the form $\eta = e^{\lambda\xi}$ where λ satisfies

$$\lambda^2 - 6(W^2\tau - \frac{1}{2})\lambda - 6(W-1) = 0.$$

Solving the quadratic equation, we find

$$\lambda = \frac{1}{2}[(W^2\tau - \frac{1}{2}) \pm \sqrt{36(W^2\tau - \frac{1}{2})^2 + 24(W-1)}].$$

There are period solutions when λ is pure imaginary, $\lambda = i\mu$, where

$$\mu = \sqrt{6(1-W)}, \qquad W = \frac{1}{\sqrt{2\tau}}.$$

For μ to be real, we require $W < 1$ which in turn requires $\tau > 1/2$. When W is different from $\frac{1}{2\tau}$, λ has a non-zero real part, and a non-zero imaginary part provided $W < 1$. Thus, the point (0,0) is a spiral. The stability of the spiral depends on the sign of $W^2\tau - \frac{1}{2}$. For $W > \frac{1}{\sqrt{2\tau}}$, we have $W^2\tau - \frac{1}{2} > 0$, and we have an unstable spiral for $\xi > 0$. For $W < \frac{1}{\sqrt{2\tau}}$ we have $W^2\tau - \frac{1}{2} < 0$, and this gives an unstable spiral for $\xi < 0$. The perturbation will determine which

side of the critical W that we will find limit cycles, and this will determine whether we find limit cycles for ξ positive or negative.

We look at the second singular point, $\eta = \eta^*$ where $\eta^* \neq 0$ and where η^* satisfies

$$W\eta^* = 1 - e^{-\eta^*}. \tag{5.11}$$

We linearize equation (5.10) about $\eta = \eta^*$ and we obtain the equation

$$\frac{e^{-\eta^*}}{6}\eta_{\xi\xi} = (W^2\tau - \frac{1}{2}e^{-\eta^*})\eta_\xi + (W - e^{-\eta^*})(\eta - \eta^*).$$

We let $\eta - \eta^* = e^{\lambda\xi}$ and obtain

$$\frac{e^{-\eta^*}}{6}\lambda^2 = (W^2\tau - \frac{1}{2}e^{-\eta^*})\lambda + W - e^{-\eta^*}.$$

and therefore

$$\lambda = 3e^{\eta*}[W^2\tau - \frac{1}{2}e^{-\eta^*} \pm \sqrt{(W^2\tau - \frac{1}{2}e^{-\eta^*})^2 + \frac{2}{3}e^{-2\eta^*}(We^{\eta^*} - 1)}].$$

From (5.11), we have

$$We^{\eta^*} = \frac{e^{\eta^*} - 1}{\eta^*} > 0$$

and thus, the quantity inside the square root is positive and the point $\eta = \eta^*$, $f = 0$ is a saddle point. Therefore, if we do have a limit cycle, we expect that η^* will bound the amplitude on the positive end. We now go to the perturbation expansion to see whether it shows periodic solutions and, if so, which side of W_0 they are found.

5.4 Perturbation Expansion

We introduce $\theta = \mu\xi$ into (5.10) so the equation becomes

$$\mu^2 P(\eta)\eta_{\theta\theta} = \mu^2 Q(\eta)\eta_\theta^2 + \mu R(\eta)\eta_\theta + S(\eta),$$

and use expansions

$$\eta(\theta) = \epsilon\eta_1 + \epsilon^2\eta_2 + \cdots$$
$$\mu = \mu_0 + \epsilon^2\mu_2 + \cdots$$
$$W = W_0 + \epsilon^2 W_2 + \cdots.$$

From successive powers of ϵ, we obtain

$$\begin{aligned}
\epsilon^1 : \quad & \mu_0^2\eta_1'' = -6(1-W_0)\eta_1 \\
\epsilon^2 : \quad & \mu_0^2\eta_2'' = \tfrac{3}{4}\mu_0^2(\eta_1')^2 + 3\mu_0\eta_1'\eta_1 + (6W_0-3)\eta_1^2 - 6(1-W_0)\eta_2 \\
\epsilon^3 : \quad & \mu_0^2\eta_3'' + 2\mu_0\mu_2\eta_1'' = \tfrac{3}{2}\mu_0^2\eta_1'\eta_2' + 3\mu_0\eta_1'\eta_2 + \tfrac{3}{2}\mu_0\eta_1^2\eta_1' \\
& +12W_0W_2\tau\mu_0\eta_1' + 3\mu_0\eta_1\eta_2' + 6W_2\eta_1 + 12W_0\eta_1\eta_2 \\
& +(3W_0-1)\eta_1^3 - 6\eta_1\eta_2 - 6(1-W_0)\eta_3 \\
& \vdots
\end{aligned}$$

where in some of the terms we have used the relation from the solution to the linear problem that $W_0^2\tau - \frac{1}{2} = 0$.

The ϵ-equation is solved by $\eta_1 = e^{i\theta} + e^{-i\theta}$, $\mu_0^2 = 6(1-W_0)$, repeating the linear equation.

The ϵ^2-equation has a solution in the form

$$\eta_2 = Ae^{2i\theta} + \bar{A}e^{-2i\theta} + M.$$

The constant M is required because of the squared terms, $(\eta_1')^2$ and η_1^2. On substituting this into the ϵ^2-equation, we find that

$$M = \frac{1}{\mu_0^2}(6 - \frac{7}{2}\mu_0^2)$$

and

$$A = \frac{1}{\mu_0^2}(\frac{\mu_0^2}{12} - 1 - \mu_0 i).$$

In terms of sines and cosines, we have that

$$\eta_2(\theta) = \frac{1}{\mu_0^2}\{(\frac{\mu_0^2}{6} - 2)\cos 2\theta + 2\mu_0 \sin 2\theta + 6 - \frac{7}{2}\mu_0^2\}.$$

From the third order equation, we only want to find W_2 and μ_2. These will come from balancing the $e^{i\theta}$ and $e^{-i\theta}$ terms in the usual way. We find that

$$W_2 = \frac{15}{8} - \frac{3}{2\mu_0^2} - \frac{13}{48}\mu_0^2,$$
$$\mu_2 = \frac{53}{8\mu_0} - \frac{21}{2\mu_0^3} - \frac{95}{48}\mu_0.$$

Since W_2 can be written as

$$W_2 = -\frac{1}{12W_0\tau}(\frac{9}{\mu_0^2} - \frac{39}{4}),$$

it is negative provided $\frac{9}{\mu_0^2} > \frac{39}{4}$, or $\tau < .698$. We find that μ_2 is also negative since we can write it as

$$-\frac{1}{\mu_0^3}[\frac{95}{48}\mu_0^4 - \frac{53}{8}\mu_0^2 + \frac{21}{2}]$$

and see that the roots are complex and hence the quantity in the square bracket is always positive. Therefore, we expect to see the period increase slightly as ϵ increases.

We have then that the perturbation solution to second order is

$$\eta = 2\cos\theta + \epsilon^2[(\tfrac{1}{6} - \tfrac{2}{\mu_0^2})\cos 2\theta + \tfrac{2}{\mu_0}\sin 2\theta + \tfrac{6}{\mu_0^2} - \tfrac{7}{2}] + \bigcirc(\epsilon^3)$$
$$\mu = \mu_0 - \tfrac{\epsilon^2}{\mu_0^3}[\tfrac{95}{48}\mu_0^4 - \tfrac{53}{8}\mu_0^2 + \tfrac{21}{2}] + \bigcirc(\epsilon^4)$$
$$W = W_0 - \tfrac{\epsilon^2}{\mu_0^2}(\tfrac{3}{2} - \tfrac{45}{24}\mu_0^2 + \tfrac{13}{48}\mu_0^4) + \bigcirc(\epsilon^4)$$

where $W_0 = \frac{1}{\sqrt{2\tau}}$ and $\mu_0 = \sqrt{6(1 - W_0)}$. Since W_2 is negative, we expect limit cycles for $W < W_0$, and hence, for $\xi < 0$.

5.5 Numerical Studies

We now compute the periodic solution which the perturbation expansion suggests exists. We use the normalized form for the equation

$$P(\eta)\eta_{\xi\xi} = Q(\eta)\eta_\xi^2 + R(\eta)\eta_\xi + S(\eta)$$

where, as before,

$$P(\eta) = \tfrac{1}{6}e^{-\eta}$$
$$Q(\eta) = \tfrac{1}{8}e^{-\eta}$$
$$R(\eta) = W^2\tau - \tfrac{1}{2}e^{-\eta}$$
$$S(\eta) = W\eta - 1 + e^{-\eta}.$$

We find that stable limit cycles are found for $\xi < 0$. Figure (5.1) is an example of this.

We look at the numerical solutions in two ways, just as in Chapter 3. We would like to compare the results from the solution to this continuous equation with those from the solution to the discrete steady profile equation that we studied in Chapter 3. The first way we look at the solutions is to fix τ and let W vary from its smallest value that we could compute up towards the critical W_0. We choose $\tau = .57$, as we did in Chapter 3, so that we can compare the results. The second way we look at the solutions is for various values of τ and we choose W as far away from W_0 as we can without the solution diverging. We look at the same values for τ as we did in Chapter 3 and compare the results.

5.5.1 Various W for fixed τ

For τ fixed, we find that the solutions are very similar to those of Chapter 3. Figure (5.2) shows the phase portraits for each W. We see that as W decreases away from W_0, the value of the maximum gets closer to the saddle point. Table (5.1) has the actual values. We also clearly see that the amplitude decreases as W gets closer to W_0.

We look now at the velocity perturbations, figures (5.3) through (5.6). We see that η is related to the velocity in the same way as $f'(\xi)$ was in

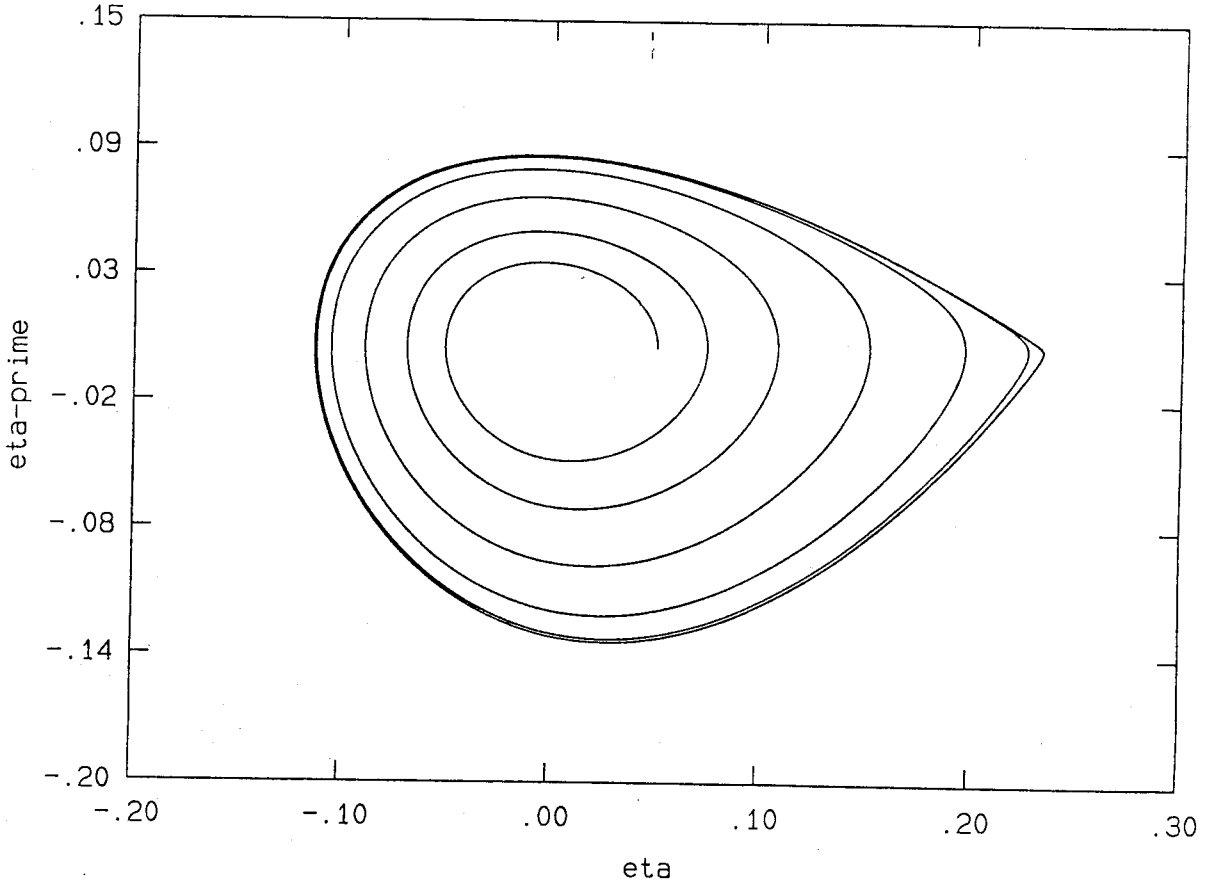

Figure 5.1: Limit cycle for $\tau = .61$ and $W = .8903$.

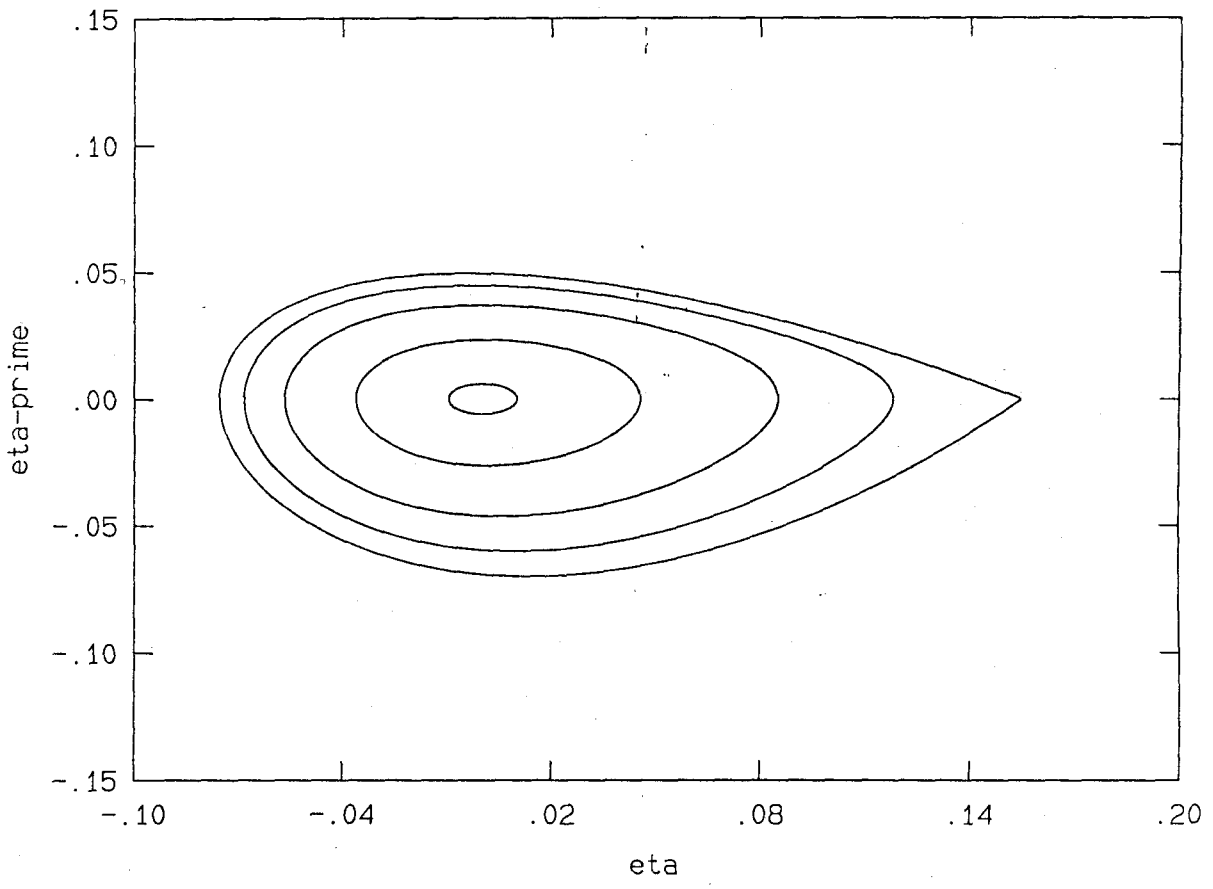

Figure 5.2: Phase portraits for $\tau = .57$ and various W.

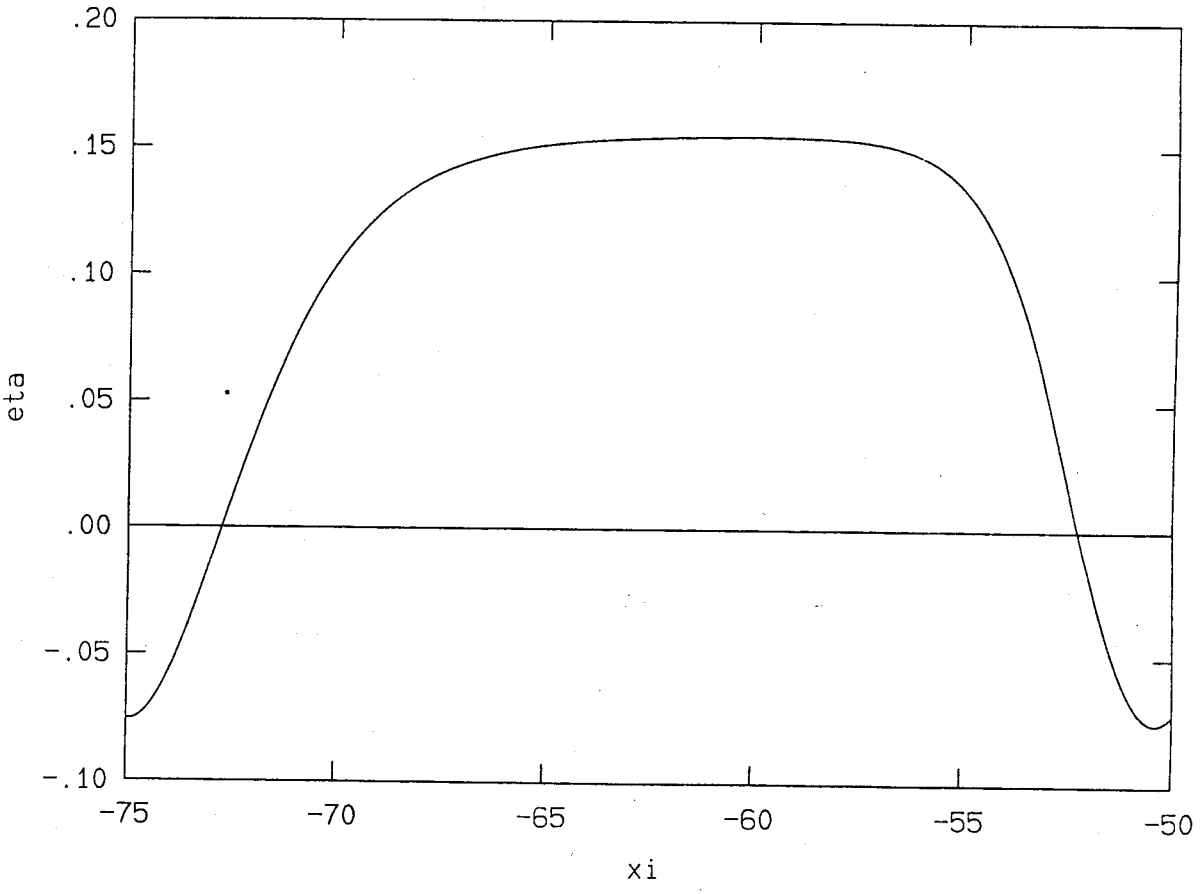

Figure 5.3: Velocity perturbation for $\tau = .57$ and $W = .9263$.

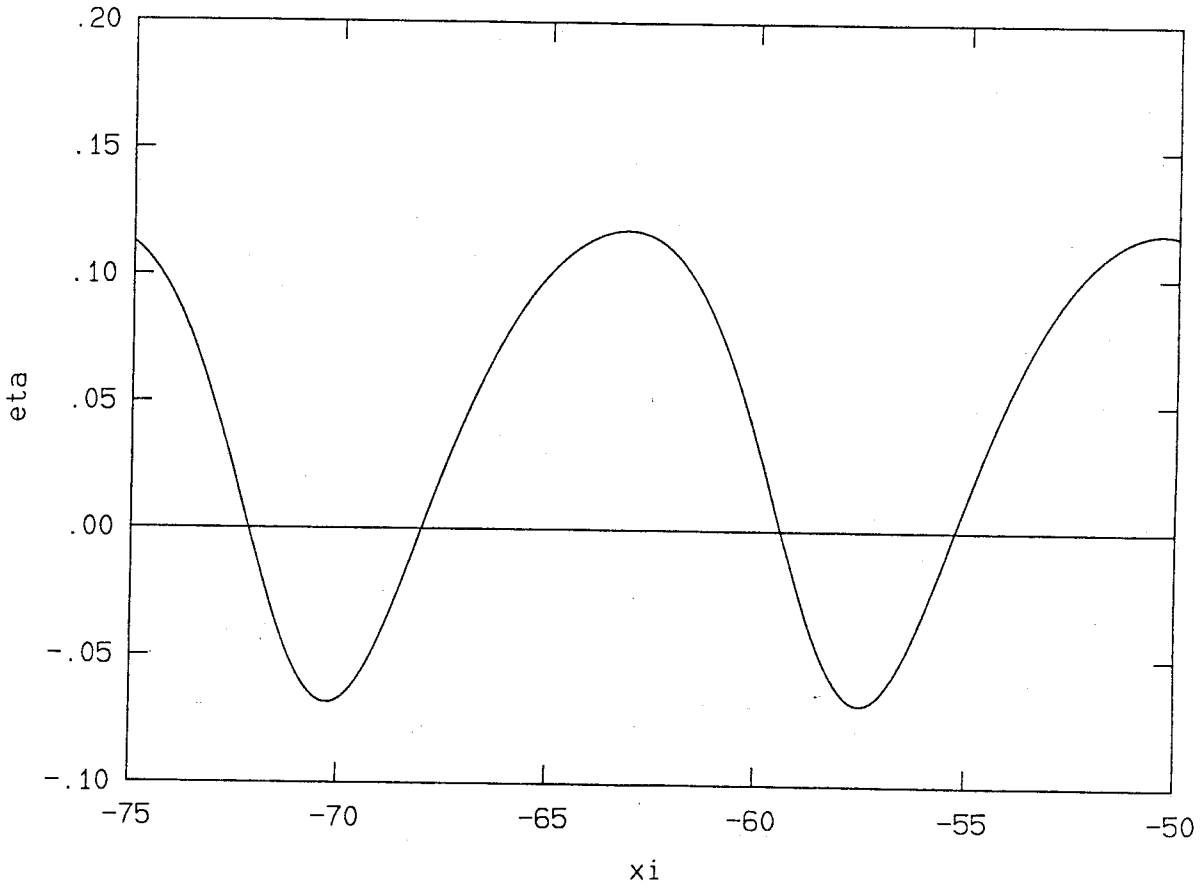

Figure 5.4: Velocity perturbations for $\tau = .57$ and $W = .929$.

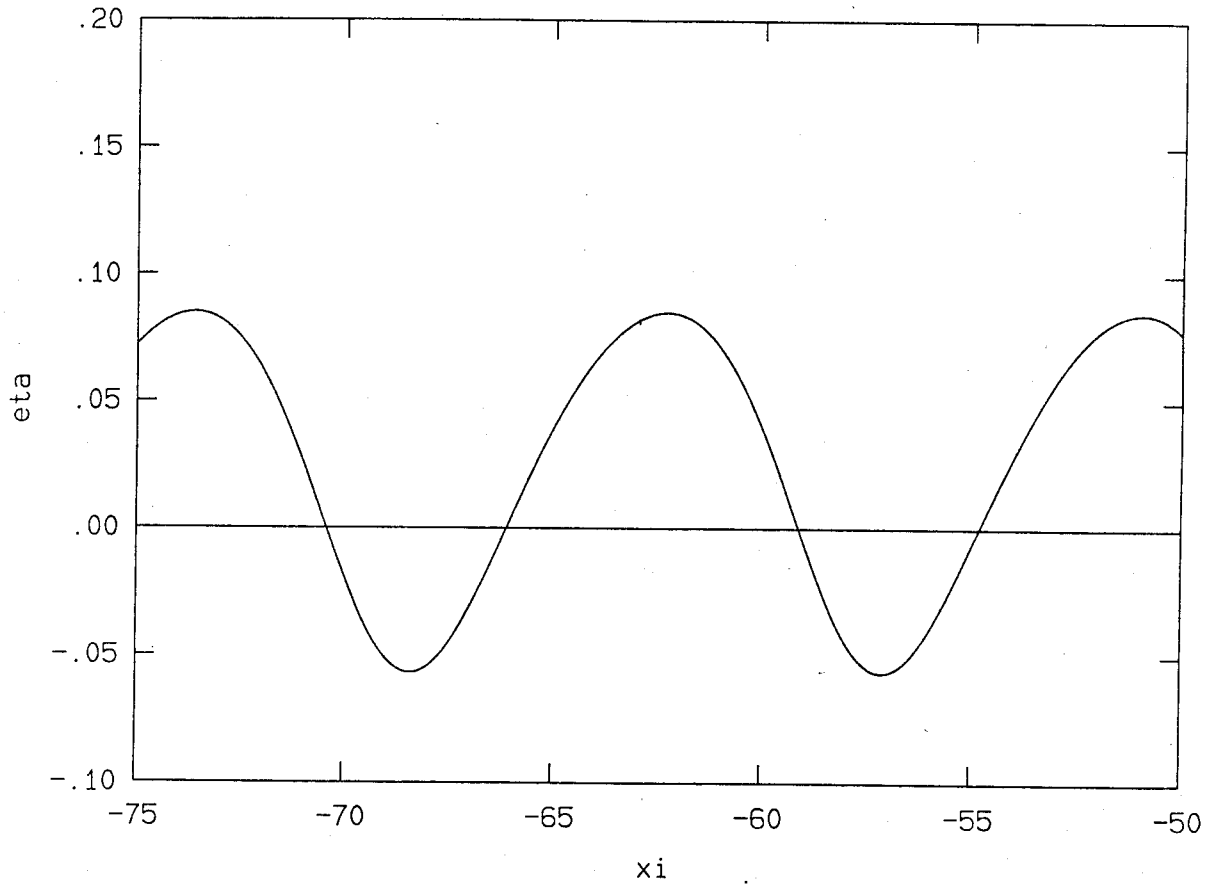

Figure 5.5: Velocity perturbations for $\tau = .57$ and $W = .932$.

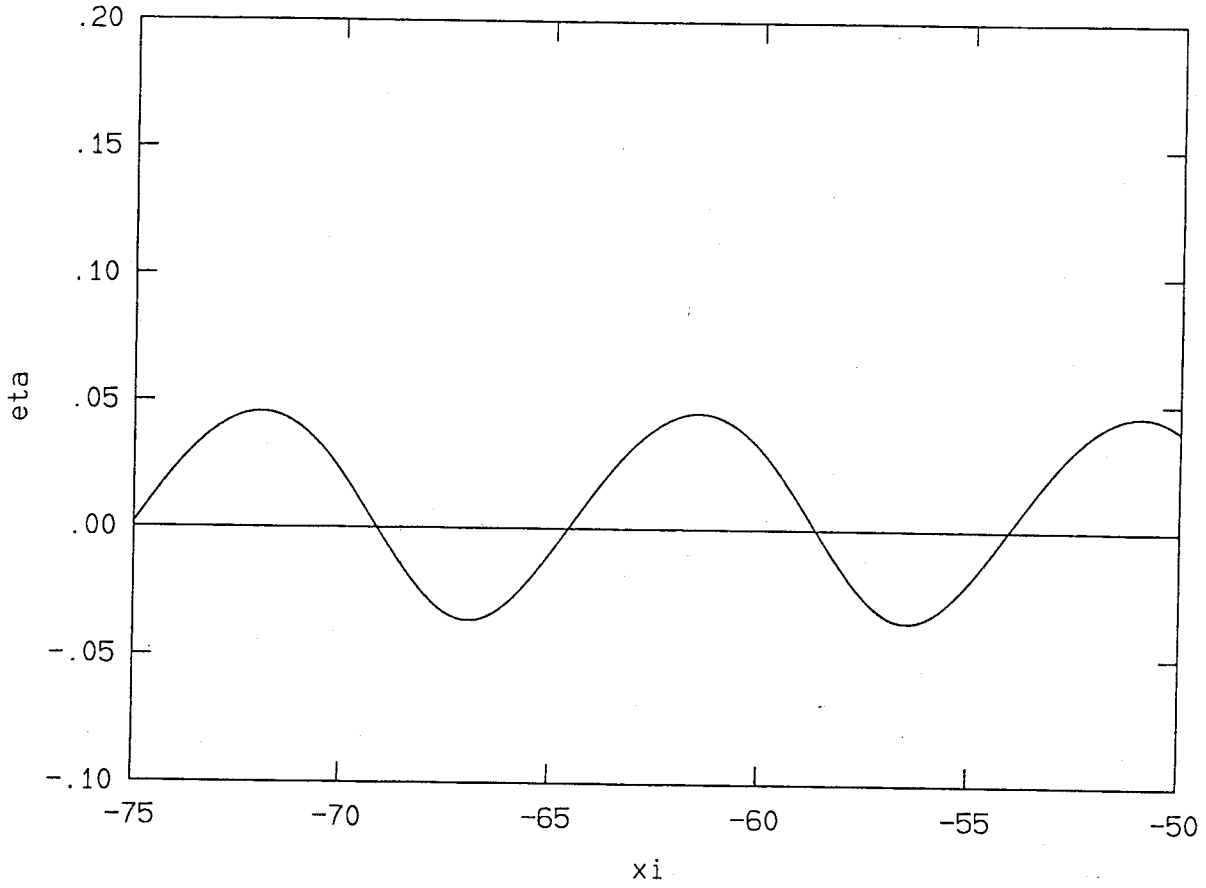

Figure 5.6: Velocity perturbations for $\tau = .57$ and $W = .935$.

Chapter 3:

$$v_n(t) = v_0 + \frac{v_f}{\lambda}\alpha W\eta.$$

Along with the increasing amplitude for $W_0 - W$ increasing, we also have the period increasing. Comparing the period here to that of the discrete equation, we find larger periods here and the increase in the period from the smallest $W - W_0$ to the largest is higher for this same value of τ. The increase here is about 14 whereas the discrete model had an increase of about 10. Table (5.2) has the values of the amplitude and period for each value of W.

From the velocity profiles, we see that as W tends to W_0, the curves become more symmetric about 0. In table (5.3), we compare the percentage of the total amplitude which is negative for each W and we see that this percentage varies from 32.8% for the largest value of $W_0 - W$, to 49% at the smallest value. A value of 50% tells us that half of the curve sits below zero and half sits above zero, thus, as $W \rightarrow W_0$, we see that the curves are tending to a symmetric function. Table (5.4) has the mean values for each case and the percentage of the total amplitude which the mean value occupies. We see that the mean increases from close to 0 as $W_0 - W$ increases. Clearly, as the amplitude decreases, the mean will also decrease. Therefore, the relevant comparison is the ratio of the mean to the total amplitude. When this is low, we see a more symmetric solution. The third column of table (5.4) shows that as $W - W_0$ decreases, so does this ratio. We see in the next sub-section that this ratio does not decrease as the amplitude decreases.

Table 5.1: This shows the value of the saddle point for each $W - W_0$ and the distance that the maximum value of η is from it.

$W - W_0$	saddle point	distance from the maximum to the saddle point
.01029	.1551	.0005
.00759	.1491	.0311
.00459	.1425	.0569
.00159	.1360	.0904

Table 5.2: The values for W, $W - W_0$, the amplitude $= \frac{max-min}{2}$ and the period.

W	$W - W_0$	A	P
.9263	.01029	.1151	24.52
.929	.00759	.0932	12.78
.932	.00459	.0713	11.30
.935	.00159	.0409	10.50

Table 5.3: The maximum, minimum and percentage of the total amplitude which is negative for each W.

W	max	min	$\% < 0 = \frac{\lvert min \rvert}{2A}$
.9263	.1546	-.0755	32.8%
.929	.1180	-.0684	36.7%
.932	.0856	-.0570	40.0%
.935	.0456	-.0362	44.3%

5.5.2 Maximum Amplitude Solutions

We see the greatest differences in the solutions to the discrete equation and the continuous equation when we look at the maximum amplitude solutions for various values of τ. Table (5.5) gives the values chosen for W for each τ as well as the resulting maximum, minimum and location of the saddle point. Figure (5.7) has the phase portraits for this case. Clearly, just as in Chapter 3, the amplitude decreases with decreasing τ. In comparing these solutions to those of Chapter 3, we notice that the amplitudes are consistently smaller here than those of Chapter 3. Table (5.6) illustrates this. Since the actual velocity depends on the value of W, and this value is different for the continuous problem and the discrete problem, we check that the actual velocities for both cases followed this same pattern. We find that the amplitudes of the velocity profiles, even though the values of W are different, are still larger for the discrete case. Table (5.7) compares the values of W times the corresponding amplitude for each τ for both cases. $W\eta$ for the continuous equation corresponds to Wf' of the discrete equation.

Next, we compare the period. Table (5.8) has this comparison. We see that the periods of the solutions to the continuous equation decrease as τ decreases, which is what we expect from the perturbation. We also see that the periods here are greater than the corresponding ones from the solutions to the discrete equations. For example, the period for the case of $\tau = .61$ for the continuous case is 16.6, and for the discrete case it is 10.9. We find in table (5.9) that the distance from the saddle point is quite small for the continuous equation. The distances are smaller than the corresponding distances for the

Table 5.4: The mean and the percentage of the total amplitude which the mean occupies for each value of W.

W	mean = M	$\frac{M}{2A}$
.9263	.0973	42.3%
.929	.0396	21.2%
.932	.0208	14.6%
.935	.0065	8.0%

Table 5.5: The value of τ, W, the maximum, the minimum and the location of the saddle point.

τ	W	max	min	saddle point
.67	.8427	.3466	-.1662	.3526
.61	.8903	.2338	-.1138	.2371
.57	.9263	.1546	-.0755	.1551
.53	.9666	.0669	-.0337	.0683
.51	.98852	.0228	-.0115	.0231

Table 5.6: Comparison of the amplitudes for the continuous case - A_c with those of the discrete case - A_d for each value of τ.

τ	A_c	A_d
.67	.2564	.3182
.61	.1738	.2090
.57	.1151	.1456
.53	.0503	.0605
.51	.0172	.0209

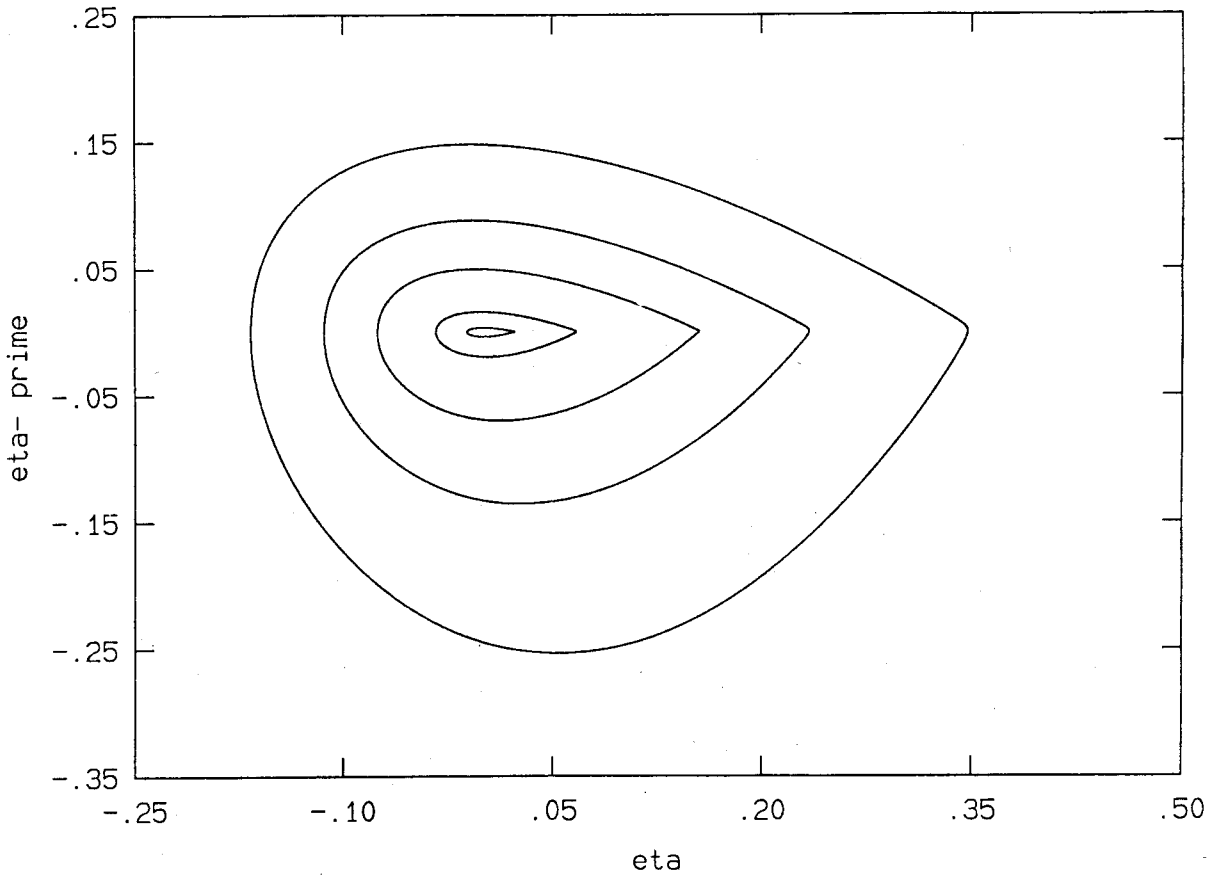

Figure 5.7: Phase portraits for the maximum amplitude solutions for various τ.

Table 5.7: Comparison of the actual velocities for the discrete and continuous cases by comparing the values of W times the amplitude for each τ.

τ	$W_c A_c$	$W_d A_d$
.67	.2161	.2577
.61	.1547	.1808
.57	.1066	.1322
.53	.0486	.0580
.51	.0170	.0206

Table 5.8: Comparison of the periods of the continuous and discrete cases for each τ.

τ	P_c	P_d
.67	13.53	10.51
.61	16.63	10.91
.57	24.53	18.75
.53	28.30	19.94
.51	50.98	34.93

Table 5.9: The location of the saddle point and the distance from it to the maximum for each τ.

τ	saddle point	distance from the maximum to the saddle point
.67	.3526	.006
.61	.2371	.003
.57	.1551	.0005
.53	.0683	.001
.51	.0231	.0003

discrete equation. Perhaps, because we have orbits closer to passing through the saddle points, we find longer periods. We see also from the velocity profiles, figures (5.8) through (5.12), that the shape is slightly different. The discrete case had more symetric profiles than the continuous case. The continuous case has profiles which lean slightly to the right and thus provide a good comparison with the discontinuous shock solution. Table (5.10) shows that for both the continuous and discrete equations, in these extreme cases, the percentage of the total amplitude which is negative is about the same — an average of 33% for the continuous case and 34% for the discrete case.

We also compare the mean velocity. Since the amplitudes are smaller here, we expect the mean to be smaller and it is. We compare the actual mean values for different values of τ for the continuous case in table (5.11). In comparing the solutions to the two equations, instead of comparing the actual means, we compare the ratio of the mean to the total amplitude. We do this in the third column of table (5.11). We find that for the continuous equation, this ratio is higher . The discrete equation gives a lower range of values, with its average slightly lower. Thus, we conclude that we have a higher mean as compared to the amplitude for the continuous equation. We can also interpret this as saying that the continuous equation gives a flatter velocity profile at the top of the curve than does the discrete equation. This is visually apparent from comparing the figures.

The overall characteristics of the periodic solutions for the continuous equation are very much the same as those of the discrete model. There are differences in the actual numbers, as is seen in the tables of this section,

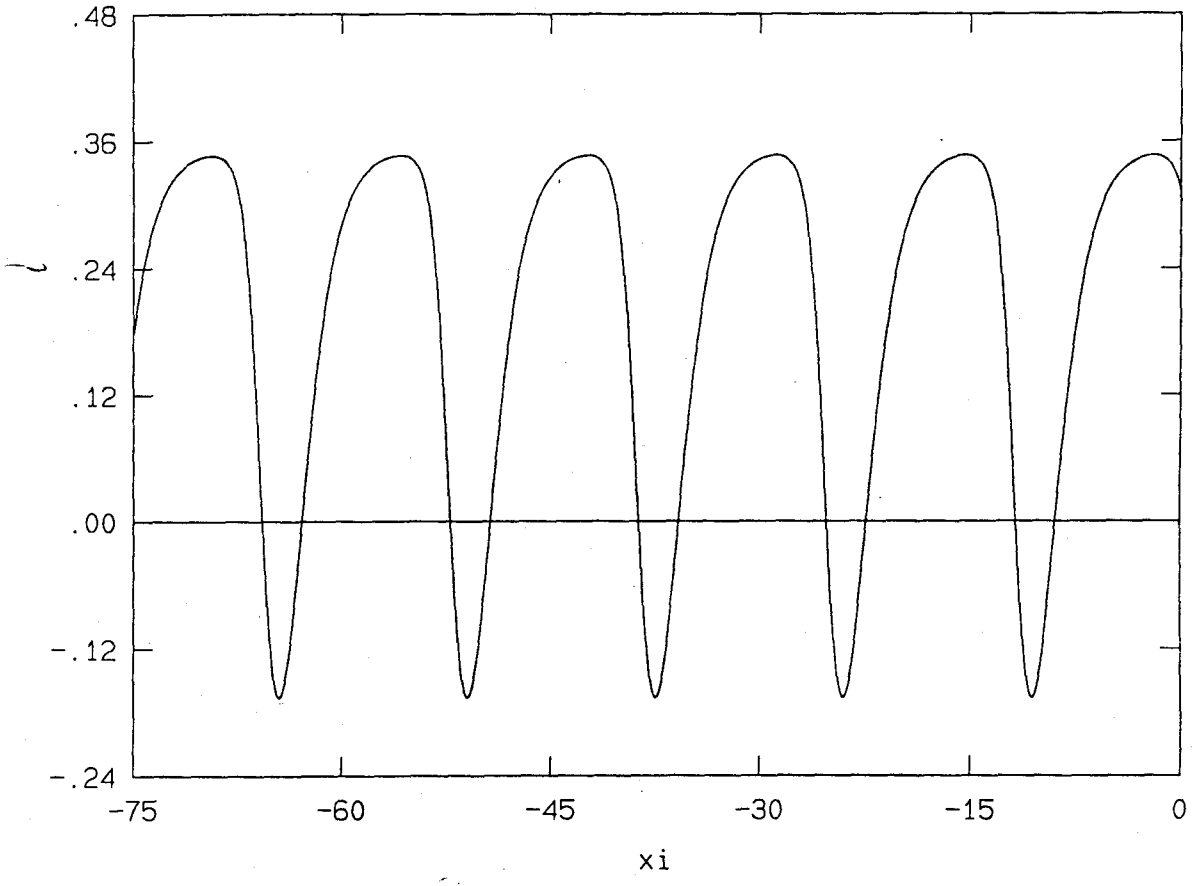

Figure 5.8: Velocity perturbation for $\tau = .67$ and $W = .8427$.

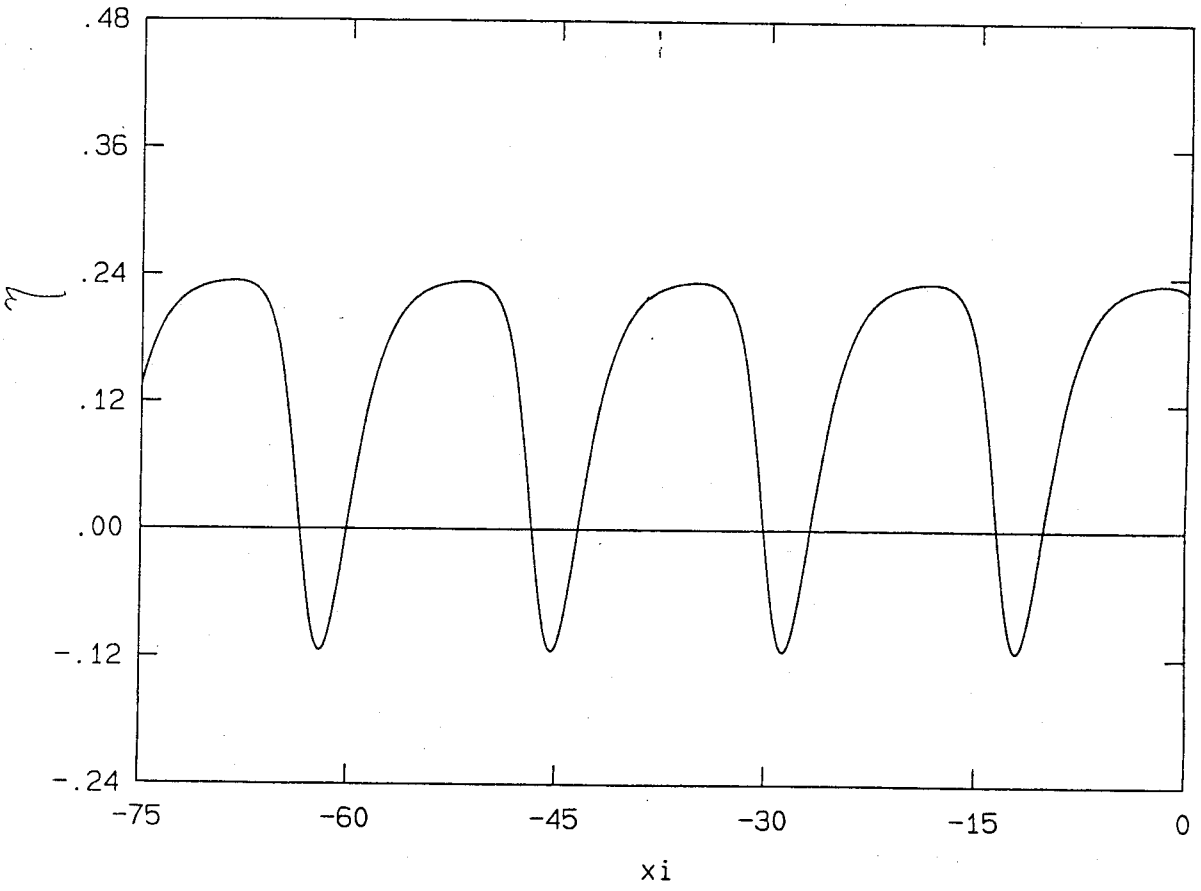

Figure 5.9: Velocity perturbations for $\tau = .61$ and $W = .8903$.

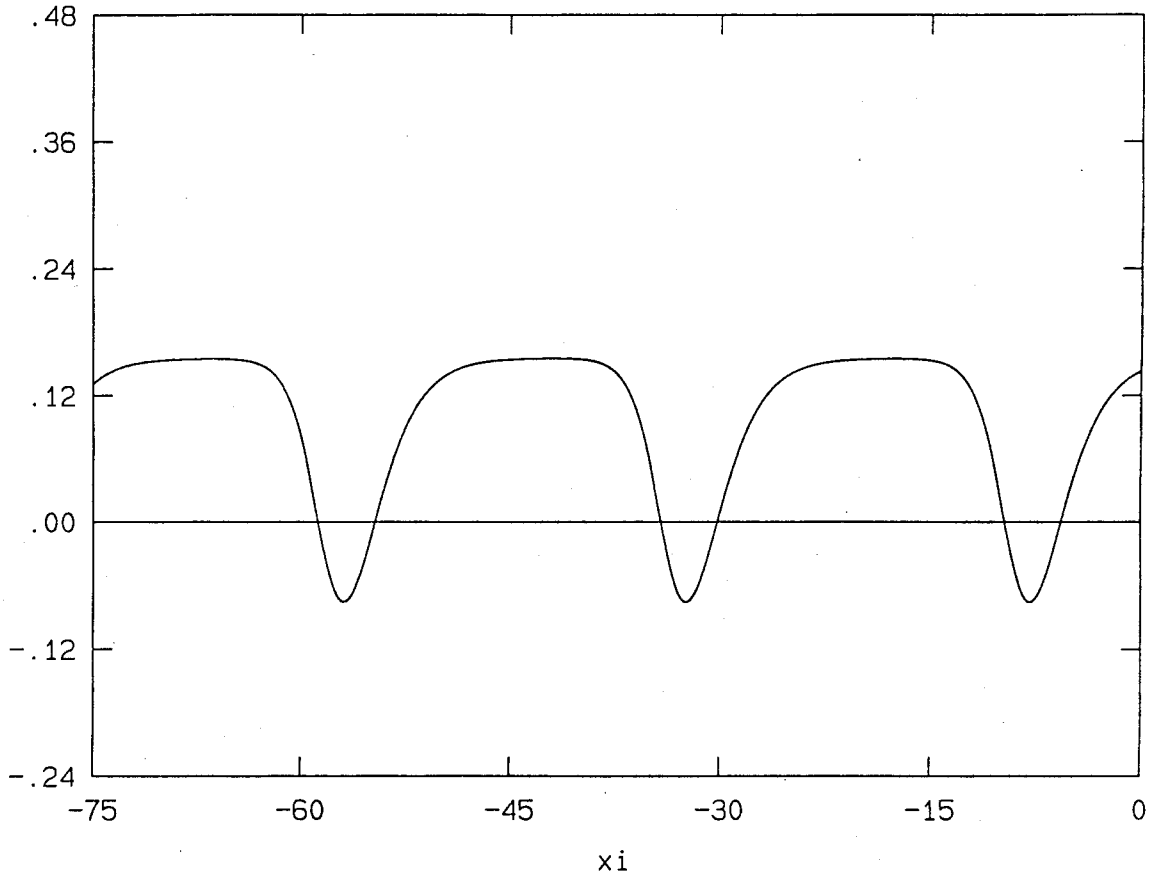

Figure 5.10: Velocity perturbations for $\tau = .57$ and $W = .9263$.

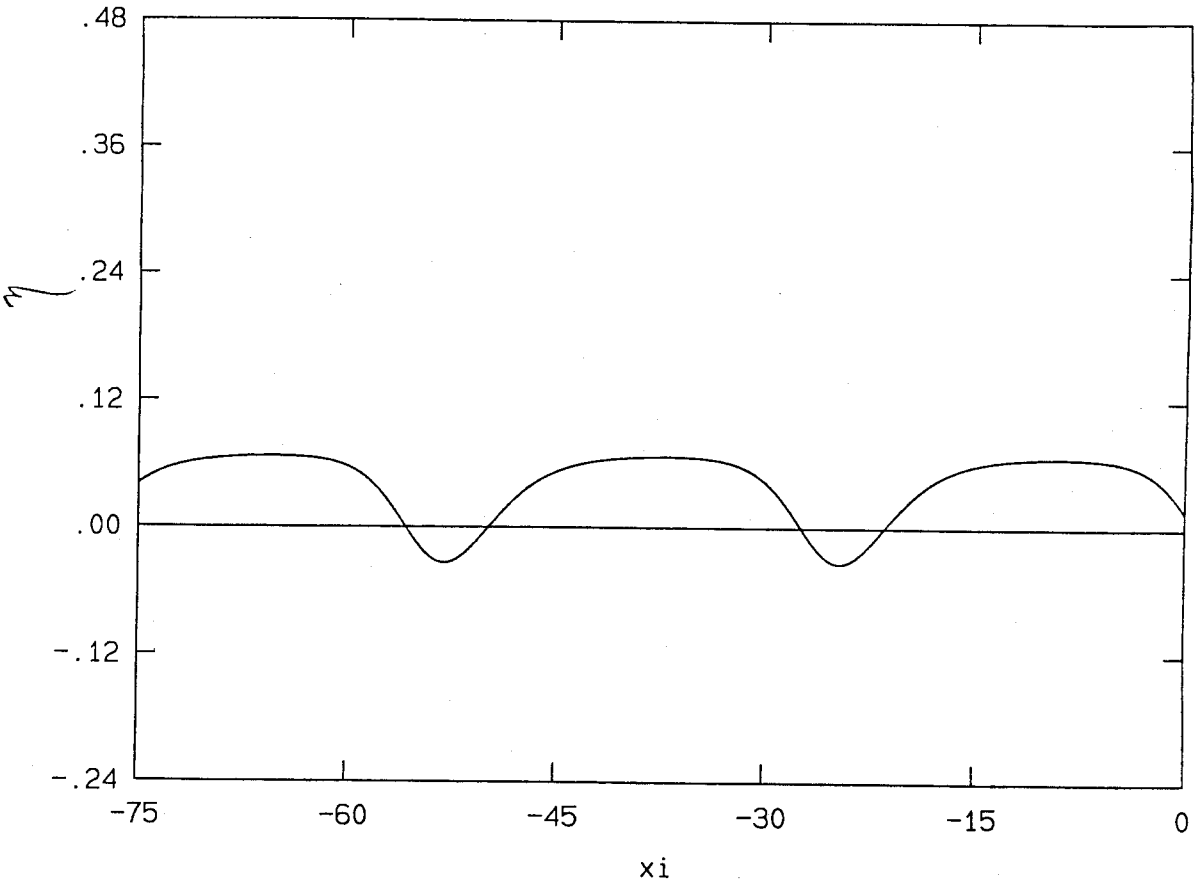

Figure 5.11: Velocity perturbations for $\tau = .53$ and $W = .9666$.

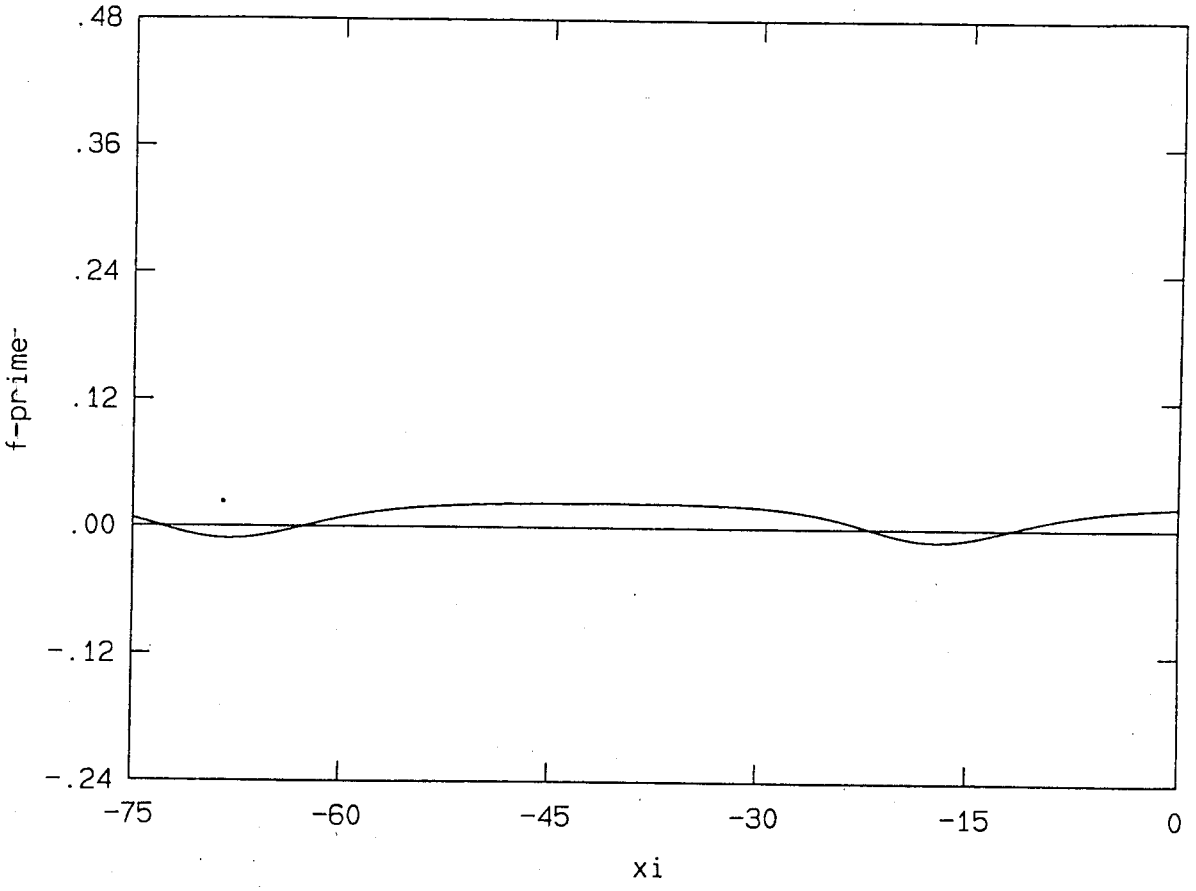

Figure 5.12: Velocity perturbations for $\tau = .51$ and $W = .98852$.

Table 5.10: Comparison of the percentage of the total amplitude which is negative for the continuous and discrete cases for each value of τ.

τ	$\frac{\lvert min\rvert_c}{2A_c}$	$\frac{\lvert min\rvert_d}{2A_d}$
.67	32.4%	33%
.61	32.7%	35%
.57	32.8%	33%
.53	33.5%	35%
.51	33.4%	35%
average	33.0%	34.2%

Table 5.11: The mean values for each τ and the comparison of the ratios of the mean to the total amplitude for the continuous and discrete cases.

τ	mean $= M_c$	$\frac{M_c}{2A_c}$	$\frac{M_d}{2A_d}$
.67	.1862	36.3%	33.0%
.61	.1298	37.3%	29.3%
.57	.0973	42.3%	38.7%
.53	.0357	35.5%	28.3%
.51	.0127	37.2%	29.2%
average		37.7%	31.7%

but they are qualitatively the same. The most notable difference is the less symetric nature of the solutions to the continuous equation as compared to those of the discrete equation and hence, the solution to the continuous equation provides a bridge between the discontinuous shock solution and the periodic solution of the discrete equation.

Concluding Remarks

We have seen that the result of instabilities is growing oscillations, the magnitude of which is determined by the extent of the instability. For shocks, we found that if the instability was not too severe, the magnitude of these oscillations stabilized and did not continue to grow down the line of cars and thus produced what appeared to be steady profile waves.

We also found oscillations in the form of periodic waves. The three theories that we considered all resulted in some form of periodic solution. The discontinuous shock theory of Chapter 1 had the velocity profile leaning all the way to the right. The car following model of Chapter 3 had more symmetric velocity profiles. The continuum model of Chapter 5 gave solutions which were continuous as in Chapter 3, but not as symmetric. The solutions leaned to the right, similar to the discontinuous solution of Chapter 1. We can think of the car following model as a model with an infinite number (and order) of derivatives which smooth out the discontinuous shock significantly more than the continuum model of Chapter 5 with only one higher derivative.

A thorough comparison with experimental data on traffic would be another nice thing to consider. One piece of experimental data was obtained from a report that was done by two surf students in the summer of 1987.

Figure (5.13) shows the velocity profile of their car on the 605 freeway at rush hour. This is a graph of the record they kept while driving through a

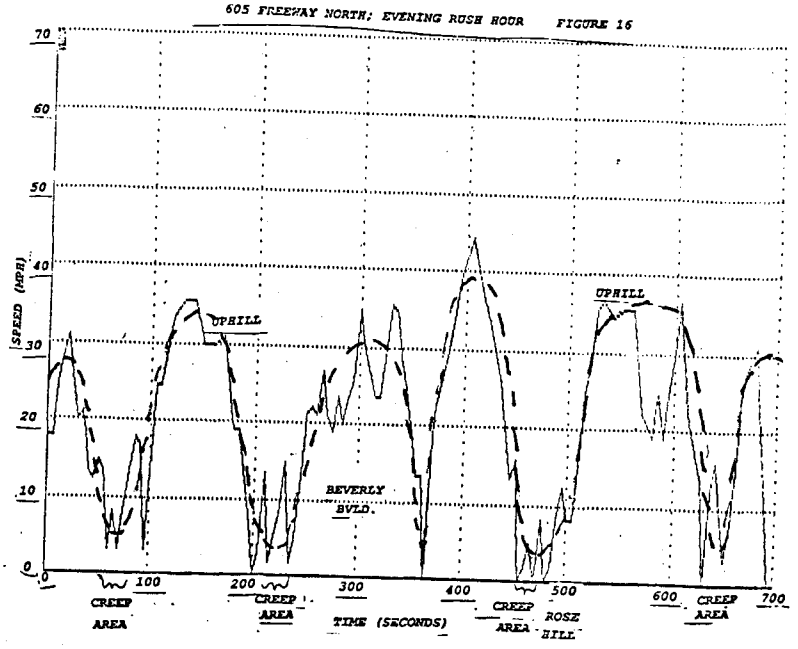

Figure 5.13: The velocity profile of a car on the 605 freeway during rush hour.

traffic jam. Although there are many short, frequent oscillations, the overall shape compares nicely with the periodic solution obtained in this thesis. The dotted line shows a smooth version of the actual velocity curve. This curve has the characteristic that it spends much of its time at a higher velocity and occasionally dips down for a short duration as do our solutions. Clearly, the actual values do not compare well at all, but this could be due to the parameter values that we chose.

In addition to the mathematical interest of these periodic and shock solutions, there is perhaps some practical interest as well. Stop and go waves clearly exist in traffic and it seems that this instability can be triggered very easily. These waves are not desirable in traffic. By lowering the mean velocity, they lower the flow and are also a source of great frustration to the driver.

Bibliography

[1] R.R. Brock, "Development of Roll-Wave Trains in Open Channels," Proc. Am. Soc. Civil Eng. Hydrodynamics Division Journal, Vol. 95, 1401-1427 (1969)

[2] R.F. Dressler,"Mathematical Solution of the Problem of Roll Waves in Inclined Open Channels," Comm. Pure and Appl. Math. 2,149-194 (1949)

[3] D.L. Gerlough, "Traffic Flow Theory", Transportation Research Board (1975)

[4] D.L. Gerlough and D.G. Capelle, "An Introduction to Traffic Flow Theory", Highway Research Board Special Report 79 (1964)

[5] R. Herman, E.W. Montroll, R.B. Potts and R.W. Rothery, "Traffic Dynamics: Analysis of Stability in Car Following," Opns. Res. 7, 86-106 (1959)

[6] D.J. Needham and J.H. Merkin, "On Roll Waves Down an Open Inclined Channel," Proc. R. Soc. Lond. A 394, 259-278 (1984)

[7] G.F. Newell, "Nonlinear Effects in the Dynamics of Car Following," Opns. Res. 9, 209-229 (1961)

[8] G.F. Newell, "Theories of Instability in Dense Highway Traffic," J. Oper. Res. Soc. Jap., 5:9-54 (1963)

[9] B. Solberg and P. Hughes, "Freeway Observations and Computer Modeling of Traffic Jams," SURF report at Caltech sponsored by G.B. Whitham (1987)

[10] G.B. Whitham, Linear and Nonlinear Waves, (Wiley & Sons, New York 1974)